

AIAA Undergraduate Aircraft Design Competition Final Design Review

Team Dolphin



AE 443: Aerospace Systems Design II

2021 Spring

Department of Aerospace Engineering

University of Illinois at Urbana-Champaign, IL, 61801

Group Member Assignments

Group Member	Discipline Assignments	Email	Signature
Travis Zook	Team Lead, Systems, Acoustics	tjzook2@illinois.edu	
Ben Schultz	Aerodynamics, Landing Gear	bks4@illinois.edu	
Ted Kim	Structures, Loads and Dynamics, Interior Design	jkim669@illinois.edu	
Julia Yoon	Mass Properties, Certification	chaewon2@illinois.edu	
Mitchell McMahon	Propulsion, Avionics, Ordnance	mem6@illinois.edu	
Ashvat Bansal	Performance, Configuration	ashvatb2@illinois.edu	
Ifeloluwa Osilaja	Stability and Control, Cost	iosila2@illinois.edu	

Table of Contents

I.Introduction	1	VI.B.Wing Design.....	22
I.A.Background	1	VI.C.High Lift Systems	23
I.B.Target Market.....	1	VI.D.Drag Buildup	25
I.C.Design Philosophy	1	VI.E.Lift Curves and Drag Polars	26
II.Concept of Operations.....	1	VII.Performance	27
II.A.Requirement	1	VII.A.Required Performance	27
II.B.Mission Profile.....	2	VII.B.Takeoff and Landing Analysis.....	27
III.Sizing Analysis	4	VII.C.Fuel and Velocity	28
IV.Configuration.....	7	VII.D.Drag Calculations	31
IV.A.Design Morphology	7	VII.E.Aircraft Performance Coefficients	32
IV.B.Interior Design & Ejection Mechanism ...	10	VII.F.Payload Range	33
IV.C.Landing Gear	11	VII.G.Payload-Time on Station	34
V.Propulsion.....	14	VII.H.Range Mach	35
V.A.Propulsion System	14	VII.I.Performance Ceilings	35
V.B.Engine Selection and Performance	14	VII.J.Flight Envelope	36
V.C.Configuration	16	VII.K.Specific Excess Power	37
V.D.Safety Consideration	17	VII.L.Trade Studies.....	38
V.E.Inlet and Exhaust	17	VII.M.Comparison to RFP Requirements	40
V.F.Inlet Validation.....	19	VIII.Stability and Control.....	40
V.G.Future Work	20	VIII.A.Empennage Design	40
VI.Aerodynamics	20	VIII.B.Control Surface Design.....	42
VI.A.Airfoil Selection	20	VIII.C.Longitudinal Static Stability	44

VIII.D.Trim Analysis	45	XI.D.Hydraulics.....	75
VIII.E.Stability Derivatives.....	47	XI.E.Pneumatics	76
VIII.F.Dynamic Stability	48	XI.F.Electric System.....	76
VIII.G.Trade Studies.....	48	XI.G.Avionics	77
IX.Structures and Loads	49	XI.H.Emergency Systems	79
IX.A.Material Selection	49	XI.I.Environmental Control System	79
IX.B.Trade Study: Armor Design	51	XII.Cost Analysis	79
IX.C.V-n Diagram	52	XII.A.Inaccuracies	79
IX.D.Load Cases and Path.....	54	XII.B.Major Costs	80
IX.E.Structural Arrangement	56	XII.C.Cost Reduction Methods	80
IX.F.Pressurization & Skin Thickness	61	XII.D.Unit Cost	81
IX.G.Landing Gear	62	XIII.Ordnance	82
X.Mass Properties	65	XIII.A.Requirements and Design.....	82
X.A.Weight Estimations	65	XIII.B.Ordnance Configurations	83
X.B.Longitudinal Center of Gravity	65	XIII.C.Inaccuracies	84
X.C.Lateral Center of Gravity	67	XIV.Survivability	84
X.D.Trade Study: Ordnance Location	69	XIV.A.Radar	85
XI.Auxiliary Systems	70	XIV.B.Infared	85
XI.A.Fuel System	70	XIV.C.Acoustic	86
XI.B.Flight Controls.....	73	XIV.D.Other	86
XI.C.Engine Controls.....	74	XV.Conclusion	88

Nomenclature

α	= angle of attack
μ	= coefficient of friction
β	= sideslip angle C_D
drag coefficient	=
C_{D_0}	= parasitic drag coefficient
C_{D_i}	= induced drag coefficient
$C_{D_{\text{trim}}}$	= drag due to trim coefficient
$C_{D_{\text{flap}}}$	= drag due to flaps coefficient
$C_{D_{L+p}}$	= drag due to leakage and protuberance coefficient
C_L	= lift coefficient
$C_{L, \text{Max}}$	= max wing lift coefficient
C_l/C_d	= lift-to-drag-coefficient ratio
C_{l_p}	= roll damping coefficient
C_{l_β}	= rolling moment due to sideslip angle
C_{l_r}	= yaw damping coefficient
$C_{l_{\delta a}}$	= rolling moment due to aileron deflection angle
$C_{l_{\delta r}}$	= rolling moment due to rudder deflection angle
C_m	= moment coefficient
$C_{m_{\delta e}}$	= pitching moment due to aileron deflection angle
C_{n_β}	= yawing moment due to sideslip angle
$C_{n_{\delta a}}$	= yawing moment due to aileron deflection angle
$C_{n_{\delta r}}$	= yawing moment due to rudder deflection angle
c'/c	= flap extension ratio
Γ	= dihedral
L/D	= lift-to-drag ratio
λ	= taper ratio
$\Lambda_{C/4}$	= quarter chord sweep
Re	= Reynolds Number
$S_{\text{flapped}}/S_{\text{ref}}$	= ratio of flapped area to reference area
$S_{\text{wet}}/S_{\text{ref}}$	= ratio of wetted area to reference area
T/W	= thrust-to-weight ratio

Acronyms

AIAA	= American Institute of Aeronautics and Astronautics
a.c.	= aerodynamic center
CAD	= Computer-aided Design
CBR	= California Bearing Ratio
CFD	= Computational Fluid Dynamics
CG	= center of gravity
ECS	= Environmental Control System
ECU	= Engine Control Unit
F124	= F124-GA-100
FADEC	= Full Authority Digital Engine Control
FCU	= Fuel Control Unit
FDR	= Final Design Review
FEA	= Finite Element Analysis
FOD	= Foreign Object Debris
HOTAS	= Hands on Throttle and Stick
HUD	= Heads-Up Display
IPPS	= Integrated Powerplant System
KEAS	= Knots Equivalent Airspeed
KTAS	= Knots True Airspeed
MAC	= Mean Aerodynamic Chord
MTOW	= Maximum Takeoff Weight
OWE	= Operating Empty Weight
PDR	= Preliminary Design Review
RDTE	= Research, Development, Testing and Evaluation Cost
RFP	= Request for Proposal
ROC	= Rate of Climb
SDB	= Small Diameter Bomb
TOFL	= Takeoff Field Length
TSFC	= Thrust Specific Fuel Consumption
FOD	= Foreign Object Damage

List of Figures

1	Diagram of Design Mission Profile	2	26	Specific Excess Power Plot	38
2	Diagram of Ferry Mission Profile	3	27	ROC vs. Velocity	39
3	Constraint Diagram	7	28	Fuel Burn vs Mach	39
4	Engine Positions	8	29	Scissor Plot for Horizontal Tail Sizing . .	40
5	Tail Configurations	9	30	Horizontal Tail of the aircraft with major dimensions measured	41
6	Inlet Positions	9	31	Vertical Tail of the aircraft with major dimensions measured	42
7	(a) Isometric View of the Cabin and Canopy Opening Mechanism (b) Cabin and Seat Dimension	10	32	Drawing of the Aileron with Dimensions .	43
8	(a) Warning Signs, Armor and Ladder Design (b) Warning Sign and Inlet Ejection Design	11	33	Optimal Trim Elevator Deflections	45
9	Landing Gear Configuration	12	34	Takeoff Trim Curves	45
10	Graphs of TSFC and Thrust vs Mach vs Altitude	15	35	Cruise Trim Curves	46
11	Graphs of TSFC vs Partial Thrust vs Mach at Sea Level and 15,000 feet	16	36	Landing Trim Curves	46
12	CAD Drawing of the Inlet	17	37	Maneuver and Gust V-n Diagram	53
13	CAD Drawing of the Nozzle	18	38	Load Cases	54
14	2D Inlet ANSYS Simulation	20	39	(a) Lift Distribution (b) Shear (c) Bending Moment For Right Main Wing	55
15	Airfoil Characteristics at Mach=0.0 from XLF5	21	40	Main Wing Structural Arrangement	57
16	NACA 63-415 Airfoil	21	41	Deflection of The Left-Side Main Wing .	58
17	Overall Wing Dimensions	25	42	Stress Throughout The Left-Side Main Wing	58
18	Aircraft Polars From XLF5	27	43	Structural arrangement of (a) Horizontal Tail (b) Vertical Tail	59
19	Design Performance Coefficients	32	44	Structural Arrangement of The Aircraft .	60
20	Ferry Performance Coefficients	33	45	Fuselage Side View	60
21	Payload Range Diagram	34	46	(a) Compartment Division at Frame Section 12 (b) Wing Attachment Fittings . .	61
22	Payload-Time on Station Diagram	34	47	Automatic Pressurization Schedule	62
23	Range Mach Diagram	35	48	Landing Gear Stowed	65
24	Max ROC vs. Altitude	36	49	Longitudinal CG envelope	67
25	Flight Envelope @ MTOW	37	50	Lateral CG envelope	68
			51	CG Imbalance Due to Ordnance	69

52	Isometric view of all major auxiliary systems components	70	60	Pneumatic System Diagram	76
53	Fuel Tank Layout	71	61	Electrical System Diagram	77
54	Diagram of Fuel System	72	62	Avionics Layout	79
55	Flight Control Diagram	73	63	Comparison of Unit Cost to Similar Aircraft	81
56	Flight Control Model	74	64	Gun Location	83
57	ECU Diagram	75	65	Pylon Locations	84
58	ECU component locations	75	66	Internal Armor Placement	87
59	Hydraulic System Diagram	76	67	External Armor Placement	87

List of Tables

1	RFP Requirements and Goals [1] compared to Orca	viii	20	Design Segment Velocities	30
2	Mission Requirements	2	21	Drag per Mission Segment for Design Mission	31
3	Design Mission Profile Breakdown	3	22	Drag per Mission Segment for Ferry Mission	32
4	Ferry Mission Profile Breakdown	4	23	Performance Coefficients Table	33
5	Similarity Analysis	5	24	Summary of Horizontal Tail Parameters	41
6	Initial Sizing Driving Parameters	6	25	Summary of Vertical Tail Parameters	42
7	Powerplant Options	14	26	Summary of Control Surface Parameters	43
8	Additional F124-GA-100 Specifications	15	27	Summary of Aileron Parameters	44
9	Targeting Pod Trade Study	19	28	Roll Parameters	44
10	Summary of Wing Parameters	23	29	Static Margin	44
11	Analysis of Different High Lift Devices	24	30	Yawing Parameters	47
12	Summary of High Lift System	24	31	List of Stability Derivatives	47
13	Cruise Component parasite Drag Buildup	26	32	Longitudinal Dynamic Stability Analysis	48
14	Complete Drag Buildup	26	33	Lateral-Directional Dynamic Stability Analysis	48
15	Aircraft Aerodynamic Information	27	34	Trade Study of Jet Driven Military Trainers	
16	Takeoff Parameters at 6,000 ft	28	35	Horizontal Tail and Elevator	48
17	Landing Parameters at 6,000 ft	28	36	Trade Study of Jet Driven Military Trainers	
18	Fuel Requirement per Mission Segment for Design Mission	29	37	Vertical Tail and Rudder	49
19	Fuel Requirement per Mission Segment for Ferry Mission	30	38	Properties of Aluminium Alloys (at Room Temperature)	50

37	Material Selection	51	45	Fuel Tank Volumes	72
38	Properties of Metal Alloys and Silicon Carbide (SiC) (at Room Temperature)	52	46	Avionics	78
39	Characteristic Velocity Data from V-n Diagram	53	47	Targeting Pod Trade Study	78
40	Landing Gear Specifications	63	48	Major Costs For a 25 Year Program (Millions of Dollars)	80
41	Tire and Shock Specifications	63	49	Unit Cost of Aircraft Based on Production	81
42	Weights and CG Locations	66	50	Ordnance Specifications	82
43	Armament Locations	68	51	Gun Specifications	83
44	Color Legend for Fig. 52	70	52	Ordnance Configurations	84

Executive Summary

The specific mission of operating in austere fields while providing close air support is currently a role that is only performed by helicopters. The AIAA RFP [1] considers this kind of mission and lays out a request for an austere field light attack aircraft capable of providing ground support on short notice. Additionally, the design should maximize cost efficiency. In order to achieve this kind of design, a design philosophy was adopted that tried to provide a 'best value' design by incorporating designs and systems that provide the performance required to complete the detailed missions while minimizing the cost. The proposed aircraft is a single turbofan top inlet design with low wing and a conventional tail. A top inlet design was chosen in order to test a less used design feature and distinguish our design from the competition.

All requirements and goals set out by the AIAA RFP were either met or exceeded. Below in Table 1, the RFP requirements and goals are listed with the proposed design's corresponding characteristics and a status of whether the design proposed has met these goals and requirements. Some key design parameters are also listed in the Orca column.

Table 1 RFP Requirements and Goals [1] compared to Orca

Type	Criteria	Requirement	Orca (Exceeded, Met, Failed)	Section
Requirement	TOFL	50 ft obstacle in \leq 4,000 ft	3,883 ft (Exceeded)	VII.B
Objective	Survivability	Considerations for survivability	Variety of features (Met)	XIV
Requirement	Payload	\geq 3000 lbs	3000 lbs (Met)	VII.F
Objective	Ordnance	Variety of ordnance \leq 500 lb	- (Met)	XIII
Requirement	Integrated Gun	Integrated gun for ground targets	Integrated M61A2 (Met)	XIII
Requirement	Service life	15,000 hours over 25 years	15,000 hours/25 Years (Met)	IX
Requirement	Service ceiling	\geq 30,000 ft	38,000 ft (Exceeded)	VII.H
Requirement	Crew	Two	Two (Met)	IV.B

The requirements we have chosen to exceed are done so more as a consequence of increasing the air-worthiness of the design rather than arbitrarily trying to increase the performance of the Orca specifically in these areas. A focus was made to meet all requirements without exceeding them in order to allow for a less expensive and more competitive design to be reached. In other words, the Orca was made so that it achieves a 'best value' design, which was another objective laid out by the RFP. It is shown in Section XII that the Orca does just that, achieving a cost of \$15.52 million for a fleet size of 200 units.

I. Introduction

A. Background

As the global pandemic has started in 2020, commercial aircraft sales has shrunk tremendously. However, the demand for light attack aircraft is on the rise. According to Market Research Future [2], the Global Light Attack and Reconnaissance Aircraft Market is expected to have annual growth rate of 4.33% by the end of 2025. A major cause of this is the evolution of light attack aircraft's role from just aerial warfare to incorporating close air support for ground forces, a role that was historically often carried out by helicopters. Though, limitations exist while operating aircraft close to the front line, as there are rarely any well built runways available. Designing a light attack aircraft with the requirements listed in the AIAA Design Competition RFP enables more powerful and swift close air support [1] as this RFP considers the operation of light attack aircraft in austere field conditions.

B. Target Market

Since 1998, the world military expenditure has increased by about 39 billion US dollars each year [3]. The designed aircraft requested can be sold to allied countries as part of their military defense. One of the emerging market segments that can be tapped into is the continent of Asia, where the trend of increasing military expenditure is also observed, especially in the countries where there are frequent territorial disputes. The aircraft, built for close air support, will provide essential support in areas where territory control and ground patrol are necessary.

C. Design Philosophy

The close air support near the front lines was often performed by helicopters as they can swiftly respond to the urgent mission notice. The purpose of the design aircraft is to be affordable, and replace the role of helicopters. The aircraft should be able to operate in harsh conditions such as austere fields with better abilities such as faster flight, longer travel distance, heavier armament, and less crew numbers. To fulfill the requirement, multiple fighter planes were considered in the process of sizing and design. The aircraft primarily used for sizing was the L-159 ALCA.

II. Concept of Operations

A. Requirement

Requirements are listed by the AIAA RFP [1]. The main goal of the aircraft design is to fulfill all of the requirements, and if possible, objectives. As the main characteristic of this military aircraft is the use of austere field, there are few requirements related runways and weaponry. Takeoff and landing should be able to be performed on semi-prepared surfaces, such as grass and dirt, must be completed under 4,000 feet. Detailed requirements can be found in Table 2.

Table 2 Mission Requirements

Category	Description	Requirement
Takeoff and Landing	50 ft obstacle in \leq 4,000 ft	Mandatory
Austere Field Performance	Density altitude up to 6,000 ft & California Bearing Ratio of 5	Mandatory
Survivability	consideration for crew survivability	Objective
Weaponry	provisions for carrying/deploying weapons	Objective
Integrated Gun	For ground targets	Mandatory
Service Life	15,000 hours over 25 years	Mandatory
Service Ceiling	Greater than or equal to 30,000 ft	Mandatory
Payload	3,000 lb of armanent	Mandatory
Crew	two with zero-zero ejection seats	Mandatory

B. Mission Profile

For this project, two different missions are presented by AIAA RFP: design mission and ferry mission. For the design mission, with the full payload requirement, the aircraft must climb to the cruise altitude, descend and loiter for four hours, climb back to the cruise altitude, and lastly, descend back to the destination. The diagram of design mission profile and detailed mission breakdown can be found in Fig. 1 and Table 3 respectively.

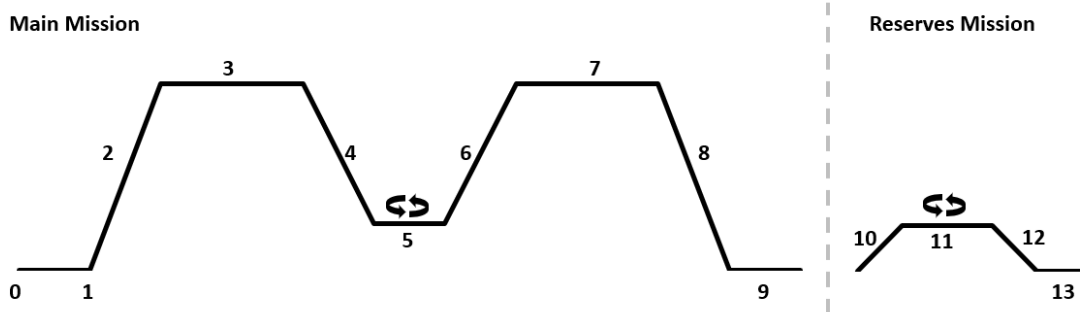


Fig. 1 Diagram of Design Mission Profile

Table 3 Design Mission Profile Breakdown

Number	Segment	Requirements
0	Warm Up / Taxi	in 5 minutes
1	Take Off	Austere field with 50 ft obstacle in $\leq 4,000$ ft of runway
2	Climb	to cruise altitude of $\geq 10,000$ ft with range credit
3	Cruise	100 nmi
4	Descent	to 3,000 ft with no range credit; completed within 20 min of initial climb
5	Loiter	4 hours on station
6	Climb	to cruise altitude of $\geq 10,000$ ft with range credit
7	Cruise	100 nmi
8	Descent / Landing	Austere field with 50 ft obstacle in $\leq 4,000$ ft of runway
9	Taxi / Shutdown	in 5 minutes
10-13	Reserves	Climb to 3,000 ft and loiter for 45 min

Another mission that needs to be completed is the ferry mission. The mission concentrates on cruising long distance of 900 nmi, with 60% of the payload requirement. The ferry mission profile and breakdown can be found in Fig. 2 and Table 4 respectively.

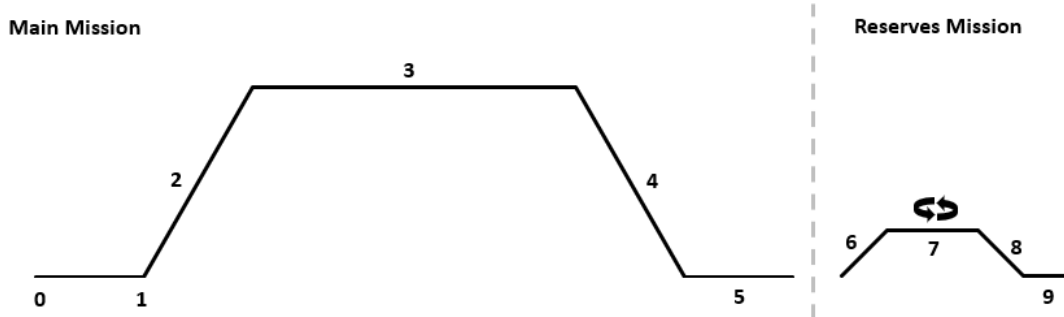


Fig. 2 Diagram of Ferry Mission Profile

Table 4 Ferry Mission Profile Breakdown

Number	Segment	Requirements
0	Warm Up / Taxi	in 5 minutes
1	Take Off	Austered field with 50 ft obstacle in \leq 4,000 ft of runway
2	Climb	to cruise altitude with range credit
3	Cruise	at best range speed at altitude \geq 18,000 ft for 900 nmi
4	Descent / Landing	Austered field with 50 ft obstacle in \leq 4,000 ft of runway
5	Taxi / Shutdown	in 5 minutes
6-9	Reserves	Climb to 3,000 ft and loiter for 45 min

III. Sizing Analysis

For the sizing of the aircraft, the options for methods were either using a seed aircraft or doing a part by part build up. A part by part build up is where the aircraft is built from scratch with many weight equations instead of making slight alterations from a similar reference aircraft like seed analysis does. These build ups take more work because each part of the plane has its own weight equation that needs to be evaluated. After all the weights are found and summed, adjustments might need to be made to the equations by checking similar aircraft and determining the proper adjustments. Seed analysis on the other hand is much quicker since a few weights like empty weight, max ramp weight, and max fuel weight of the reference aircraft are researched. Then all the weights have a change in weight applied and a sizing is iterated until it converges to a solution. Since the seed method requires much less time commitment and greater confidence with the design parameters, it was decided to go ahead with that method for the initial sizing.

In order to determine initial sizing parameters, the Embraer EMB 314 Super Tucano, Aero L-159 ALCA, and Aero L-39 Albatros were selected for a sizing analysis. The rationale of the selection was that all selected aircraft met or exceeded all mission profile requirements set out by the AIAA RFP [1]. As it was decided to have a turbofan engine, the L-159 and L-39 were selected as examples of light attack turbofan aircraft. Parameters for a turbofan design based on the Super Tucano could then be estimated. This was done using design principles and equations set out by Raymer [4].

Table 5 Similarity Analysis

Parameter	Super Tucano [5]	L-39 Albatros [6]	L-159 ALCA [7]
Wing Area [sq ft]	209	202	202.4
Wingspan [ft]	36.58	31	31.33
Aspect Ratio	6.41	4.4	4.8
Empty Weight [lb]	7,055	7,617	9,590
MTOW [lb]	11,905	10,362	17,637
Maximum Payload [lb]	3,307	2,535	5,159
Engine Spec	1,604 hp	3,790 lb thrust	6,300 lb thrust
TSFC	0.54 lb/hph	0.6 lb/lbh	0.78 lb/lbh
Ferry Range [nmi]	1,562	940	1,398
Thrust-to-Weight (or Power-to-Weight)	2.14 hp/lb	4.914 lb/lb	5.3 lb/lb
Wing Loading	56.96	51.3	87.14

For parameters that could not be estimated directly, a seed aircraft was used. This was done in part so that estimations would be more accurate (as opposed to taking averages across the different designs of multiple aircraft) and that the final design would be both achievable in performance and meeting or exceeding AIAA requirements. As it had already been decided that the Super Tucano would be the basis for the design, it was selected as the seed aircraft. This decision was made as the Super Tucano met all AIAA criteria and had a conventional design that could be easily iterated on for future changes/considerations made by the team during the design process, though some of the dimensional parameters were taken from L-159 ALCA and L-39 Albatros. Key parameters used in initial sizing are presented in the Table below

Table 6 Initial Sizing Driving Parameters

Parameter	Value
Range [nmi]	1200
Balanced Field Length [ft]	3500
Payload [lb]	3000 (armaments)
Fuselage Length [ft]	41.75
TSFC [lb/lb]	0.8
T/W IPPS	5.24
Cruise Altitude [ft]	18,000
Cruise Speed [KTAS]	345

Another major constraint is the need for the aircraft to be able to take off from austere fields. The nature of the aircraft being designed is to provide fast, effective air support to ground based allies. For this to be possible, it must be capable of taking off from airfields that may not have optimal terrain. This affects things such as inlet placement and landing gear height which in turn affect the maximum payload and fuel space available both on the wings and within the body of the aircraft.

Certain requirements were allocated for the initial sizing of the aircraft and others were derived from the initial sizing analysis. A TSFC of 0.78 was input into the sizing analysis from a similarity analysis of similar aircraft. It is also noted that keeping the TSFC below this value will only increase the efficiency of the aircraft which was a goal moving forward. Two other input values were the $C_{L_{max}}$ of 2.1 at landing, and 2.4 at takeoff and these values were also obtained from the similarity analysis and would be designed around moving forward from the sizing analysis. From these initial parameters input into the sizing analysis there were several values that were obtained from initial sizing. Wing areas and aspect ratios were iterated over various ranges in an effort to minimize the weight of the aircraft. As a result of this analysis, without compromising too much for the thrust required of the aircraft, it is seen that a wing area of 230 ft^2 and aspect ratio of 6 would minimize the fuel weight of the aircraft. Additional initial sizing results include but are not limited to, a max ramp weight of 17,000 pounds with a fuel weight of 4430 pounds, thrust required of just under 4,000 pounds, and an L/D of 11.7. These values were utilized as starting points for the detailed aircraft design outlined throughout the remainder of the paper. The constraints mentioned above provided a constraint diagram shown in Fig. 3, maximum velocity as Mach 0.8.

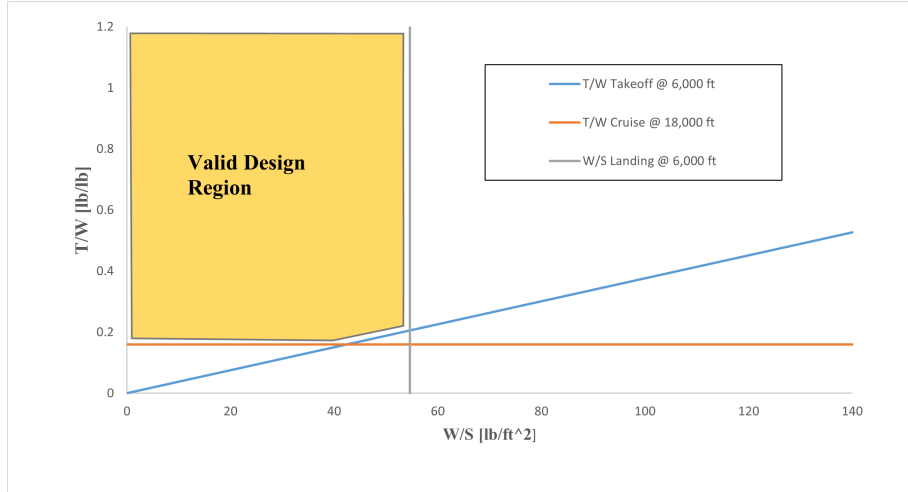


Fig. 3 Constraint Diagram

IV. Configuration

Several configurations were considered when initially designing the aircraft. The first decision was the position and the number of engines that would be on the aircraft. Based on the requirements for the RFP [1], a single engine configuration was chosen to keep the aircraft's weight low. Electric motors were ruled out as inclusion of an electric engine is not feasible by the stated introduction of the aircraft. Turbojets and turboprops were considered, but were eventually set aside in favor of a turbofan, as efficiency or speed singularly are not the primary concerns for the aircraft, and a turbofan is a good mix of both efficiency and speed, enabling the Orca to fly at relatively high subsonic speeds if required.

A. Design Morphology

1. Engine Placement

With a single turbofan configuration, the engine placement was the next configuration to be decided upon. The positions considered are shown below

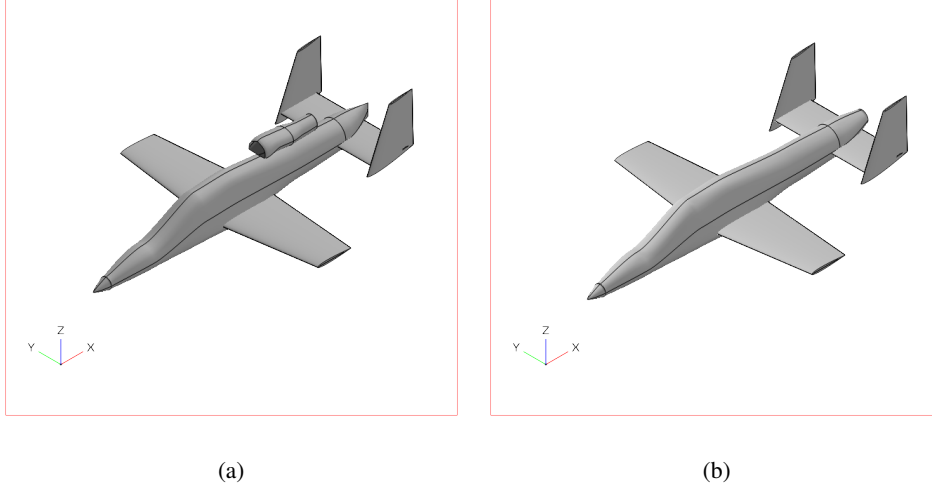


Fig. 4 Engine Positions

Figure 4a shows the engine placed at the top of the aircraft, similar to Cirrus Vision SF50, while the Fig. 4b displays the engine placed at the rear of the aircraft. The engine placement on the top also tied in with the tail configuration, as a conventional tail or T-Tail would not work, and hence a Twin Tail was considered, as seen on the Fairchild Republic A-10 Thunderbolt. Though the engine on top had certain benefits, such as hiding the heat signature of the plume using the twin tail, it was discarded in favor of the engine being placed at the rear, as engine mounted on the top of the aircraft would lead to challenges such as instability during maneuvering due to CG being higher than normal, and it was determined that the heat signature for the aircraft with engine placed at the rear could be reduced by adding a cooling system.

2. Tail Configuration

The tail configuration was chosen as a conventional tail. The H-Tail was discarded due to having a higher weight, cost, and structural complexity. A T-Tail was considered, but was dropped due to the possibility of the aircraft entering a deep stall condition at high angles of attack.

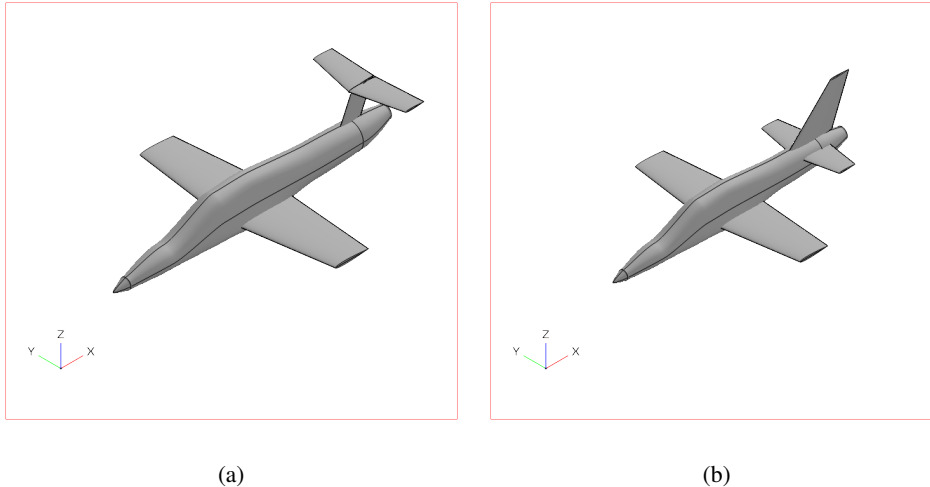


Fig. 5 Tail Configurations

3. Inlet Placement

For the rear engine configuration, the inlet placements of side inlets, as seen on L-159 ALCA, and a top bottom inlet, were considered. Between the two, the top mounted inlet configuration was picked for the design aircraft. This was done for a few reasons. Inlets pose a risk of detection, as radar waves can be deflected in many directions from inside the inlet. Having a top mounted inlet reduces this risk. Another reason was the weight, and thus the cost. Having 2 S-ducts instead of 1 would increase the weight of the aircraft. A bottom mounted inlet was also considered, but was dropped in the favor of the other two as the aircraft is to be designed to operate from Austere Fields, and a bottom mounted inlet runs the risk of having FOD ingested into the engine through the inlet. Analysis for effect of the pressure recovery in the inlet decrease of thrust due to bleed air was also considered, and is shown in a later section. Shown below are the configurations considered.

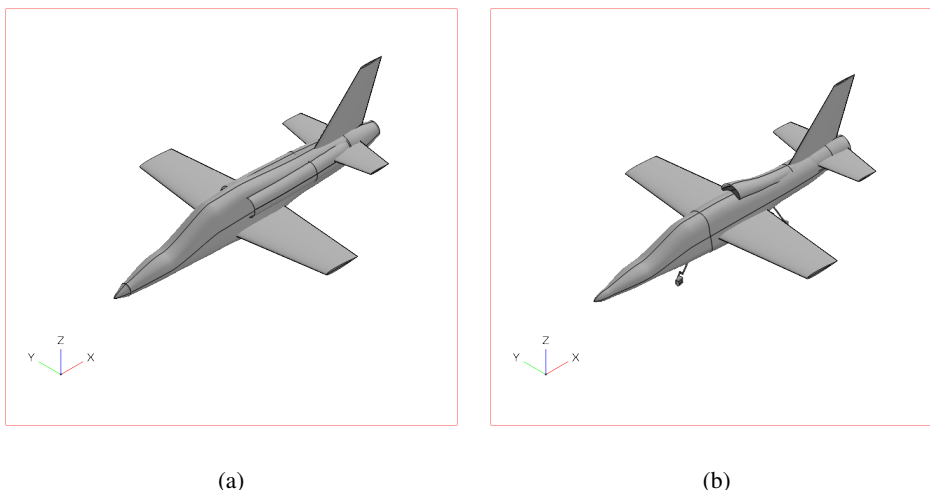


Fig. 6 Inlet Positions

B. Interior Design & Ejection Mechanism

A primary consideration for the interior design is two zero-zero ejection seats, as they are required by the proposal. Aces 5 ejection seat from Collins Aerospace is chosen [8]. The ejection angle is given to be 96.5° from Collins Aerospace, which is a driving parameter for the interior design. As shown in Fig. 7, total 7 frame sections are allocated for the cabin, and the ejection seats are placed where the inlet and cockpit do not interrupt the seats during the ejection process. The canopy opens to the right to prevent any unexpected situation due to inlet airflow above the canopy. The cabin uses the entire width of the fuselage where the side frames and longerons are exposed inside the cabin. Fig. 8(a) shows that both sides of the cabin are protected by the armors, which is discussed in the later section.

The cabin is completely sealed to prevent any air leak since the cabin is fully pressurized through Environmental Control System (ECS). Oxygen masks are integrated with the ejection seats to provide additional equipment in case of malfunctioning ECS. Also, the air from ECS defogs and deices the canopy to give better visibility to pilots. As shown in Fig. 7(b), a front pilot takes advantage of having wider front visibility, 11.2° , where the pilot has primary control of the integrated gun, maneuvering, and taxiing. A rear pilot has a 2.1° front view, but has a broader side view, as the pilot has primary control of navigation, communications, and ordnance.

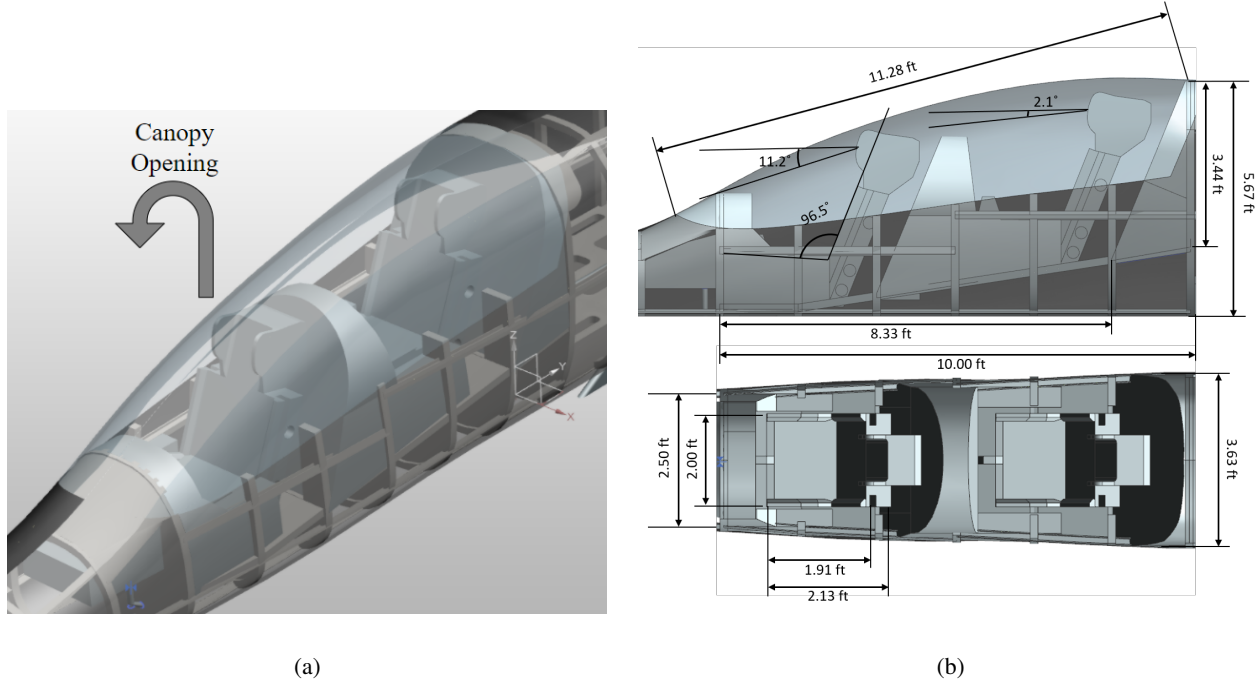


Fig. 7 (a) Isometric View of the Cabin and Canopy Opening Mechanism (b) Cabin and Seat Dimension

During the ejection process, the engine will be shut off first. Then, the inlet surface at the back will be ejected outside, and the front inlet will be blocked, as shown in Fig. 8(b). This mechanism prevents disruption from the front inlet airflow during the seat ejection since the engine would not be completely shut down during the ejection process. Second, the canopy will be exploded. Finally, the pilots will be ejected one by one from the back.

In addition to the ejection system, a ladder and recessed drop-down step are integrated in the fuselage to help pilots and technicians access the cabin more conveniently, especially in the austere field, as illustrated in Fig. 8(a). The ladder and its door are mechanically locked during the operation to ensure safety. Also, in case of any emergency on the ground, they are used to escape the cabin. Warning and emergency signs are marked on the fuselage skin to ensure safety of the flight and ground crews. If any external doors are opened during or before flight, the warning light in the cockpit will be turned on.

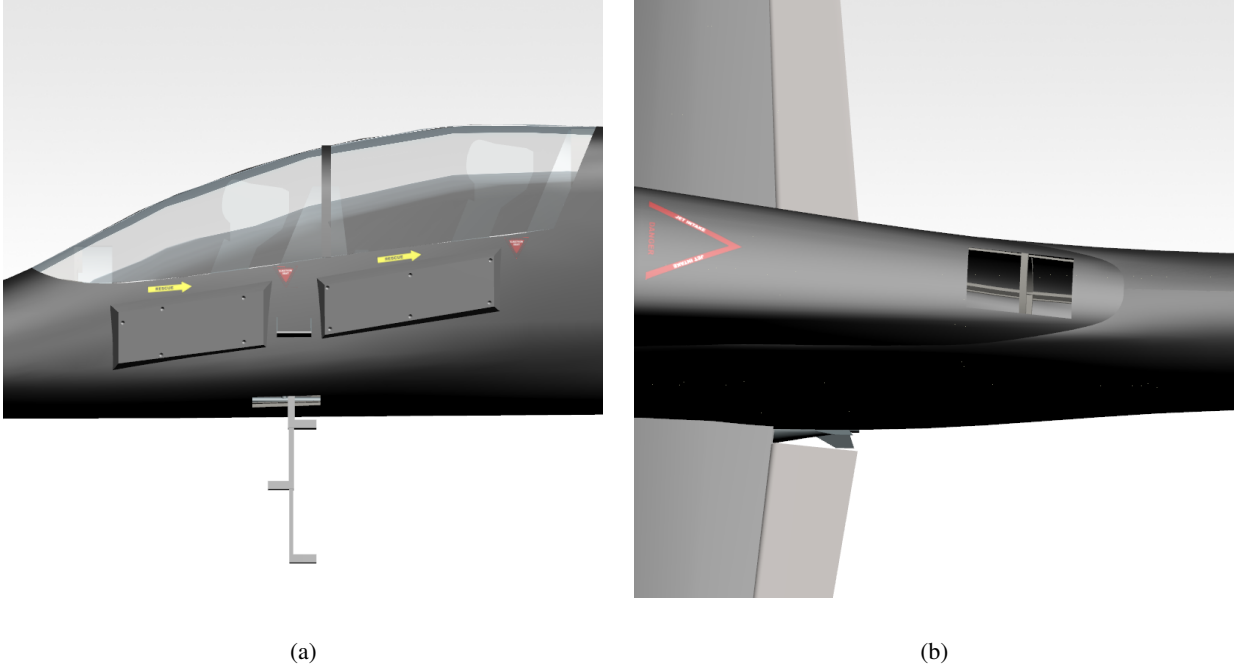


Fig. 8 (a) Warning Signs, Armor and Ladder Design (b) Warning Sign and Inlet Ejection Design

C. Landing Gear

For the design of a landing gear system two primary configurations were considered: taildragger and tricycle style. Analyzing the configuration of landing gear the four considerations that were considered were aerodynamics, loads, storage, and stability. This light attack aircraft will be utilized on austere fields and having landing gear that is able to withstand loads from rough conditions in addition to minimizing the impact of these loads on the body of the aircraft is a necessity. Additionally, the landing gear configuration plays an important role in keeping all exterior payload and aircraft components sufficiently distanced from the effects of FOD. With respect to sufficiently keep debris away from the aircraft the tricycle gear is superior due to the aircraft being in a level configuration. With regards to stability the tricycle style landing gear is also superior. Although taildragger landing gear provides increased lift during takeoff, the layout is inherently unstable during taxiing and could become catastrophic during taxiing along an austere field [4]. Additionally the taildragger style landing gear points the plume from the jet exhaust at the ground which can cause instability in control with the tail while on the ground [9]. As a result, the aircraft will utilize a tricycle style

configuration of landing gear due to its ability to keep all exterior payload and aircraft components sufficiently distanced from FOD as well allowing for stability while maneuvering on the ground. Additionally, it was determined that the landing gear will be retracted during flight to decrease the drag on the aircraft overall. The main landing gear will be mounted on the wings aft of the CG and the nose gear will be mounted on the center of the fuselage forward of the flight deck.

The height and location of the tricycle style landing gear was driven by the avoidance of FOD while on the ground and satisfying of dynamic stability requirements as well as avoidance of tip back [4]. These details along with other landing gear sizing are detailed below in section IX. A general configuration of the landing gear with a ground line can be seen below in Fig. 9.

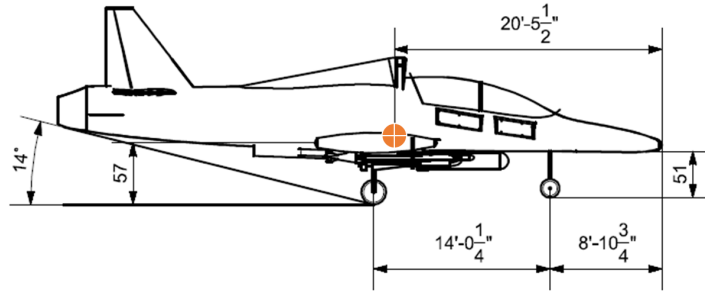


Fig. 9 Landing Gear Configuration

THIS DRAWING HAS BEEN PRODUCED USING AN EXAMPLE
TEMPLATE PROVIDED BY SIEMENS PLM SOFTWARE

A

H

C

G

F

E

D

C

B

A

H

G

F

E

D

C

B

A

H

G

F

E

D

C

B

A

H

G

F

E

D

C

B

A

H

G

F

E

D

C

B

A

H

G

F

E

D

C

B

A

H

G

F

E

D

C

B

A

H

G

F

E

D

C

B

A

H

G

F

E

D

C

B

A

H

G

F

E

D

C

B

A

H

G

F

E

D

C

B

A

H

G

F

E

D

C

B

A

H

G

F

E

D

C

B

A

H

G

F

E

D

C

B

A

H

G

F

E

D

C

B

A

H

G

F

E

D

C

B

A

H

G

F

E

D

C

B

A

H

G

F

E

D

C

B

A

H

G

F

E

D

C

B

A

H

G

F

E

D

C

B

A

H

G

F

E

D

C

B

A

H

G

F

E

D

C

B

A

H

G

F

E

D

C

B

A

H

G

F

E

D

C

B

A

H

G

F

E

D

C

B

A

H

G

F

E

D

C

B

A

H

G

F

E

D

C

B

A

H

G

F

E

D

C

B

A

H

G

F

E

D

C

B

A

H

G

F

E

D

C

B

A

H

G

F

E

D

C

B

A

H

G

F

E

D

C

B

A

H

G

F

E

D

C

B

A

H

G

F

E

D

C

B

A

H

G

F

E

D

C

B

A

H

G

F

E

D

C

B

A

H

G

F

E

D

C

B

A

H

G

F

E

D

C

B

A

H

G

F

E

D

C

B

A

H

G

F

E

D

C

B

V. Propulsion

A. Propulsion System

The thrust required for the proposed aircraft was determined to be 6,200 pounds at sea level. This thrust requirement was determined from thrust required calculations at different altitudes during the design mission. From all these thrust required calculations at different altitudes, it was found that an engine above 6,200 pounds of thrust would satisfy the takeoff requirements with an engine weight of 1,050 pounds. The engine type selection of the proposed aircraft is a low bypass turbofan. A low bypass turbofan can provide more thrust than turboprop and reciprocating engines, while having less weight and a smaller diameter than a high bypass turbofan. Some drawbacks of a low bypass turbofan is that a high bypass turbofan can produce more dry thrust, but since this is a light attack aircraft a very large dry thrust is not necessary. High bypass turbofans will also have a lower TSFC, but the increase in weight and size makes a low bypass turbofan a better choice for the proposed aircraft. Table 7 shows a good high bypass turbofan (PW306B) and the table shows its diameter, which is much larger than the other engines and would not fit in the rear of the plane [10]. While turboprops will pass the requirements set in the RFP, low bypass turbofans allow the aircraft to travel much faster, which gives the Orca a distinct advantage over helicopters for similar missions. The higher thrust from low bypass turbofans allows the aircraft to carry more weight, which increases the survivability by increasing the amount of armor. Lastly, a low bypass turbofan allows the Orca to climb much faster than a turboprop could, which is important for meeting the takeoff requirement.

Table 7 Powerplant Options

Model	Dry Thrust [lb]	Dry TSFC [1/hr]	Bypass Ratio	Diameter [in]	Dry Weight [lb]
M88-2	11,240	0.78	0.3	27.4	1,977.6
EJ200	13,500	0.77	0.4	29	2,200
AI-222-25F	5,512	0.66	1.18	24.6	1,235
F124-GA-100	6,280	0.78	0.49	36	1,050
PW306B	6,050	0.685	4.5	44.8	1,151

B. Engine Selection and Performance

Table 7 shows the powerplants considered for the Orca. From these options, the F124 [11] was selected as the engine for the Orca. Looking at the top four engines in Table 7, the F124 has the lowest weight of all the engines. This factor was very important for the selection process since cost is tied to the weight and one of the main selling points of light attack aircraft is that they are much cheaper than their counter parts. For example, the EMB 314 Super Tucano is less than 1/20th the cost of the F-16 and less than 1/60th the cost of the F-22 [12]. The EJ200 [13] and M88-2 [14] are

too heavy to be considered for the Orca since they would make the Orca too expensive. The TSFC of the AI-222-25F [15] is the lowest which makes this engine desirable, while the TSFC of the other low bypass engines are about the same. However, the thrust of the AI-222-25F does not pass the thrust requirement, while the M88-2 and the EJ200 have the opposite problem where they provide unnecessary amount of thrust. The thrust of the F124 passes the thrust requirement, while not being excessive. The diameter of the F124 is larger than desired, but it is still small enough to fit in the fuselage. The other low bypass turbofans have better sized diameters. Taking all these engine performance parameters into consideration, the F124 has the best combination of parameters mainly due to its low weight and weight being the most important parameter.

Table 8 Additional F124-GA-100 Specifications

Parameters	Value
Airflow [lb/s]	92.6
Pressure Ratio	19.4
Length [in]	102.1
T/W	5.98

Additional specifications of the F124, which were not given in Table 7 are given above in Table 8 [11]. These specifications are given for sea level standard day conditions. As the proposed aircraft flies to higher altitudes, the thrust decreases and TSFC increases. Also the thrust decreases and the TSFC increases as the mach increases.

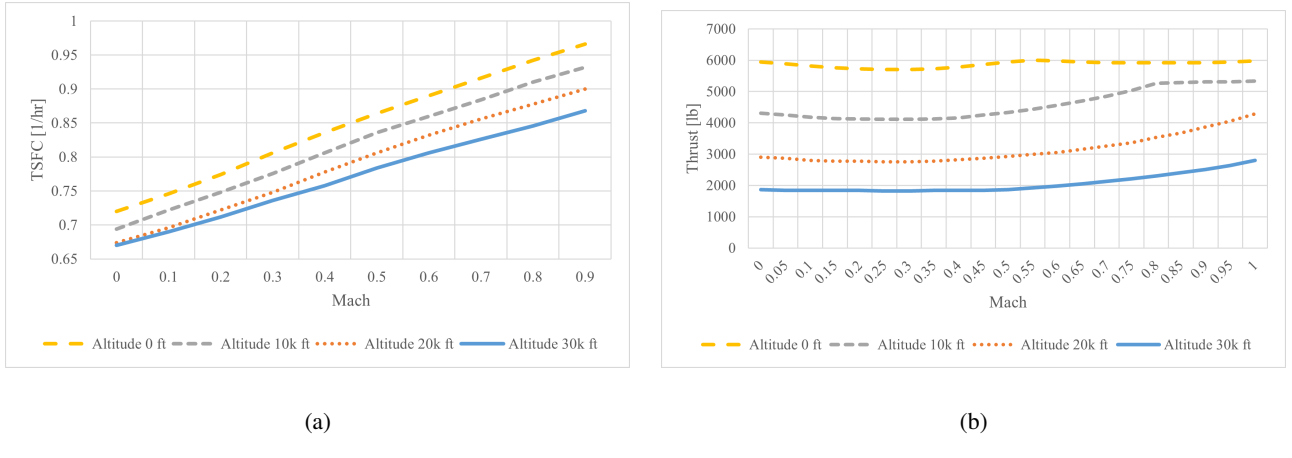


Fig. 10 Graphs of TSFC and Thrust vs Mach vs Altitude

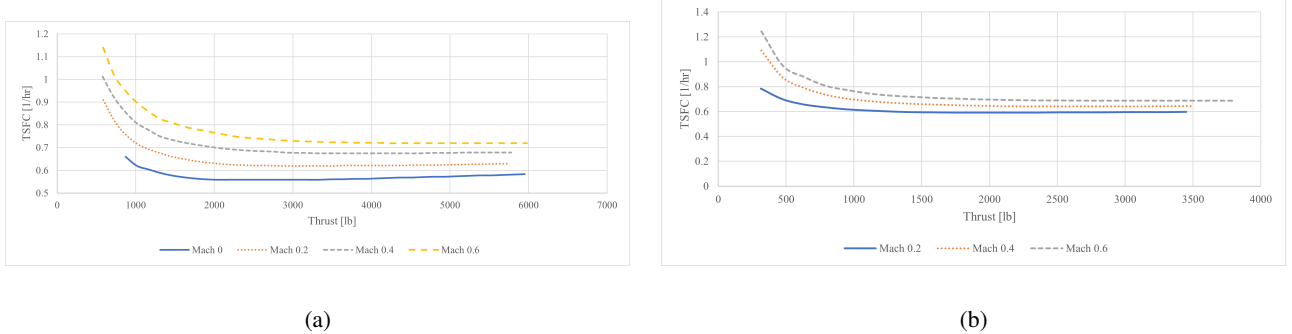


Fig. 11 Graphs of TSFC vs Partial Thrust vs Mach at Sea Level and 15,000 feet

Fig. 10a shows the relationship between TSFC, mach, and altitude, while Fig. 10b show the relationship between thrust, mach, and altitude. Fig. 11a and Fig. 11b show the TSFC at two altitudes and different mach for varying amounts of thrust. These curves were determined by taking experimental engine performance data for low bypass turbofans from the Appendix E of Raymer and scaling it to the F124 [4]. Fig. 10a was additionally modified by including expected improvement in TSFC per year (0.5%). The 0.5% yearly decrease in TSFC is a historical pattern rather than a trend that was calculated. After scaling, the thrust values in Fig. 10b were additionally decreased accounting engine installation. The two factors in the engine installation calculations are the pressure recovery in the inlet and the bleed air. The effect of the pressure recovery in the inlet decreased thrust by 5.4% while the decrease of thrust due to bleed air was 2%. The adjustments to Fig. 11a and Fig. 11b besides scaling the TSFC are the same TSFC yearly adjustment and changing the thrust values by scaling them with the max thrust found at the appropriate mach and altitude from Fig. 10b.

C. Configuration

The chosen propulsion system configuration is one engine integrated in the rear. This configuration was chosen because only one F124 is necessary to meet the thrust requirement and it reduces complexity. Two smaller low bypass turbofans on the rear of the aircraft would lose efficiency from interference due to being placed next to each other. Podded engines can not be placed on the wing due to the requirement to take off and land on an austere airfield. The austere airfield condition means that FOD would get sucked into podded engines potentially causing engine failures. Two engines integrated in the wing would reduce the aerodynamic performance of the wing. One engine on top of the aircraft was an option that was considered, however this configuration was decided against due to the thrust being directed far away from the cg. This causes a downward pitching moment, pushing the nose down and the aircraft would need to counteract this moment, which would increase drag. An engine integrated into the rear of the aircraft avoids this problem due to the thrust being directed through the cg. Some problems with an engine integrated into the rear are maintenance is harder and a more complicated inlet duct is required. These problems were determined to be less important than the increased drag on the aircraft with an engine on top.

D. Safety Consideration

In the event of the engine failing the pilot should activate the brakes to try to stop the plane and attempt another launch. If the speed of the aircraft at the moment of engine failure is above 25% of the takeoff speed the pilots will eject with the zero/zero seats and parachutes will be deployed from the fuselage above the wings. The brakes will still be activated by the CMC Cockpit 4000 avionics suite. If the speed of the aircraft is below 25% of takeoff speed the pilots will not eject and instead will brake. Once the aircraft stops, the aircraft will taxi back to the beginning of the runway to try again. If engine failure occurs while the aircraft is in the air, the pilot should keep the aircraft relatively level and make sure the plane does not stall while the ECU is restarting the engine.

E. Inlet and Exhaust

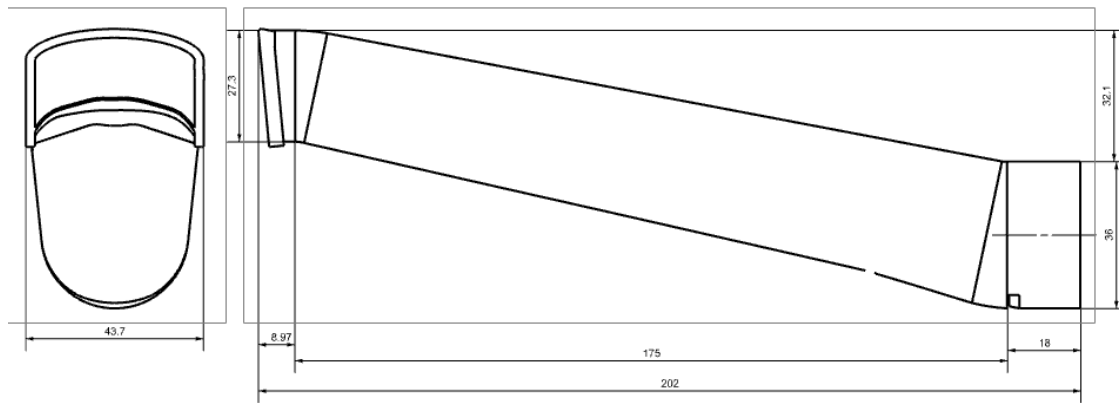


Fig. 12 CAD Drawing of the Inlet

The inlet is modeled using CAD in Fig. 12. The inlet chosen for the proposed aircraft is a top inlet that uses an S-duct to get the air from the higher inlet entrance location to the lower engine entrance location. Design of S-ducts has to be done carefully to make sure shocks or flow separation does not occur. To accomplish this the maximum angle with the center line is 14.2, which is less than the maximum angle with the center line without separation forming stated in Nicolai, 15°[16]. The top inlet was chosen to avoid FOD and it will also not suck in any smoke from the gun since the gun is below the fuselage. Additionally, a top inlet has the benefit of reducing the radar cross section. A top inlet was chosen over side inlets since side inlets require a complex double S duct geometry, which can stall the engine due to pressure instability and can have vortex issues if the merge is not designed properly [4]. A bottom inlet would conflict with the austere airfield requirement from the RFP since FOD would be sucked into the inlet. One difficulty with the top inlet is that the fuselage can block airflow into the inlet at high angles of attack. However, this was not deemed to be too problematic since this aircraft will not be flying on missions that require steep climbs nor will it engage in dogfights where agility is very important.

A boundary layer bypass duct was placed in front of the inlet to not let the low energy boundary layer air enter the inlet. Low energy boundary layer air entering the inlet can cause flow separation, so it is critical to not allow it in the

inlet. The boundary layer bypass duct is one inch tall and in addition to removing boundary layer air from the inlet, provides cold air to the pneumatic system. Excess air not needed for the pneumatic system is dumped behind the inlet face. There is an additional boundary layer duct that removes boundary layer air right before the engine. This duct is much smaller and this air is used to cool the engine. The two design drivers of the inlet for the Orca are the inlet capture area and the S duct geometry. The inlet capture area was the first to be chosen. Raymer explains that air entering a turbofan should only be travelling at Mach 0.4 [4]. If the air is moving much faster than Mach 0.4 the compressor will not be as effective. Using equations 10.16 and 10.17 from Raymer, which relate the area of the inlet to the area of the engine and area to choked area in terms of mach respectively, the inlet area was determined to be 760 in^2 . Typically the inlet capture area is 70-80 percent of the engine area and this inlet capture area is 74.7% of the engine area [4]. Additionally, the inlet leans forwards at 5.4° to make the inlet more effective at capturing air at higher angles of attack. This was decided due to the weakness of top inlets described earlier. To create the S duct geometry and keep from becoming too long, the majority of the duct is a straight diagonal duct with the angle along the bottom being 14.2° . At the ends of the diagonal the duct curves smoothly so it is parallel to the center line. Along the S duct the area of the inlet slowly increases to the area of the engine face.

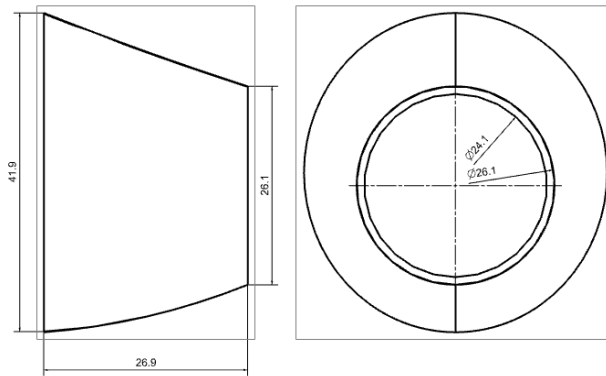


Fig. 13 CAD Drawing of the Nozzle

The nozzle design was much simpler than the inlet since the flow does not need to move up or down. The nozzle is modeled in CAD in Fig. 13. The two main types of nozzles are converging or converging diverging nozzles. Converging diverging nozzles add weight and are designed to increase the performance of supersonic flow, which the proposed aircraft will not have. Therefore a converging nozzle was chosen. Converging nozzles can be fixed or variable. Converging nozzles can be fixed or variable, but the performance improvements from a variable nozzle are outweighed by the increased complexity and weight. Fixed converging nozzles have more drag than most other nozzles besides ejector nozzles, however the increased drag is not a huge problem. Therefore, a fixed converging nozzle was chosen. The trade study completed to decide on the nozzle type is shown in Table 9. From Raymer, the nozzle area should be 50-70 percent of the inlet area [4]. The nozzle area was decided to be 60 percent of the inlet area since the design mach values for fixed converging nozzles are between 0 and 1.4 and the Orca will fly at Mach 0.6.

Table 9 Targeting Pod Trade Study

	Weight	Drag	Complexity	Design Mach Number	Score
Importance	2	3	1	5	
Nozzle Types					
Short Convergent	5	1	5	5	43
Iris	4	5	3	3	41
Convergent Divergent Iris	3	5	3	1	29
Simple Ejector	3	4	2	2	35
Fully Variable Ejector	2	4	1	1	22
Blow in Door Ejector	3	2	1	1	18
Plug	2	3	4	1	22
Isentropic Ramp	1	5	5	1	27

F. Inlet Validation

In order to further validate the implementation of the top inlet design, a 2D simulation was performed using ANSYS Fluent to ensure that the inlet will receive sufficient airflow at high angles of attack. From the simulation we were able to validate that the inlet will receive flow comparable to cruise conditions up to 13° relative to the incoming flow. The resulting simulation can be seen below in Fig. 14. As a result of this simulation we were able to conclude that the top inlet receiving sufficient flow is not a point of concern for angles of attack less than 13° .

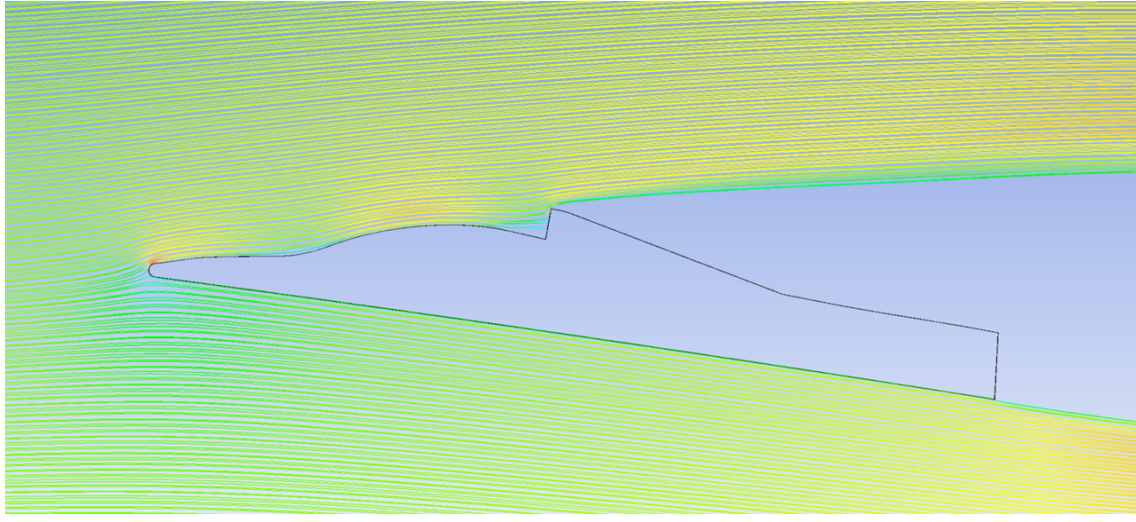


Fig. 14 2D Inlet ANSYS Simulation

G. Future Work

The future work for propulsion is limited to calculating the takeoff speed that the pilots should eject at for an engine failure that occurs at takeoff.

VI. Aerodynamics

A. Airfoil Selection

To choose an airfoil a trade study was performed on several different airfoils. The characteristic that was most valued was the C_l/C_d of the airfoil. Due to the austere field requirement from the RFP it was determined that having a high C_l/C_d would be of benefit to the performance of the aircraft [1]. A secondary characteristic that was considered was the C_m of the airfoil. This value was to be minimized if possible to improve stability during maneuvering and decreasing the overall tail size. The primary tool utilized to analyze these characteristics of airfoils was the vortex lattice method software *XFLR5* in conjunction with experimental data [17].

Airfoil choices for the trade study began with a compilation of airfoils from other light attack aircraft as well as aircraft that perform well on austere fields. From this compilation the four airfoils being considered were the NACA 63-412, NACA 63-415, NACA 64-012, and the USA 35b. Each airfoil was plotted for C_l vs α , C_l/C_d vs α , C_l vs C_d , and C_m vs α which can all be seen in Fig. 15 below. The three NACA airfoils were cross referenced to airfoil data from Abbott and Von Doenhoff and each demonstrated similar data for the same characteristics which validates the vortex lattice software for future uses [17]. Specifically, the graphs below were made from simulation at $Re = 6,000,000$ which matches the corresponding airfoil data for α smaller than 14 and bigger than -12 from the experimental data [17].

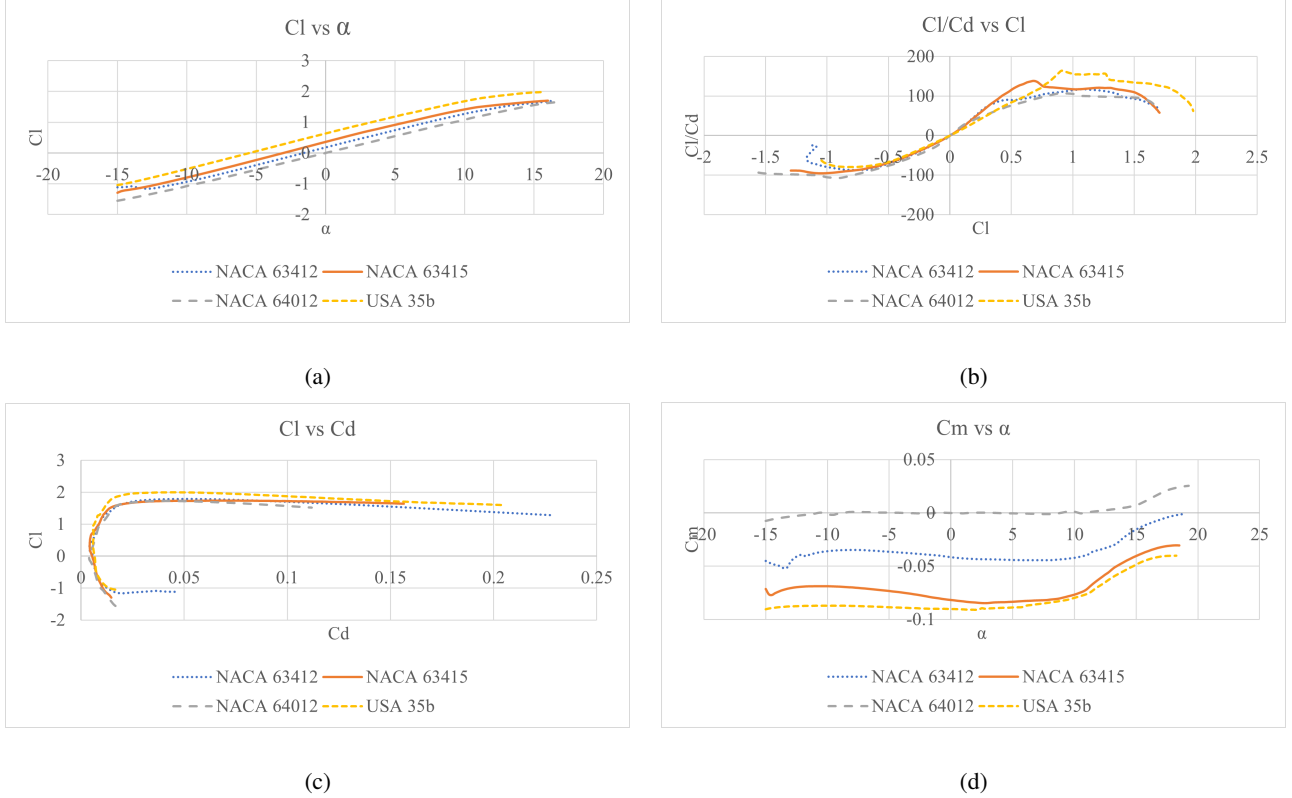


Fig. 15 Airfoil Characteristics at Mach=0.0 from XLFM

Based upon the airfoil polars in figure 15 above it is clear that the NACA 64-012 and NACA 63-412 airfoil do not meet the requirement of maximizing C_l/C_d so they are ruled out. With the NACA 63-415 and USA 35b airfoils left its apparent they both have comparable C_l/C_d so moving to the secondary requirement of minimizing C_m we can also rule out the USA 35b airfoil because it has a larger pitching moment. Overall, the final airfoil that will be utilized is the NACA 63-415 because of its high C_l/C_d characteristics. The airfoil can be seen plotted below in figure 16.

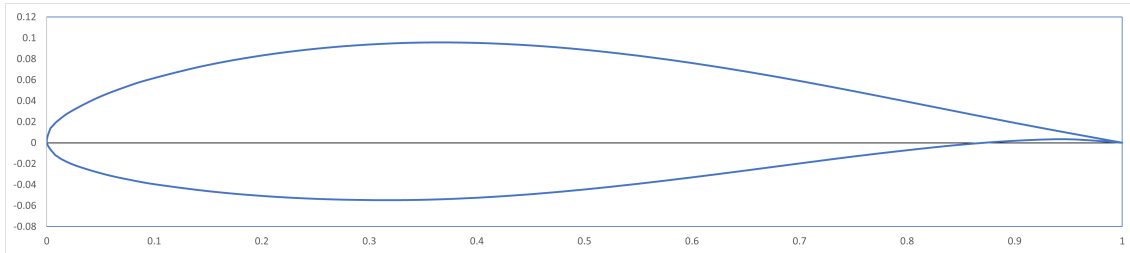


Fig. 16 NACA 63-415 Airfoil

B. Wing Design

1. Area and Aspect Ratio

From the initial sizing analysis that is outlined in section III above, iterations were performed over various wing areas and aspect ratios. Within this analysis the primary driving factor was to minimize fuel weight however, at the minimum fuel weight the thrust required was larger than desired for the power plants being analyzed. As a result, a slight adjustment was made to compromise between both factors. The resulting wing area is 230 ft^2 and the aspect ratio is 6 which leads to a wing span of 37.2 feet. These details along with the other wing parameters can be found in Table 10 below.

2. Sweep and Taper Ratio

Within Raymer it is noted that excessive wing sweep can be detrimental to an aircraft, causing it to pitch up at high α [4]. Due to the light attack aircraft having the potential to be in many different maneuvers, pitch-up will want to be avoided which can be achieved by utilizing Fig. 4.21 in Raymer [4]. In this graph it is noted that the quarter chord sweep should be as little as possible, specifically less than 10 degrees of sweep. On the contrary a slight leading edge sweep is beneficial to limit radar detection [4]. As a result, to provide increased stability, as well as minimizing detectability, it is determined that the quarter chord sweep is to be 3° . Further, through a similarity analysis of additional light attack aircraft it is seen that many of them also utilize minimal sweep.

In order to decrease the cost to operate the aircraft, decreasing the induced drag on the aircraft during cruise was analyzed with respect to λ . As shown in Prandtl's wing theory it is noted that the least induced drag occurs when there is an elliptical lift distribution for an unswept wing [4]. In an effort to decrease induced drag, a taper ratio of 0.5 is chosen for the aircraft to create as close to an elliptical lift distribution as possible during cruise conditions [4].

3. Twist and Dihedral

With regards to twist, stability during flight and maneuvering were the primary considerations. As a result, a negative twist will be utilized due to it being beneficial to creating washout which prevents tip stall to retain the effectiveness of the ailerons [4]. There will be a 2 degree negative linear twist over the length of the wing to create washout.

Similar to the other parameters listed, dihedral was analysed with respect to stability. In order to allow for stability while banking, a 2° dihedral will be implemented. This value was derived from table 4.2 in Raymer which outlines the general guidelines for dihedral [4]. Further, it is seen that similar aircraft also utilize a slight positive dihedral.

4. Angle of Incidence

The driving factor with choosing the angle of incidence was the desire to fly in steady level flight during cruise. It is calculated that at a cruise altitude of 18,000 feet and Mach 0.6, C_L needs to be 0.27. From a 3D analysis in XFLR5 of the wing that is described above, it is determined that the angle of incidence must be 1.0° to provide the desired lift

characteristic during cruise. All of the wing parameters can be seen within table 10 below. Additionally, figure 17 below shows all the major dimensions of the wing.

Table 10 Summary of Wing Parameters

Parameter	Value
Wing Area	230 ft ²
AR	6
Span	37.2 ft
λ	0.5
$\Lambda_{C/4}$	3°
Twist	-2°
Γ	2°
Angle of Incidence	1°

C. High Lift Systems

Takeoff and landing performance are an essential part of the requirements defined in the RFP [1]. As a result, the sizing of the high lift systems was driven by the requirements of C_{Lmax} at takeoff and landing. Within the initial sizing of the aircraft, outlined in section III, it was input that a C_{Lmax} of 2.1 and 2.4 were needed at takeoff and landing respectively in order to satisfy the requirements of field length.

To effectively determine the most effective high lift device, a trade study was performed analysing plain, slotted, Fowler, and double slotted flaps. Within the trade study it was assumed the length of flap extension would remain constant if applicable. Further it was assumed that the flap would be of uniform width which lead to $\Lambda_{H,L}$ of 4°. For the trade study the primary goal would be to analyze the flapped area of the different devices and their impact it would have assuming a constant ΔC_L of 0.97 in order to reach the desired C_{Lmax} value of 2.4 needed during landing. Utilizing the equations of flap sizing in Raymer, the necessary $\frac{S_{flapped}}{S_{Ref}}$ was determined [4]. Table 11 below has a summary of the data obtained from the trade study.

Table 11 Analysis of Different High Lift Devices

Device	$\Delta C_{l_{max}}$	$\frac{c'}{c}$	$\frac{S_{flapped}}{S_{ref}}$
Plain or Split flap	0.9	N/A	1.21
Slotted Flap	1.3	N/A	0.84
Fowler Flap	$1.3 \frac{c'}{c}$	1.2	0.70
Double Slotted	$1.6 \frac{c'}{c}$	1.2	0.57

From the trade study data on high lift systems, seen in table 11 above, it becomes apparent that a plain or split flap will not be able to be utilized because the required flapped area is not possible. Additionally, the slotted flap was also ruled out because the necessary area spans nearly 70 percent of the wing which leaves minimal space for the ailerons needed for a maneuverable light attack aircraft. Finally, the double slotted flap was ruled out due to added complexity and weight of such a design. The resulting high lift system determined was the Fowler flap with an extension ratio of 1.2. A full compilation of the Fowler flap specs can be seen below in table 12.

With the lift device determined the corresponding flap angles to achieve the desired lift characteristics at takeoff and landing must be determined. Using the techniques present within Raymer, an estimate of the change in lift coefficient was achieved [4]. From these estimates we note that for take off the desired C_L is achieved with flaps set to 20° and $\alpha = 9^\circ$. Likewise for landing it is noted that with flaps at 30° and $\alpha = 9.25^\circ$ the desired C_L is achieved. Additionally the full wing dimensions can be seen below in figure 17

Table 12 Summary of High Lift System

Parameter	Value
Flap Span	11 ft
Flapped Area	163 ft^2
Flap Extension Ratio	1.2
Hinge Angle	4°

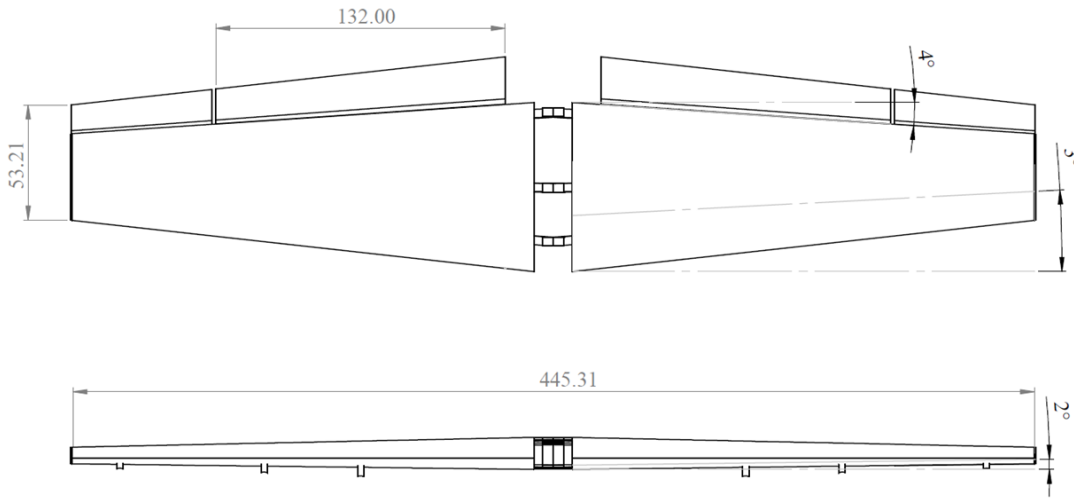


Fig. 17 Overall Wing Dimensions

D. Drag Buildup

Utilization of an effective drag buildup is essential to further analysis of performance of the aircraft. The drag buildup that was performed utilized the component buildup method outlined within Raymer [4]. For the parasitic drag of the aircraft it is noted that the biggest contributions are from the fuselage, wing, and ordnance. All of the components utilized for the parasitic drag buildup can be seen below in table 13. Further, a complete drag buildup of the aircraft during cruise, takeoff and landing can also be seen below in table 14. It is noted here that the engine nacelle is incorporated into the fuselage drag, the takeoff and landing drag are prior to takeoff, and it was assumed leakage and protuberance drag was approximately 5 percent of the total C_{D_0} [4].

Table 13 Cruise Component parasite Drag Buildup

Component	Swet/Sref	CD0
Fuselage	2.39	0.0093
Wing	2.06	0.0079
Vertical Tail	0.30	0.0011
Horizontal Tail	0.42	0.0016
Ordnance	0.77	0.0048
External Tanks	.34	0.0014
Total	6.3	0.026

Table 14 Complete Drag Buildup

Component	Takeoff	Cruise	Landing
C_{D_0}	0.027	0.026	0.027
C_{D_i}	0.013	0.0046	0.029
$C_{D_{trim}}$	0.001	0.001	0.001
$C_{D_{flap}}$	0.011	0	0.021
$C_{D_{L+P}}$	0.0013	0.0013	0.0013
Total	0.053	0.033	0.079

E. Lift Curves and Drag Polars

Complete aircraft lift curves and drag polars can be seen below in Fig. 18. The data for the polars were compiled from *XFLR5* and it is noted that it was simulated with a point drag for components other than the wing and tail. The data from XFLR5 was adjusted slightly at takeoff and landing conditions to account for the Fowler flaps. Additionally, complete aircraft data can be seen in table 15 below for takeoff, cruise, and landing. Each segments mission point is denoted with a black star on the graphs.

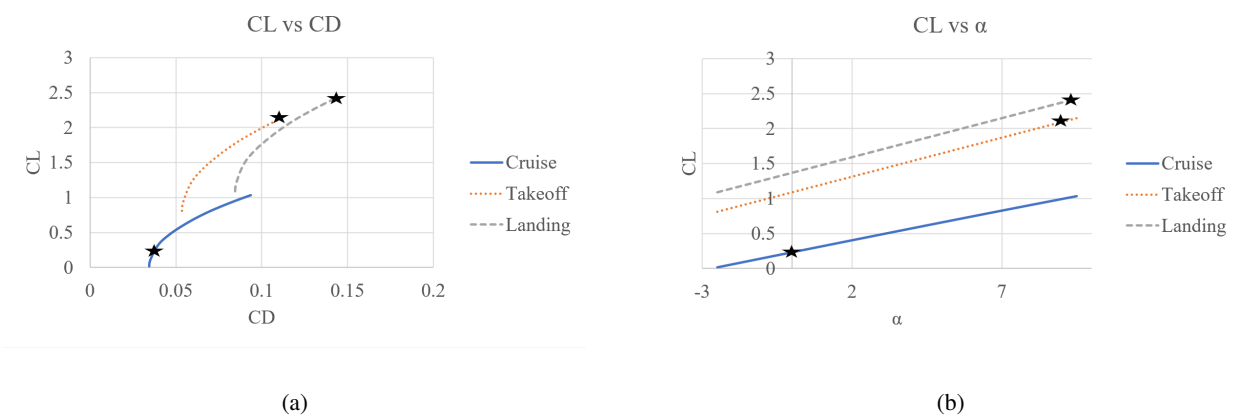


Fig. 18 Aircraft Polars From XLFR5

Table 15 Aircraft Aerodynamic Information

Parameter	Takeoff	Cruise	Landing
C_L	2.1	0.27	2.41
C_D	0.11	0.033	0.14
α	9.0°	0°	9.25°

VII. Performance

A. Required Performance

As mentioned in Table 1, the aircraft is required to takeoff and land over 50 ft obstacle within 4,000 ft from austere fields, with reserves sufficient enough to be able to climb to 3,000 ft and loiter for 45 minutes. The aircraft must also have a range of at least 900 nm with 60% of payload capacity at minimum 18,000 ft to satisfy the requirements for the Ferry Mission, as mentioned in Conops. Additional requirements include being able to complete the first segment of cruise and descent for the design mission within 20 minutes of initial climb.

B. Takeoff and Landing Analysis

To accurately account for conditions mentioned in the RFP [1], all the takeoff and landing performance were simulated at ISA+15°C conditions. The analysis was done under the assumption of the aircraft operating from fields made up of Firm Dirt to simulate the austere fields with California Bearing Ratio of 5, at an altitude of 6,000 ft above sea level. The obstacle distance was assumed to be 50 ft, as mentioned in the RFP [1]. Equations from Raymer [4] were used to calculate the various Take-off and Landing components of Transition, Ground Roll, Rotation, Approach etc. The values were simulated using time step in excel from initial velocity to final velocities. Table 16 shows the various

components for Takeoff, while Table 17 shows the components for Landing for both altitudes of 0 ft and 6,000 ft.

Table 16 Takeoff Parameters at 6,000 ft

Mission	Altitude	Ground Roll	Rotation Distance	Transition Distance	Climb Distance	TOFL
Design	6000 ft	2874 ft	187 ft	812 ft	0 ft	3883 ft
Ferry	6000 ft	2178 ft	171 ft	701 ft	0 ft	3049 ft
Design	0 ft	1950 ft	181 ft	744 ft	0 ft	2875 ft
Ferry	0 ft	1247 ft	167 ft	688 ft	0 ft	2102 ft

Table 17 Landing Parameters at 6,000 ft

Mission	Altitude	Approach Distance	Flare Distance	Free-Roll Distance	Braking Distance	LFL
Design	6000 ft	318 ft	317 ft	367 ft	1903 ft	2905 ft
Ferry	6000 ft	409 ft	252 ft	323 ft	1502 ft	2481 ft
Design	0 ft	311 ft	280 ft	336 ft	1620 ft	2546 ft
Ferry	0 ft	585 ft	191 ft	317 ft	1481 ft	2573 ft

C. Fuel and Velocity

The mission segment fuel requirements were calculated by time stepping implemented in excel by adding up the amount of fuel used within each step. Tables 18 shows the amount of fuel required for the design mission. A total of 5293 lb of fuel is required to successfully complete the design mission. The reserves were calculated such that there is 0 lb of fuel is left after climb to 3,000 ft and cruise for 45 minutes.

Table 18 Fuel Requirement per Mission Segment for Design Mission

Mission Segment	Fuel Requirement [lb]
Warm-up, Taxi	82
Takeoff	41
Climb 1	157
Cruise 1	394
Descent 1	11
Loiter	3510
Climb 2	66
Cruise 2	331
Descent 2	27
Landing	2
Taxi, Shutdown	82
Reserves	590
Total	5293

The mission segment fuel requirements for the ferry mission were calculated as well. Table 19 shows the amount of fuel required for the ferry mission. 3257 lb of fuel is required for the ferry mission to be completed successfully. Given below are the fuel requirements for each segment of the ferry mission.

Table 19 Fuel Requirement per Mission Segment for Ferry Mission

Mission Segment	Fuel Requirement [lb]
Warm-up, Taxi	82
Takeoff	29
Climb	224
Cruise	2291
Descent	48
Landing	2
Taxi, Shutdown	82
Reserves	500
Total	3257

The fuel values were calculated by using the TSFC values, which were estimated by scaling the figures provided in Raymer [4] and plotting a regression line by linearly interpolating for the TSFC values, using Mach number as the input. To calculate the fuel requirements, the velocities needed to be determined as well. Since the weight of the aircraft was a concern, the velocities that minimized the amount of fuel burn were utilized, which reduced the amount of fuel that the aircraft needed to carry. Though for Ferry, velocity that maximized range was utilized, as specified in the RFP [1]. Fig. 20 shows the important velocities used in design mission segments, as the design mission was the more restrictive mission that the aircraft needed to be designed around.

Table 20 Design Segment Velocities

Mission Segment	Velocity [KCAS]
Takeoff	105
Cruise 1	312.5
Loiter	180
Cruise 2	235
Landing	100
Reserve Loiter	165

For the Ferry mission, the Orca cruised at 245 KCAS, with Takeoff being at 98 KCAS and Landing being at 97.5

KCAS. The cruise velocity was chosen as that was the best range velocity given using performance parameters, which will be discussed in a later section.

D. Drag Calculations

The Drag force on the aircraft constitutes of 2 major parts. The parasitic drag which is the intrinsic drag of the aircraft due to its structure, and the induced drag which depends on factors such as velocity, density and flight path angle. Table 21 shows the average drag values calculated at each segment of the design mission. The Takeoff and Landing calculations, as mentioned before, were done at Δ ISA+15 conditions, and the cruise altitude for the design mission was chosen as 10,000 ft.

Table 21 Drag per Mission Segment for Design Mission

Mission Segment	Drag [lb]
Takeoff	2597
Climb 1	1528
Cruise 1	1815
Descent 1	1448
Loiter	1130
Climb 2	1058
Cruise 2	1187
Descent 2	1096
Landing	3321

Table 22 shows the average drag values calculated at each segment of the ferry missions. The Takeoff and Landing calculations were also done at Δ ISA+15 conditions. The cruise altitude for the ferry mission was at 18,000 ft.

Table 22 Drag per Mission Segment for Ferry Mission

Mission Segment	Drag [lb]
Takeoff	2222
Climb	1031
Cruise	1064
Descent	874
Landing	2842

E. Aircraft Performance Coefficients

Since there was no minimum cruising velocity requirement for the design mission listed in the RFP [1], the velocities were chosen to minimize the fuel consumption. These velocities were initially estimated from the performance coefficients 19, and then tuned to account for changes in weight due to fuel burn. The performance coefficients were plotted for Design Mission Take off Weight cruising altitude of 10,000 ft and are provided below.

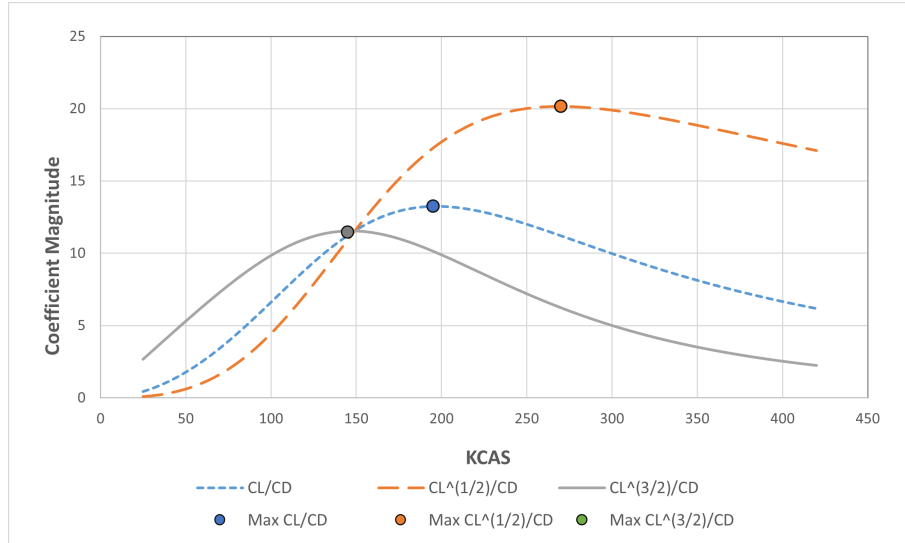


Fig. 19 Design Performance Coefficients

Similarly, the performance coefficients were utilized to estimate maximum range velocity, as required by the RFP [1]. Again, the plots were generated at Ferry Mission Takeoff Weight for a cruising altitude of 18,000 ft, and are shown below.

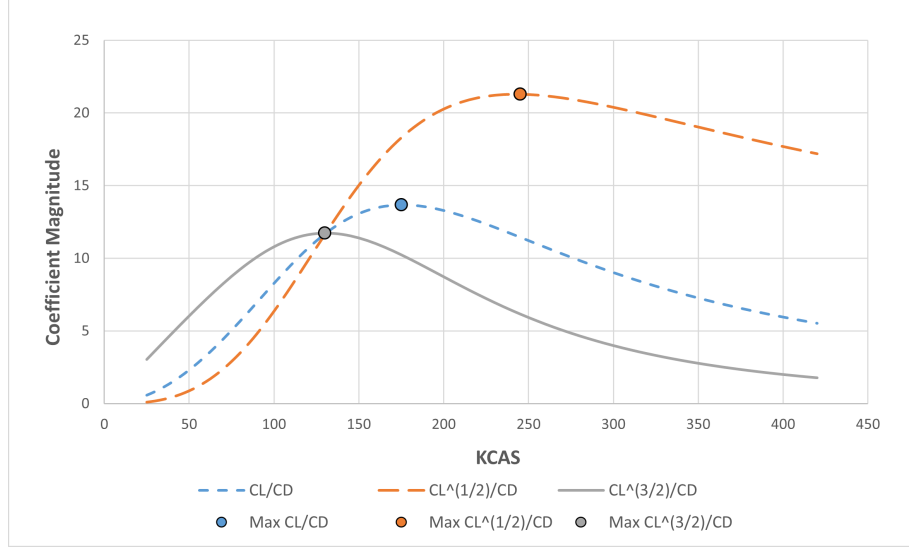


Fig. 20 Ferry Performance Coefficients

The three coefficients each represent the performance of the aircraft in different scenarios. $(\frac{CL}{CD})_{max}$ represents the most efficient velocity for loiter. At this point, the aircraft consumed the least amount of fuel to stay aloft. $(\frac{CL^{1/2}}{CD})_{max}$ represents the best range performance of the aircraft. At this point, the aircraft will be able to achieve the maximum range. Finally, $(\frac{CL^{3/2}}{CD})_{max}$ represents the endurance performance of the aircraft. With this maximized, aircraft consumes minimum amount of power, and can stay airborne the longest. These values can be seen tabulated for the different segments in Table 23 below

Table 23 Performance Coefficients Table

	$(\frac{CL}{CD})_{max}$	$(\frac{CL^{1/2}}{CD})_{max}$	$(\frac{CL^{3/2}}{CD})_{max}$
Design Mission Value	13.24	20.16	11.55
Design Cruise KCAS	195	270	145
Ferry Mission Value	13.29	21.29	11.73
Ferry Mission KCAS	175	245	130

F. Payload Range

The RFP [1] details the amount of payload to be set at 3,000 lb for the design mission. However, it is possible to increase the range of the aircraft by decreasing the payload. A payload-range diagrams visualizes the gains in range by decreasing the payload equipped. As seen in Fig. 21, with the design payload, the maximum range of the aircraft is 1200 nmi when flying at an altitude of 10,000 ft with a velocity of 280 KTAS. If the payload is reduced in favor of maximum fuel capacity, the range increases to 1450 nmi, and without any payload the aircraft is capable of flying till 1696 nmi.

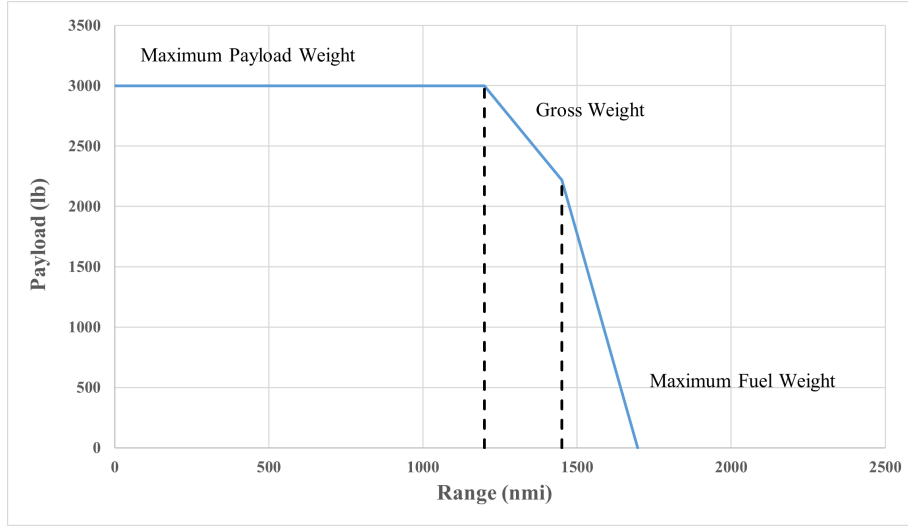


Fig. 21 Payload Range Diagram

G. Payload-Time on Station

Though the RFP [1] requires a payload of 3,000 lb for the design mission, it is possible to increase the endurance of the aircraft if the total amount of payload is reduced in favor of maximum fuel capacity. It can be seen in Fig. 22 that with the design payload, the aircraft is able to stay aloft for roughly 4.3 hours. If the amount of payload is sacrificed in favor of carrying maximum amount of fuel, the endurance increases to 5.2 hours. With no payload carried by the aircraft, the Orca is able to maintain flight for 6.1 hours.

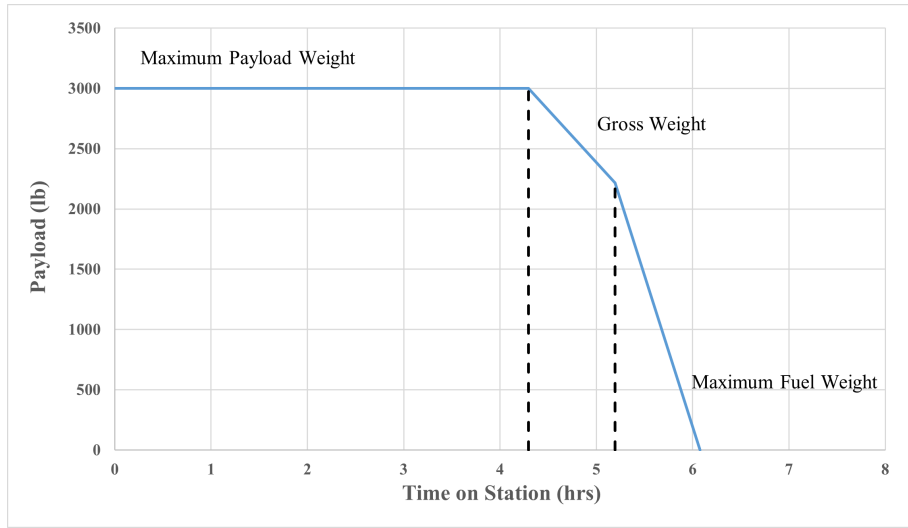


Fig. 22 Payload-Time on Station Diagram

H. Range Mach

The Range of an aircraft depends on the velocity the aircraft is flown at, along with the total weight of the aircraft. Using a Range Mach diagram, the affects of variation in velocity (or Mach) can be seen on the range of the aircraft. It can be seen in Fig. 23 that the best range for the Orca flown at 10,000 ft is when the aircraft is Mach 0.44, with a range of 1157 nmi. It is important to note that this analysis was done using the Maximum Takeoff Weight of the aircraft and the design payload of 3,000 lb. The range was estimated using the Breguet Range equation from Raymer [4].

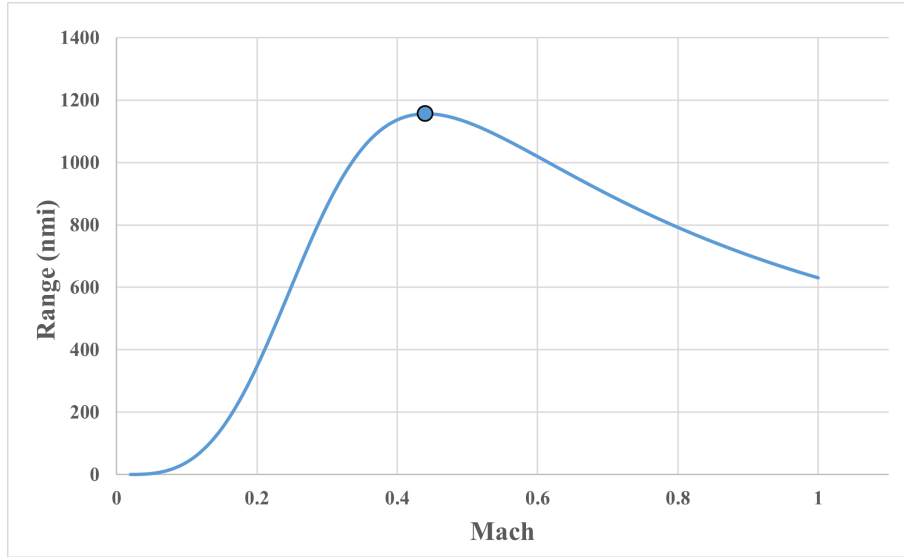


Fig. 23 Range Mach Diagram

I. Performance Ceilings

The RFP [1] requires the aircraft to have a service ceiling of minimum 30,000 ft. The service ceiling is the altitude at which the rate of climb for an aircraft equals 100 ft/s (for military aircrafts). The calculation was done at best rate of climb velocity, which was obtained using Raymer [4]. Given below is the plot for Maximum ROC vs Altitude.

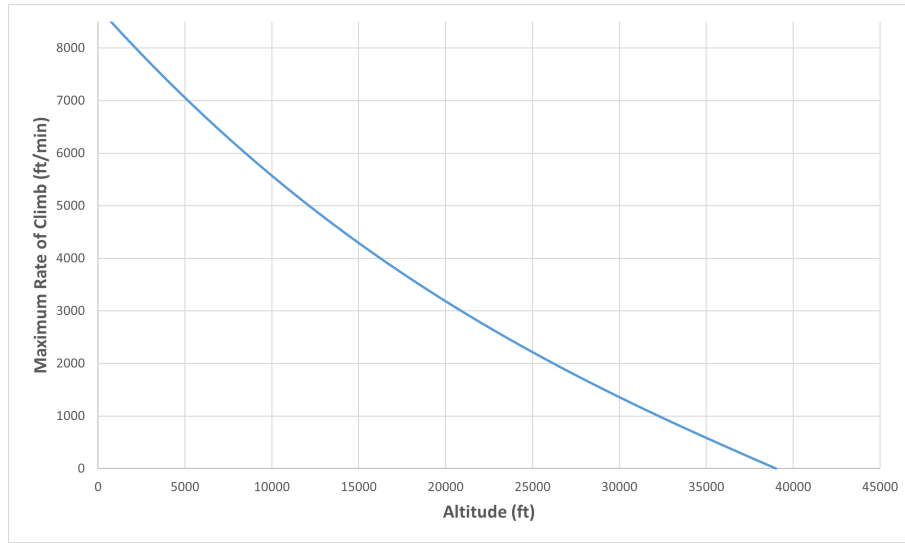


Fig. 24 Max ROC vs. Altitude

The starting weight used for the calculation was the Maximum Takeoff Weight of 17,239 lb, which was calculated earlier for the design mission. Using the mentioned values, the aircraft was able to achieve its service ceiling at 38,000 ft, and its absolute ceiling at 39,000 ft.

J. Flight Envelope

The flight envelope for the ORCA at maximum takeoff weight is shown in Fig. 25. The absolute ceiling of the aircraft was 39,000 ft. Notice that the minimum velocity possible for lower altitudes is defined by the stall velocity of the aircraft and not the calculated minimum velocity possible.

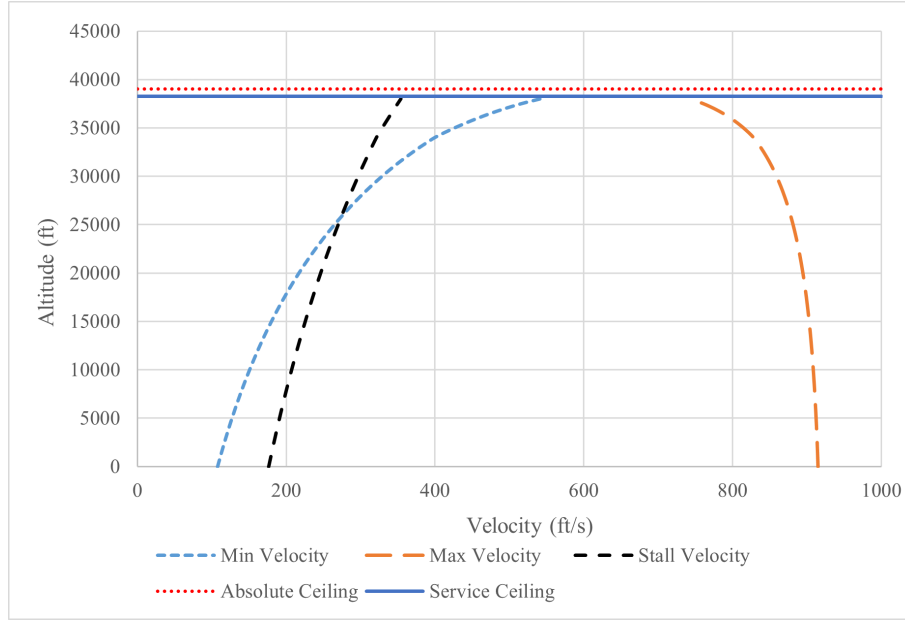


Fig. 25 Flight Envelope @ MTOW

K. Specific Excess Power

To study the climb performance of the aircraft, a specific excess power contour was plotted (Fig. 26. This plot shows the power available to climb at certain speeds and altitudes. For example, for takeoff from 0 ft altitude and at a velocity of 180 ft/s, the diagram suggested specific excess power was roughly 50 ft/s. The red line denotes the stall velocity for the aircraft as specific altitudes.

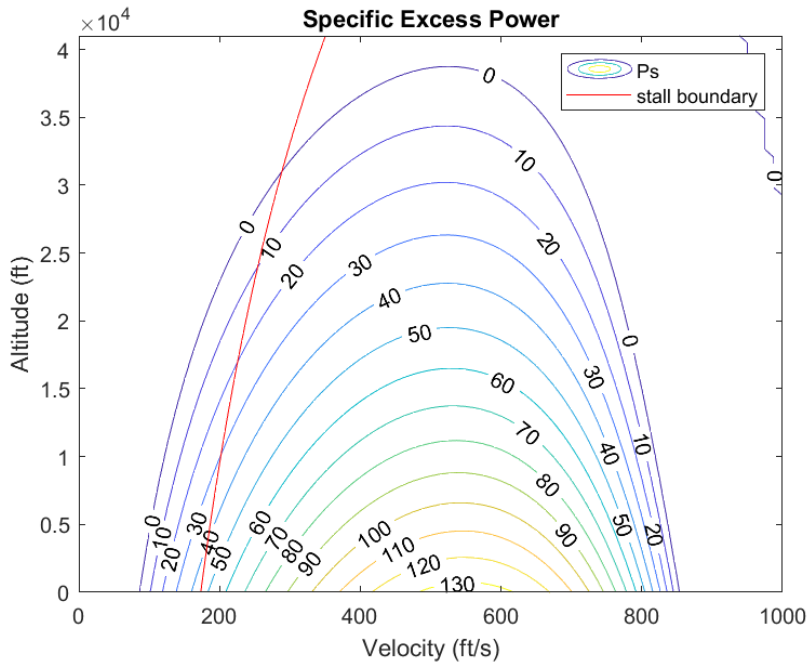


Fig. 26 Specific Excess Power Plot

As it can be seen, the control line for specific excess power of 0 ft/s matches up pretty well with the flight envelope for the aircraft. In fact, it also defines the flight envelope of the aircraft, as at that point there is not excess power available for the aircraft to climb further.

L. Trade Studies

One of the flight parameters to be studied is the best rate of climb velocity. Fig. 27 shows the variation in the rate of climb as the velocity is varied. The analysis was done at 0 ft of altitude. From the plot, it can be concluded that the maximum rate of climb occurs at a very specific velocity, and was needed to be determined to estimate the service and absolute ceiling of the Orca.

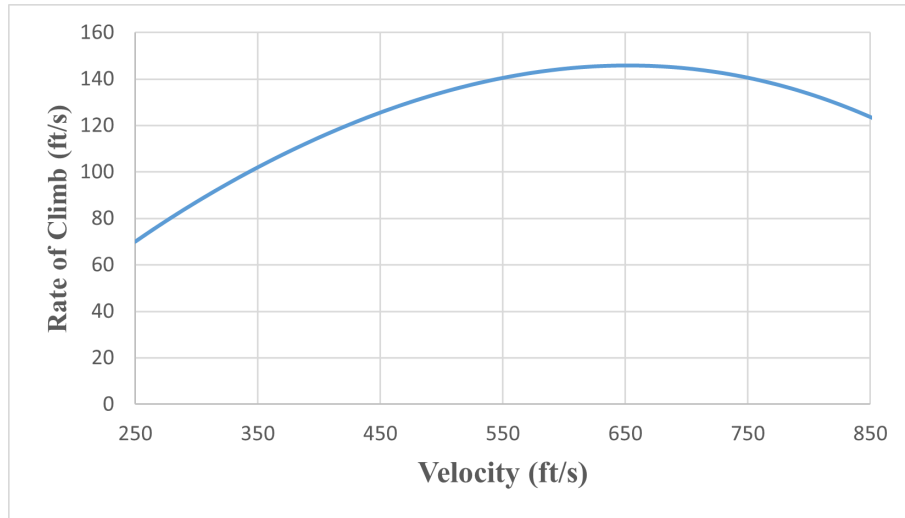


Fig. 27 ROC vs. Velocity

Another important parameter is the velocity at which the minimum fuel consumption occurs. By reducing the amount of fuel consumed, the design weight of the Orca can be decreased, with benefits multiple parameters. Fig. ?? shows the amount of fuel burned as the Mach is varied, with the analysis done at MTOW. It can be seen from the plot that at Mach 0.44, the aircraft burned the least amount of fuel. This plot also helped identify that during the dash section of design mission, minimum possible velocity that enables dash to be completed within 20 minutes should be used to minimize fuel burn, as the dash occurs at a speed higher than the point of minimum fuel consumption.

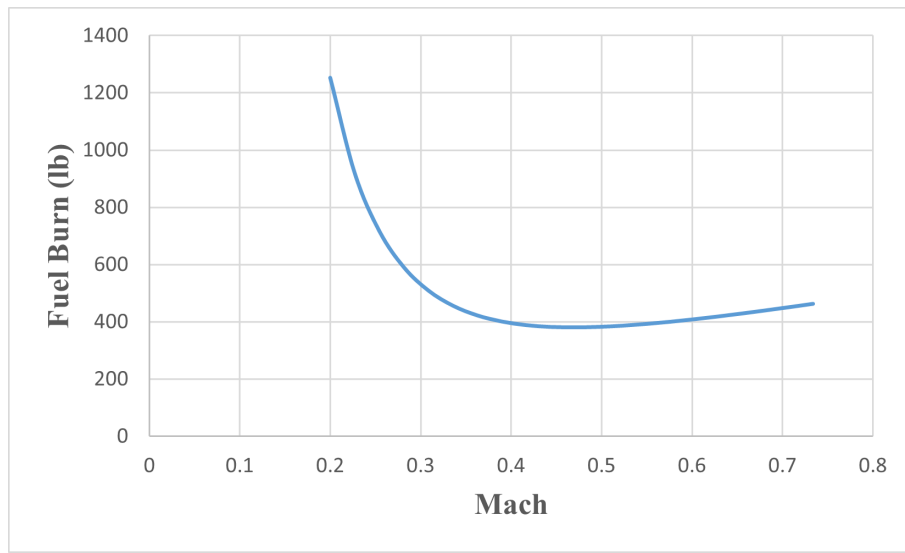


Fig. 28 Fuel Burn vs Mach

M. Comparison to RFP Requirements

Using the parameters for the design of the Orca, the aircraft was able to meet all the requirements listed in the RFP [1], while exceeding the requirements for some, which include the landing field length along with the service ceiling. Plots were provided to show the performance of the aircraft and as validation for the design.

VIII. Stability and Control

A. Empennage Design

1. Horizontal Tail

The design of the horizontal tail is based on values obtained from the scissor plot in fig. 29. Horizontal tail size is a major contributor to pitch stability and counteracts the moment about the CG of the aircraft caused by the main wing during the different flight regimes. Extra area was included above the true optimum size to allow for more pitch control for the sake of keeping the aircraft under the maximum α for sufficient inlet flow. The aspect ratio and taper ratio were chosen based on the trade stud in Raymer[4] Table 4.3, for fighter aircraft. Though the design aircraft is not a fighter, that was the the most similar category to light attack, so to compensate for the difference in aircraft type the highest aspect ratio was chosen at 4 while the average taper was chosen at .3. No incidence or dihedral were applied to the tail in the interest keeping cost low by keeping parts identical for easily maintained. The full parameters of the horizontal tail are displayed in Table [24] and a dimensioned diagram is in fig 30.

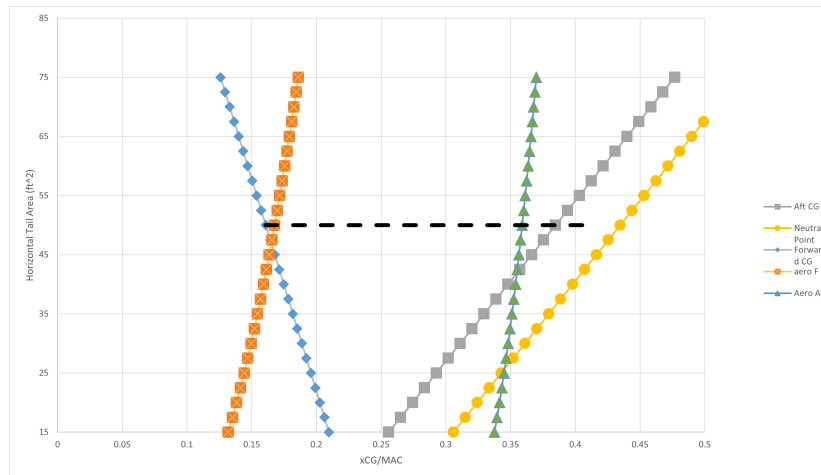


Fig. 29 Scissor Plot for Horizontal Tail Sizing

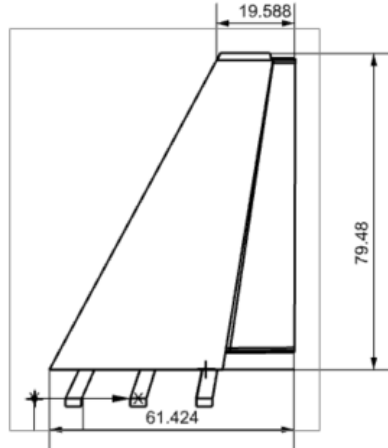


Fig. 30 Horizontal Tail of the aircraft with major dimensions measured

Table 24 Summary of Horizontal Tail Parameters

Parameter	Value
Horizontal Tail Area	50 ft ²
AR	4
Span	14.14 ft
λ	0.3
$\Lambda_{C/4}$	23.8°

2. Vertical Tail

Vertical stabilizer is the main surface responsible for maintaining yaw stability and must be appropriately sized to impart a moment large enough to prevent spin. The vertical tail is designed using historical ratios for area, where the chosen value is one quarter of the main wing area resulting in a vertical tail area of 28.75 sq. ft. The full parameters of the vertical tail are listed in Table [25]. Also, the NACA 0012 thin airfoil was chosen for both the vertical and horizontal tails because of its symmetry, low drag and cost to manufacture when compared to wings made of thinner airfoils which require more support

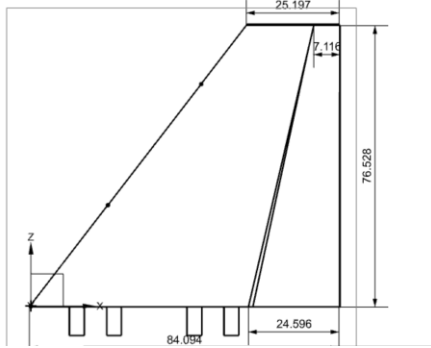


Fig. 31 Vertical Tail of the aircraft with major dimensions measured

Table 25 Summary of Vertical Tail Parameters

Parameter	Value
Vertical Tail Area	28.75 ft ²
AR	1.4
Span	6.34 ft
λ	0.3
$\Lambda_{C/4}$	37.6°

B. Control Surface Design

1. Elevator Design

Elevator sizing was done using a trade study on similar aircraft, which cluster around the chosen value of 30 percent and the surface will cover the entire span. The total area of the surface, then is 15 sqft. The parameters are listed in Table 26

2. Rudder Design

The rudder sizing also is based on a trade study, displayed in Table 35, which produce an average rudder chord ratio of 30 percent as well and the surface at this point covers the full span of the vertical tail, resulting in a rudder area of 8.625 sqft.

Table 26 Summary of Control Surface Parameters

Parameter	Elevator	Rudder
Chord Ratio	.3	.3
Span Ratio	1	1
Area	15 ft^2	8.625 ft^2
δ_{max}	$\pm 20^\circ$	$\pm 25^\circ$

3. Aileron Design

Ailerons for the aircraft were sized using historical values from Roskam[[18]], the parameters are listed in Table 27. For ease of maintenance, the hinge line of the aileron is the co-linear to that of the flaps. The maximum deflection angle was chosen to be 20 degrees in either direction to avoid flow separation. The roll requirement for a trainer aircraft is listed as a 90°bank angle in 1.3 seconds, the effectiveness of the ailerons were tested using methods from McCormick[19] in loiter conditions. The chosen situation for roll performance evaluation was loiter in consideration of responsiveness in combat airspace. In a ground support situation, the aircraft may be in loiter around the airspace and need some maneuverability to respond to changes in the landscape of the battle. The requirement for an attack aircraft is to roll 90°in under 1.3 seconds. Assuming quasi-steady state, the aircraft is able to reach the required roll rate with an aileron deflection much less than the maximum. The results are displayed in Table 28.

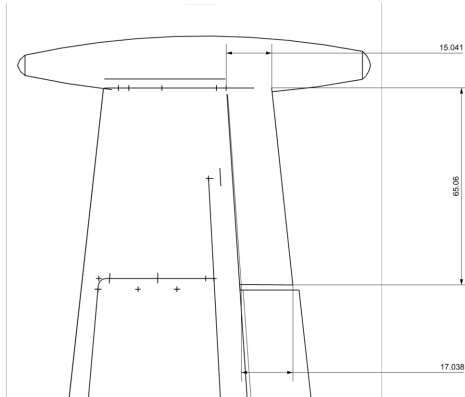


Fig. 32 Drawing of the Aileron with Dimensions

Table 27 Summary of Aileron Parameters

Parameter	Value
Chord Ratio	.2
Aileron Span	5.63 ft
Span Ratio	.65 - .95
Area	15 ft^2
δ_{max}	$\pm 20^\circ$

Table 28 Roll Parameters

Parameter	Value
V_{Loiter}	280 ft/s
C_{lP}	-.435
Roll Rate	69.23 $^\circ/s$
$C_{l\delta A}$	0.00294 $^\circ$
δ_A	11.87 $^\circ$

C. Longitudinal Static Stability

Longitudinal static stability is achieved by designing surfaces such that the change in the moment about the center of gravity of the aircraft always opposes any perturbation in the angle of attack. Static margin a value that gives an idea of the stability characteristics of the aircraft. Using the calculation method from Raymer[4], the approximate neutral point of the aircraft is at 20.96 ft from the nose while the range of the CG movement is from about 11 to 35 percent of the MAC. The static margin is show in Table 29.

Table 29 Static Margin

Parameter	Value
Neutral Point	43.47% MAC
Minimum Static Margin	5% MAC
Maximum Static Margin	27% MAC

D. Trim Analysis

Trim analysis of the aircraft was done using methods described in Raymer [4]. The pitching moment was calculated for each flight regime and the optimal elevator deflection angle was solved for by iterating. These optimal cases are displayed in fig. 33. Further analysis was done to show α at different elevator deflections for each flight regime as well in figures 34, 35, and 36. In these representations the stability and trimmability of the aircraft is proven for all regimes without surpassing the maximum deflection angle of the elevator.

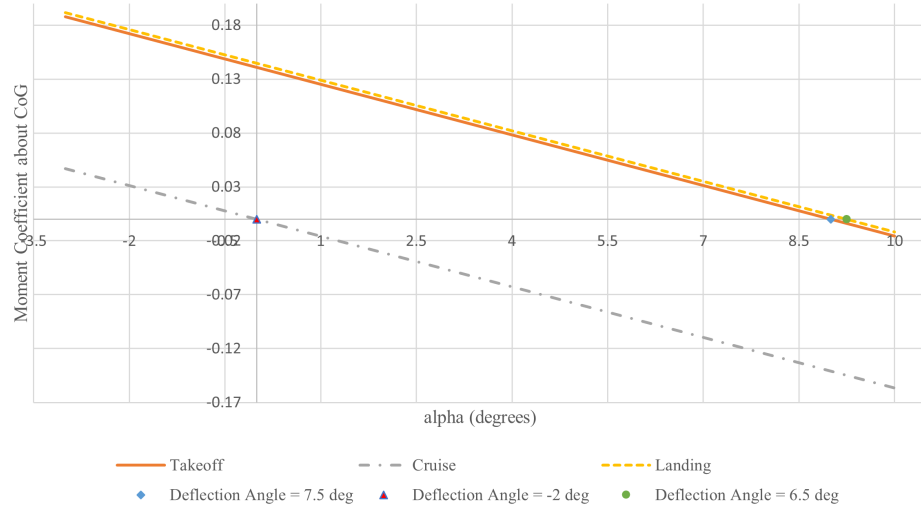


Fig. 33 Optimal Trim Elevator Deflections

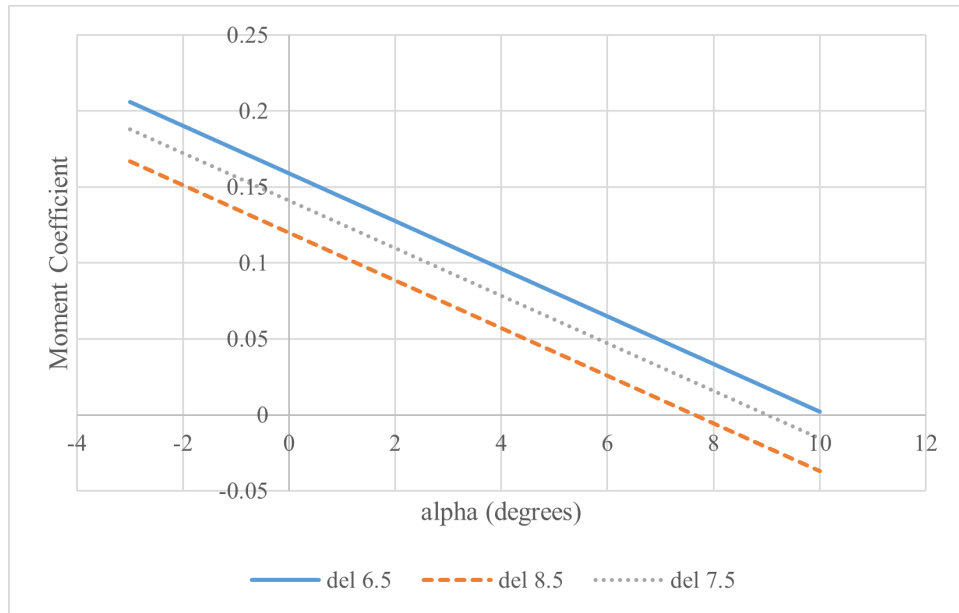


Fig. 34 Takeoff Trim Curves

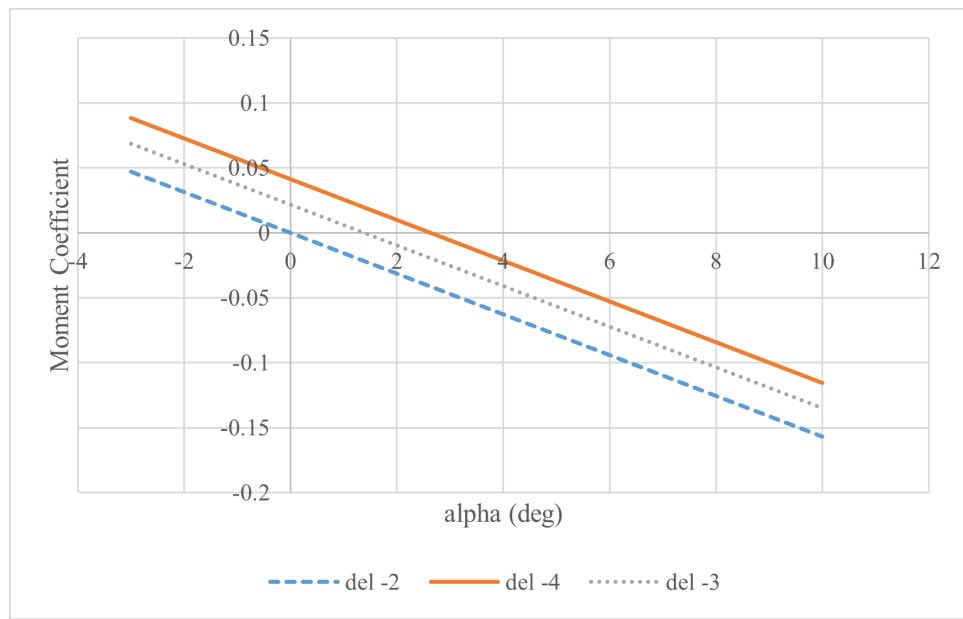


Fig. 35 Cruise Trim Curves

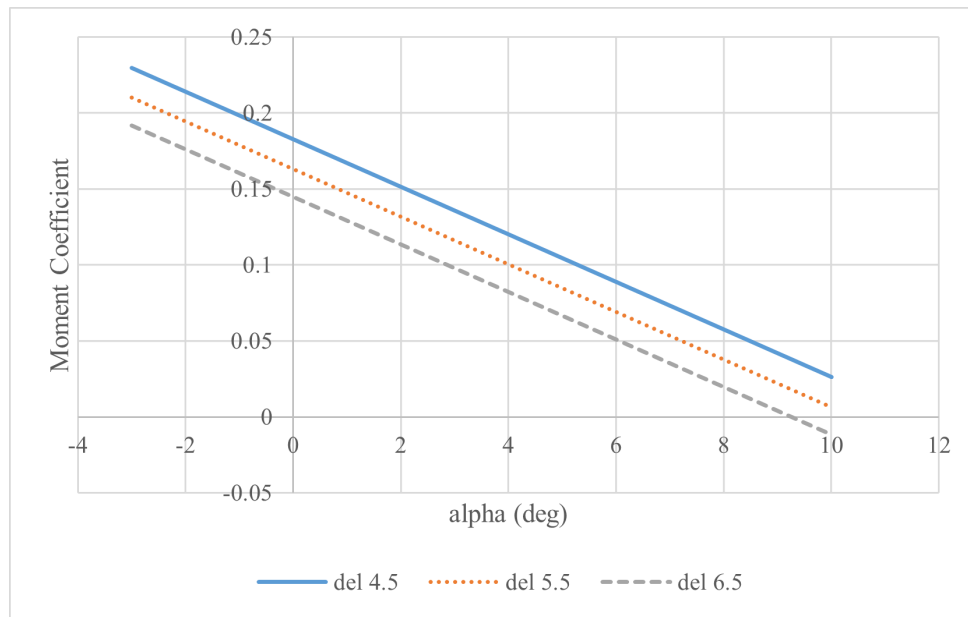


Fig. 36 Landing Trim Curves

The rudder trim was also considered for a takeoff case with a crosswind of 20 of the takeoff speed and a sideslip angle of 11.5° . For this analysis, the contribution of the aileron to yaw was not considered as to focus on the ability of the rudder to trim. The result is shown in Table 30, the major sizing term is the required rudder deflection angle which in this case is below the maximum .

Table 30 Yawing Parameters

Parameter	Value
V_β	36 ft/s
β	11.5°
δ_R	19.26 °

E. Stability Derivatives

The stability derivatives used in the moment and trim calculations are displayed in Table 31 for cruise conditions. The negative value for C_{m_a} indicates that there is a negative pitching moment on the plane and therefore longitudinal static stability. The negative C_{l_β} value indicates that the Orca is laterally stable and produces a restoring response to roll given a change in slideslip angle. Similarly, the positive value of C_{n_β} indicates that the Orca produces a restoring yaw moment given a change in sideslip angle and in conjunction with C_{l_β} proves that the aircraft is both laterally and directionally stable.

Table 31 List of Stability Derivatives

Derivative	Value	Method
C_{L_a}	4.94 per rad	Raymer[4]
C_{m_a}	-0.7765 per rad	Raymer[4]
$C_{m_{\delta e}}$	-1.1222 per rad	Sadraey[20]
ϵ_α	.5093	Sadraey[20]
$C_{l_{\delta a}}$	0.1686 per rad	McCormick[19]
$C_{n_{\delta a}}$	0.00573 per rad	XFLR5
C_{l_β}	-0.06481	McCormick[19]
C_{n_β}	0.23463	XFLR5
C_{l_r}	0.13813 per rad	XFLR5
C_{n_r}	-0.34645 per rad	XFLR5
$C_{l_{\delta r}}$	0.0198 per rad	XFLR5
$C_{n_{\delta r}}$	-0.1206 per rad	XFLR5

F. Dynamic Stability

Dynamic stability was analyzed by constructing a model of the Orca in XFLR5 and implementing all of the control surfaces and wing bodies along with weights, moments of inertia and cruise conditions. The model was run using the XFLR5 native stability analysis which incorporates both Vortex Lattice and 3-D Panel methods of analysis on the structure. The characteristics for both the longitudinal and lateral-directional analyses are presented in Tables 32 and 33. The analysis resulted in negative real values for the roots of all of the modes besides the spiral mode, proving that the aircraft design is dynamically stable for all

Table 32 Longitudinal Dynamic Stability Analysis

Dynamic Mode	Roots	ω_n	ζ
Phugoid	$-1.03276 \pm 3.84432i$.634 Hz	.259
Short	$-.00095 \pm .11424i$.018 Hz	.008

Table 33 Lateral-Directional Dynamic Stability Analysis

Dynamic Mode	Roots	ω_n	ζ	$T_{1/2}$
Roll	$-73.51 + 0i$	0 Hz	0	.009 s
Dutch Roll	$-.21635 \pm 2.72585i$.435 Hz	.079	-
Spiral	$.00855 + 0i$	0 Hz	0	81.03 s

G. Trade Studies

Trade studies were done on empennages of established light attack aircraft to determine approximate sizes for the horizontal tail as well as the vertical tail and their control surfaces. The results are displayed in Table 34 and Table 35.

Table 34 Trade Study of Jet Driven Military Trainers Horizontal Tail and Elevator

Aircraft	S_e/S_t	S_t	Chord Ratio
Aero L39C	.23	54.6	.4
MB-339A	.23	46.9	.31
PZL TS-11	.33	38.1	.31
SM S-211	.40	36.4	.4
Orca	.3	50	.3

Table 35 Trade Study of Jet Driven Military Trainers Vertical Tail and Rudder

Aircraft	S_r/S_v	S_t	Chord Ratio
Aero L39C	.28	37.8	.36
MB-339A	.26	25.5	.34
PZL TS-11	.31	24.2	.33
SM S-211	.40	27.7	.36
Orca	.3	28.75	.3

IX. Structures and Loads

A. Material Selection

A study on material selection is essential to initiate the structure and load analysis. Also, material selection is one of the critical components for determining survivability and manufacturing cost. This section aims to find the optimal material for each part of the structure to balance survivability, weight, service life, and manufacturing cost. Three representative metal materials are studied as well as their applications on the Orca. Then, the material for each part of the aircraft structure is selected.

Although the composite material has become a primary material for aircraft structure, it is not considered for this project. Our designed aircraft must maximize the ability to do repair and maintenance in a short time due to the high risk of being attacked from the ground. Compared to metal materials, composite materials significantly increases the level of repairability in large scales due to complex strength and stiffness characteristics. Most importantly, the composite material's manufacturing and maintenance cost is not acceptable in our design approach.

1. Steel Alloy [21]

Steel alloy has been widely used since the early stage of aircraft development due to its ability to weld for fuselage structures. However, it is not mainly used today because many advanced materials with low density and high strength have been introduced. Still, they are used in some areas where they require high fatigue and heat resistance. Our designed aircraft will mainly use steel alloys in the landing gear, engine mounts, and fitting parts such as hardpoints and wing attachment fittings.

2. Aluminum Alloy [22]

Aluminum alloy has been used in the aerospace industry for a long time because of its low weight, high strength, and high corrosion resistance. The price is comparably lower than any other advanced materials, such as composite materials. Many types of Aluminum alloy are developed to be suitable for aircraft use, and some of the alloys are

certified to be used in military aircraft. Also, aircraft skins made of Aluminum alloy are ideal for ground support fighters because it is easier to replace in case of any damage. Therefore, Aluminum alloys will be mainly used for this aircraft.

3. Titanium Alloy [22]

Titanium has a very high weight-to-strength ratio, which reduces the aircraft's weight with the same or better structural integrity. It is also highly resistant to corrosion since it forms a passive oxide coating when exposed to air or oxygen at high temperatures. Lastly, it has a significantly low thermal expansion rate. However, it has high density and manufacturing cost. Therefore, Titanium alloy is expected to be used only in the armor around the cabin. The armor is essential in the designed aircraft to increase the pilots' survivability and protect the ejection seats where they must eject pilots regardless of any damage or attack. A trade study on armor is conducted in the next section to design the armor for this aircraft.

Table 36 below shows the properties of Aluminium alloys that are certified for military and aircraft manufacturing. Properties of composite materials, steel and Titanium alloys are in Table 38.

Table 36 Properties of Aluminium Alloys (at Room Temperature)

Parameters	Al 2024-T4 [22]	Al 6061-T6 [22]	Al 7075-T6 [22]
Density [lb/in^3]	0.1	0.0975	0.102
Fatigue Strength [psi]	20000	14000	23000
E [ksi]	10600	10000	10400
G [ksi]	4060	3770	3900
Elongation at Break [%]	15	17	11
Yield Strength [psi]	47000	40000	73000

Based on this study, the material is chosen for each structural component to best follow our design approach and optimize the structure of the Orca, as shown in Table 37. In conclusion, Al 7075-T6 is mainly used in this aircraft due to high fatigue and yield strength. Al 7075-T4 is chosen for the skins with a consideration of repair and manufacturing cost while having optimal properties for the aircraft.

Table 37 Material Selection

Components	Material
Fuselage Frame & Longeron	Al 7075-T6
Fuselage I-Beam	Al 7075-T6
Skin	Al 2024-T4
Spar	Al 7075-T6
Rib	Al 7075-T6
Landing Gear	Steel 4340
Fitting & Joint part	Steel 4340
Armor	Ti-6A1-4V

B. Trade Study: Armor Design

One of the concerns while designing the structure is how to protect the Orca from ground fires. In this section, a trade study on armor design around the cabin is conducted to reduce the aircraft's vulnerability, and based on this study, the armor is designed and implemented to the Orca. Total three aircraft are discussed in this section.

P-47 Thunderbolt was entirely made with Steel alloys [23]. A pilot was protected from the gunfire by a hardened, thick Steel alloy armor plate located in the cockpit's forward and after ends. Fairchild A-10 Thunderbolt is the first aircraft in the US that significantly reduced the aircraft vulnerability. The A-10 adopted a bath-tub shape armor to protect pilots using 0.5-inch thick Ti-6A1-4V Titanium alloy sheets [24], which is capable of repulsing direct hits from a 23 mm shell.

On the other hand, when A-29 Super Tucano was first built, it used detachable Ti-6A1-4V plates on both sides of the cabin with a 1.5-inch thickness. The detachable plates made it possible to efficiently manage the structural weight depending on the aircraft's mission [5]. Recently, an upgrade was made in A-29 to reinforce the armor by using composite material, Silicon Carbide (SiC), inside the whole cockpit area [25]. Not only for A-29, using the armor made of composite material has become a new trend for many military aircraft since it consumes fewer structural weights than the typical Titanium alloys.

The armor design and material must be chosen to increase survivability effectively. However, due to our design approach, the priority is that the armor must not be designed to increase the manufacturing and operating costs significantly. These aircraft suggest that a primary reason for the armor is to protect the pilots, but it is designed with different materials and shapes. Based on the study, the A-29 armor design, detachable armor, is chosen to be the armor design for the Orca because it covers the most vulnerable area of the cabin and reduces the operating cost by flexibly

controlling the aircraft's empty weight. The thickness of the detachable armor is chosen to be 1 inch, which is thicker than the A-10 armor. Total four detachable armors are attached on both sides of the cabin, using bolts.

The "bath-tub" in A-10 is the most reliable armor design, but it significantly increases the structural weight since more area is covered with the heavy material than any other aircraft. P-47 design is not an ideal design for the Orca since it does not protect the side of the cabin. Although the composite material has the best mechanical properties, it is eliminated during material selection due to the highest cost among the three materials in Table 38. Therefore, Ti-6A1-34V is selected for armor material since it has a twice lower density but higher yield strength than the Steel alloy, generating high specific strength. Using Titanium alloy would not increase the manufacturing cost too much because it is used in a small region.

Table 38 Properties of Metal Alloys and Silicon Carbide (SiC) (at Room Temperature)

Parameters	Ti-6A1-4V [22]	Steel 4340 [21]	SiC [26]
Density [lb/in^3]	0.16	0.284	0.112
E [ksi]	16510	29000	59500
G [ksi]	6380	11300	26100
Elongation at Break [%]	14	12.2	N/A
Yield Strength [psi]	160000	125000	N/A
Used in	A-29 & A-10	P-47	Modern Fighters
Cost	High	Low	Highest

C. V-n Diagram

V-n diagrams are used to visualize the aircraft's capability of a design in terms of flight speed and load factor. V-n maneuvering diagram in Fig. 37 is plotted based on military specification MIL-A-8861 [27] and MIL-A-8860 [28]. V-n gust diagram is plotted based on FAR25 certification. Equations in Roskam Section 12.4 [18] and MIL-A-8861 are used to calculate values at each point.

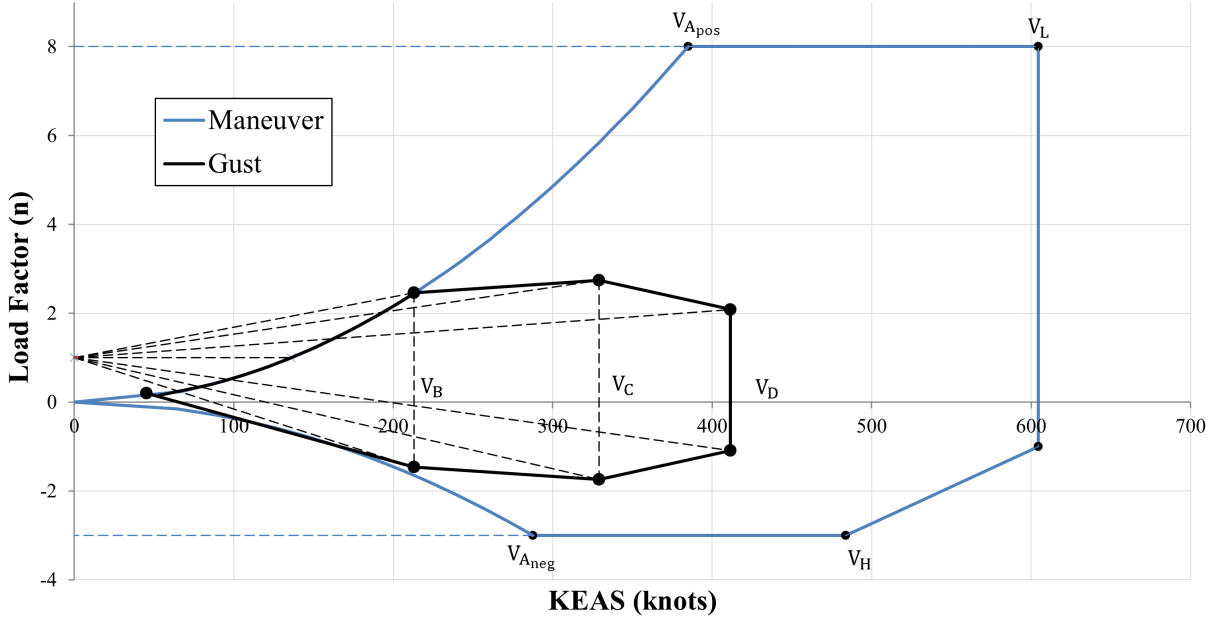


Fig. 37 Maneuver and Gust V-n Diagram

Fig. 37 shows that the gust line for the Orca is far within the maneuvering V-n diagram, which means that the gust load does not affect the maneuver load. The engine has more than enough thrust to fly faster than the design cruise speed, which increases the aircraft survivability, especially when the aircraft needs an instantaneous maneuvering operation during the attack. The maneuvering load factors are limited from -3 to 8 , according to MIL-A-8861[27] and Raymer[4]. An additional factor $K = 1.25$ was multiplied to determine the positive stall line slope and designed maneuvering speed V_{Apos} . The V-n diagram confirms that the aircraft is capable of high-speed flight and heavy maneuvering. Table 39 shows some characteristic velocities (in KEAS) obtained from the V-n diagrams.

Table 39 Characteristic Velocity Data from V-n Diagram

Parameter	Symbol	KEAS (knot)
Design Speed for Max. Gust Intensity	V_B	213.3
Design Cruising Speed	V_C	329.1
Design Diving Speed	V_D	411.4
Max. Level Flight Speed	V_H	483.7
Max. Dive Speed	V_L	604.6

D. Load Cases and Path

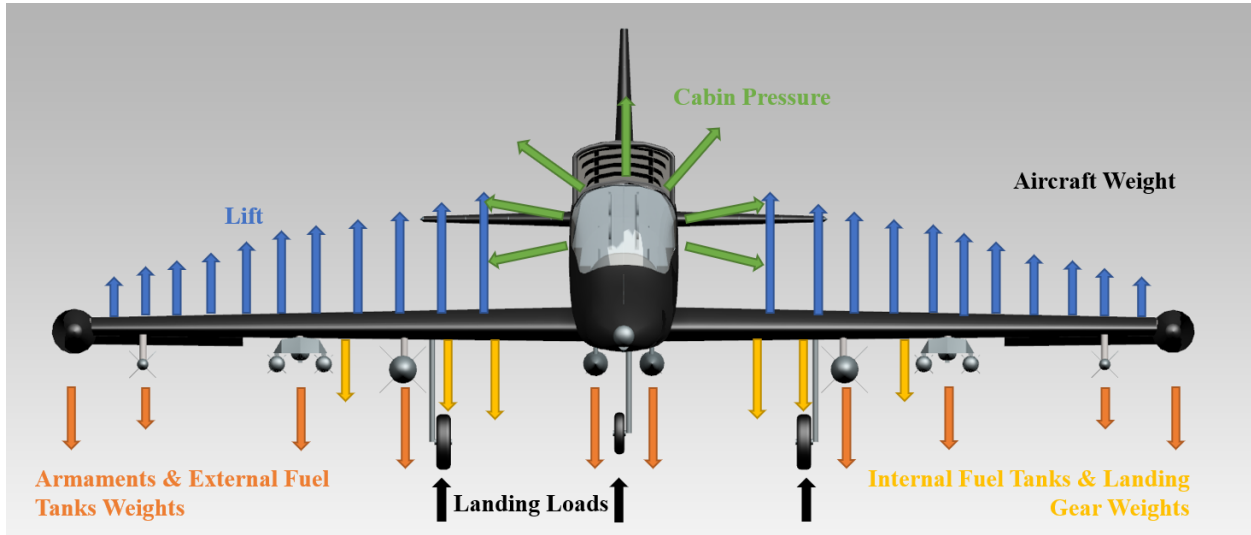
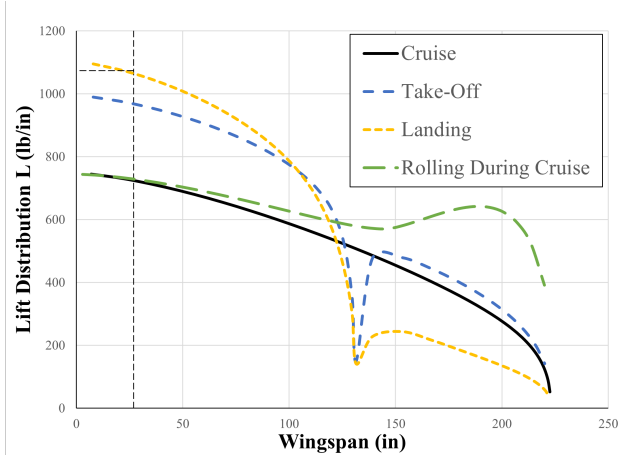


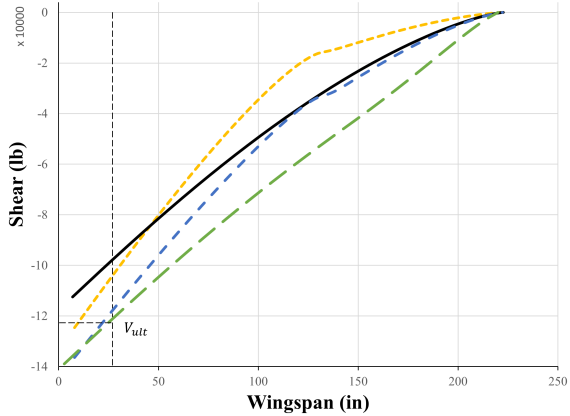
Fig. 38 Load Cases

A schematic of some load cases of interest on the Orca is shown in Fig. 38. Some load cases on the main wing are considered point masses, such as armaments, external fuel tanks, internal fuel tanks, landing gear weight, and landing loads. Distributed forces on the main wing are the lift and structural weight of the wing. The lift is varied by how the pilots maneuver the aircraft, such as take-off, landing, rolling, and cruise, and they are defined from the lift and pressure distribution data from XFLR for further analysis. The landing load, cabin pressure, and aircraft weight (including structure, powerplant, fixed equipment, payload, and fuel weight) are defined on the fuselage. Weight and c.g location for every element are described in the later section, Table 42.

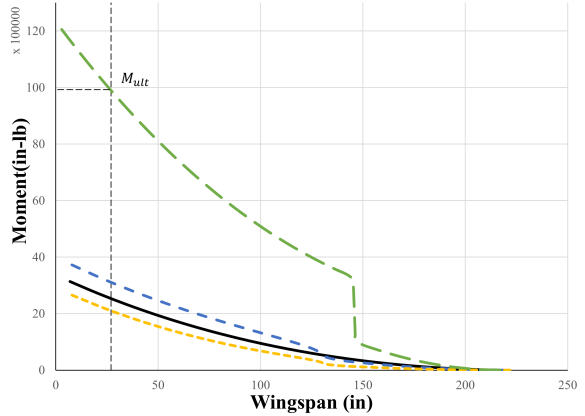
The loads on the wing are distributed through multiple ribs and spars, and then they are transferred into the fuselage via wing carry-through structure. The front landing gear is directly connected to the keel beam in the fuselage, efficiently distributing the load. The rear landing gears are attached between the spars in the wing. Strong fittings and torque boxes are used to connect the landing gear and spars for better load distribution. Pressure force from the cabin is distributed through fuselage skin, frames, and longerons. The structural design is done with a consideration of these load cases and paths.



(a)



(b)



(c)

Fig. 39 (a) Lift Distribution (b) Shear (c) Bending Moment For Right Main Wing

As stated before, the lift distribution plot on the main wing is obtained using the speed, altitude, and lift coefficient data from XFLR at each mission segment. Then, the shear and moment plots are calculated to define the ultimate values. These plots and values are used to size the ribs and spars of the main wing and verify that the selected material and structural design are suitable for any mission segments and extreme conditions. As shown in Fig. 39, four important maneuvering segments are analyzed: cruise, take-off, landing, and clockwise rolling during the cruise. Only the left side of the main wing is considered since the clockwise rolling gives maximum moment and shear (absolute) on the left-wing.

Fig. 39(a) shows that the lift distribution from cruise and rolling follows the same trends at the beginning of the span, but they demonstrate a significant difference at the end where the aileron is located. This is because the aileron is fully down during rolling, creating more lift at the end of the wing. Similarly, the lift distribution during take-off and

landing shows a similar behavior initially, but at the end, they also show a large difference because, during take-off, the aileron is also used to increase the lift quickly.

From Fig. 39 (b) and (c), the absolute maximum shear and bending moment are located at the root of the wing, and the absolute minimum at the tip of the wing. The ultimate shear and moment are determined at the outboard of the centerline, at a 27-inch wingspan, and they are selected based on the absolute maximum value among the four mission segments to ensure that the wing can withstand the extreme condition.

Finally, The ultimate shear is determined to be $-12.2 \cdot 10^4$ lb, and the ultimate moment to be $100 \cdot 10^5$ in-lb.

E. Structural Arrangement

This section aims to find an optimal structural arrangement of the Orca, based on the previous studies on loads. Each structural element is placed and sized to effectively distribute the load and increase the structural stability during designed missions and unexpected situations. Also, unlike commercial aircraft, redundancy of the structure is necessary to reduce the aircraft vulnerability, which is done by implementing additional spars on the wing. A primary source to determine the structural arrangement and sizing is from Roskam [18], and the rib and spar sizes for all wings are initially designed using the ultimate shear and moment from the previous section. However, they are ultimately determined after multiple iteration process using FEA Nastran solver in the NX12 program.

1. Main Wing Structure

The main wings are designed to hold a large load due to the fuel tanks(internal and external), landing gears, landing loads, and armaments attached at the hardpoints. Ribs and spars are placed based on the internal fuel tanks, weapon hardpoints, flap, and landing gear locations. In Fig.40, the front and rear spars are located at 15% and 75% of the wing chord, which are determined using Roskam [18]. Another spar is added to reduce the aircraft vulnerability and distribute the loads more evenly, at 40% of the wing chord. The spars are designed with an I-beam shape made of a 0.6-inch spar web, 4-inch width and 0.5-inch thick spar cap.

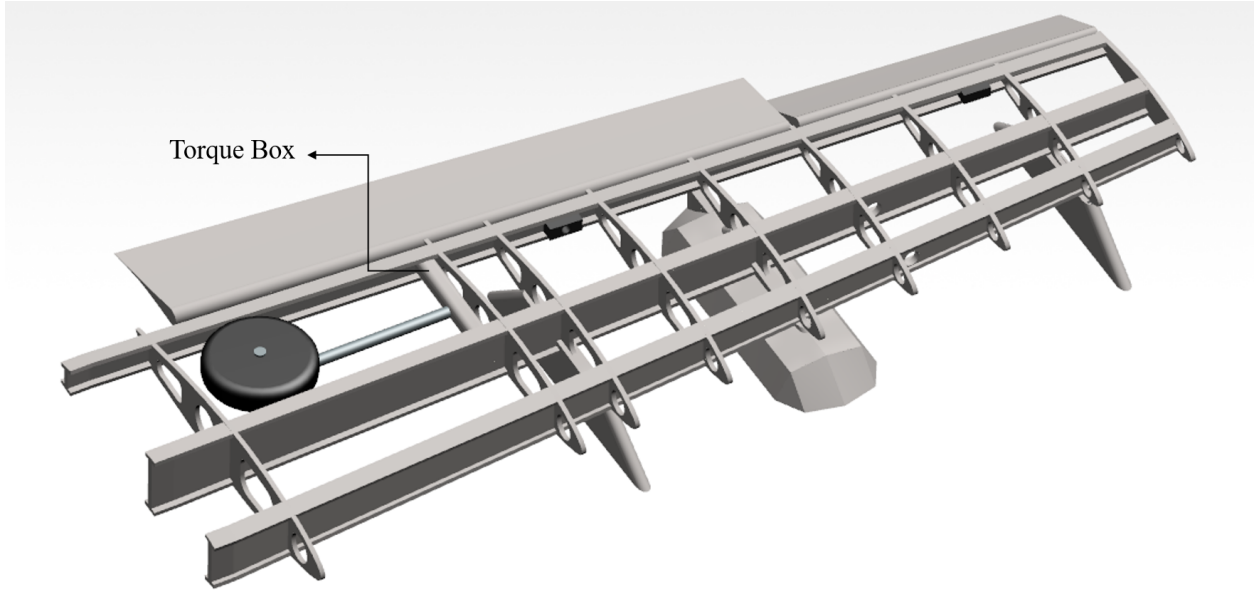


Fig. 40 Main Wing Structural Arrangement

Total nine ribs are integrated into the main wing. The ribs have multiple cutouts to reduce weight while enduring the same strength and drag load. They are also for the flight control and fuel systems to pass through each rib. All spars are made with a 0.6-inch thick plate. The hardpoints are directly connected to the ribs and attached at the front and middle spars to reduce the shear. The rear landing gear has a torque box between the middle and rear spars to withstand a large number of loads and shear, effectively distributing the landing load through the spars. In addition to these, aeroMETAL honeycomb sandwich panels from Collins Aerospace [29] are used to build the leading edges and flaps to reinforce the structure.

As stated previously, the main wing's rib and spar sizes were finalized after multiple iterations through FEA to find an optimal design that is both light and durable for extreme conditions. The lift distribution during rolling in the cruise was used to test the left-side main wing since it was the most radical segment among the other three mission segments defined in Fig. 39. Since it was desired to observe stresses experienced in the ribs and spars, skins were excluded in the CAD design, and the lift was distributed at the top surface of ribs and spars. The armament weights were excluded for FEA load cases to make the wing condition even more extreme. Only weights from necessary elements during the flight were applied: structural weight, landing gear, flight control system, hardpoints, internal and external fuel tanks (including fuel weight). They were treated as point forces and applied at the exact locations. Fixed constraints were applied at the roots of the spars. These load cases were fixed during the size iteration process. The results are shown in Fig. 41 and Fig. 42, with 1:1 scale.

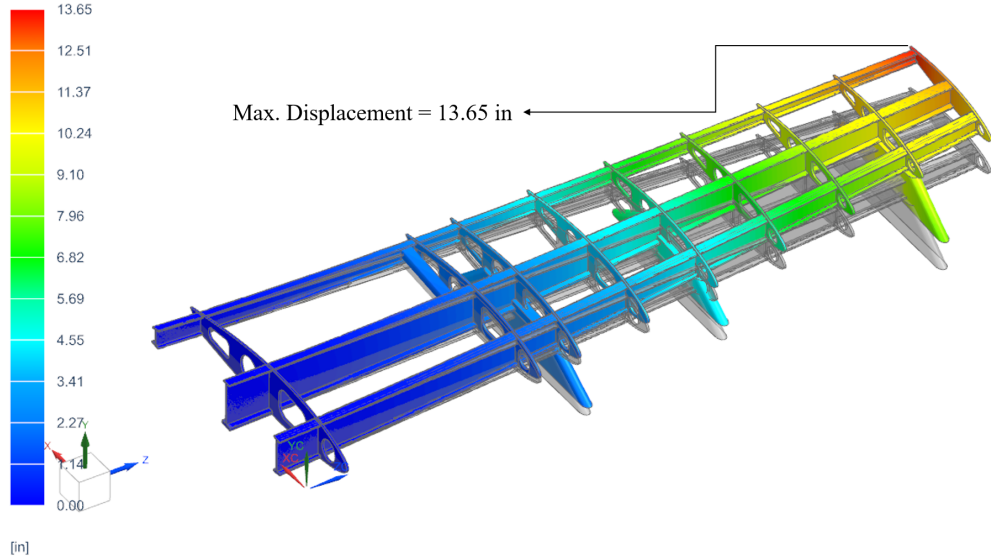


Fig. 41 Deflection of The Left-Side Main Wing

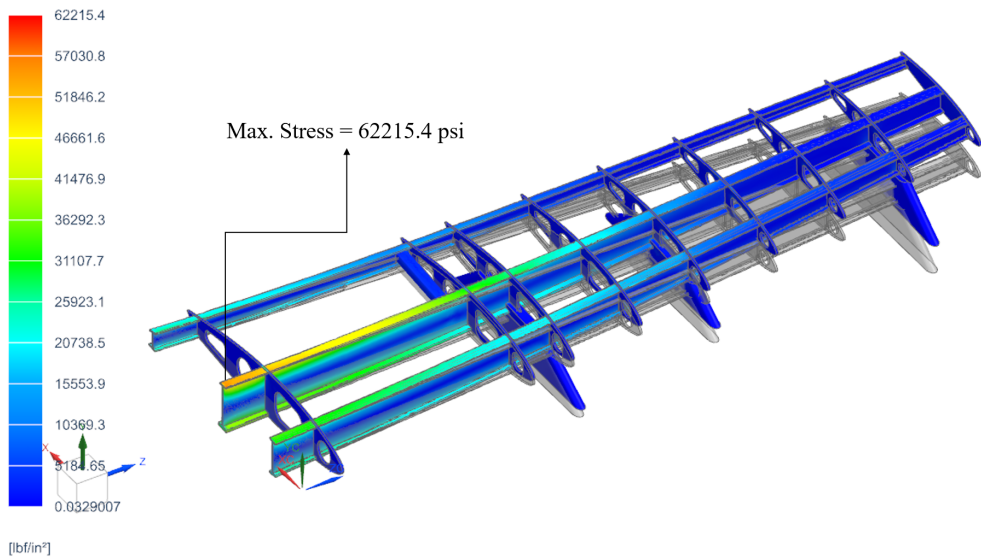


Fig. 42 Stress Throughout The Left-Side Main Wing

Fig. 41 indicates that the maximum deflection is 13.65 inches at the rear tip of the wing, and Fig. 42 shows that the maximum stress is 62215.4 psi at the root of the middle spar. It should be noted that the maximum stress that occurred at the root is not ideal since loads at the root will be distributed through the wing-box structure and wing attachment fittings at the fuselage. Also, in an actual operation, the root will not have the fixed constraints. The average stress throughout the wing is visually observed to be around 35000 psi. Regardless of a difference between the FEA simulation and reality, both average and maximum stress from the simulation are within the chosen material's yield strength, Al 7075 T6, 73000 psi in Table 37. The deflection on the wing is acceptable since it would have minimal

effects on the flight control and fuel system, based on visual observation. Therefore, it is confirmed that the wing can withstand most extreme cases, with the chosen rib and spar sizes.

2. Empennage Structure

The horizontal and vertical tail wings are designed in the same way as the main wing, based on Roskam [18] and the location of rudder and elevator. As shown in Fig. 43, additional spars are implemented to reduce the aircraft vulnerability so that they can still function after attacks from the ground. For both tails, the front and rear spar are located at 15% and 65% of the wing chord. An additional spar is located at 40% of the chord for the horizontal tail. For the vertical tail, two extra spars are located at 27% and 53% of the chord. The spars for both wings are designed with an I-beam shape made of 0.3-inch spar web, 2-inch width and 0.2-inch thick spar cap. Both wings have five ribs with a spacing of 16.3 inches for the vertical tail wing and 21.50 inches for the horizontal tail wing. All ribs are made with a 0.3-inch thick plate. Again, aeroMETAL honeycomb sandwich panels from Collins Aerospace [29] are used to build the leading edges, elevator, and rudder.

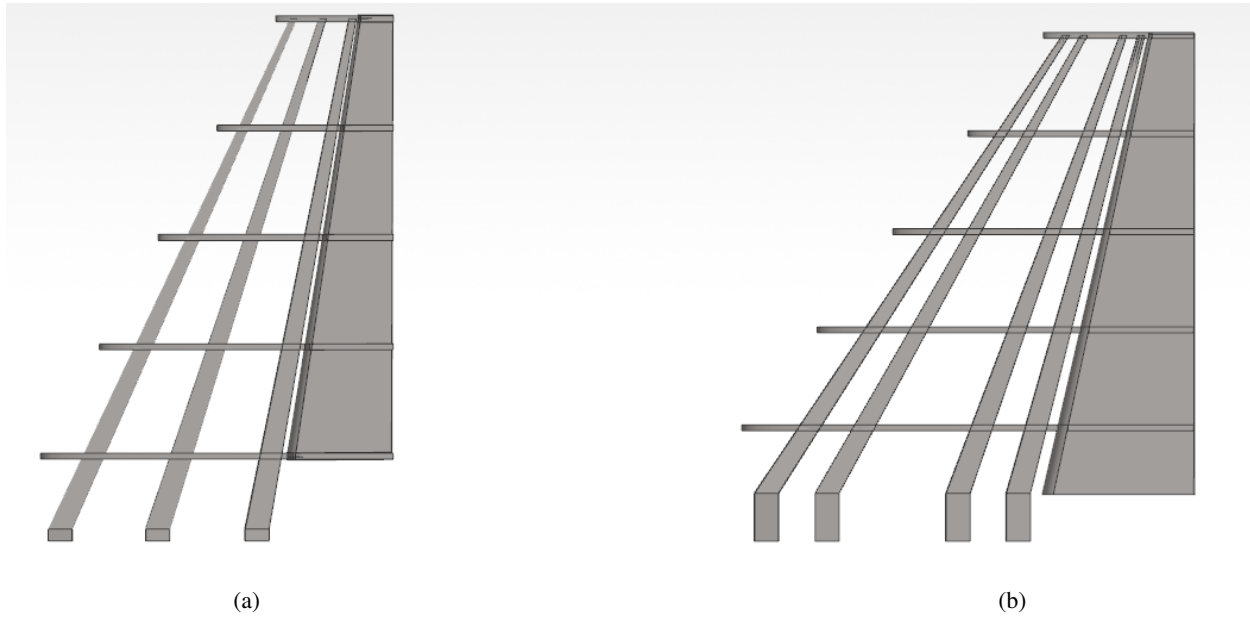


Fig. 43 Structural arrangement of (a) Horizontal Tail (b) Vertical Tail

3. Fuselage Structure

The Orca has a dynamic shape of the fuselage where every element of the aircraft must be integrated perfectly with the fuselage structure to endure the loads. The size of each component for the fuselage is determined using Roskam [18]. As shown in Fig. 44, total 27 frames, including two bulkheads, are used with a 20-inch spacing. They are 2 inches thick T-shape beams, and some frames where the wings are attached are 4-inch thick, frame sections 11, 14, 23, and 24. Bulkheads are located at the front and back of the cabin, frame sections 5 and 11, with 1-inch thickness. They help the

cabin's pressurization and work as firewalls to separate the engine and internal fuel tank from the cabin, preventing the cabin from fires or any hazardous materials. The cabin and bulkheads are fireproof and sealed with close-fitting as required by 14CFR 25.1191 [30].

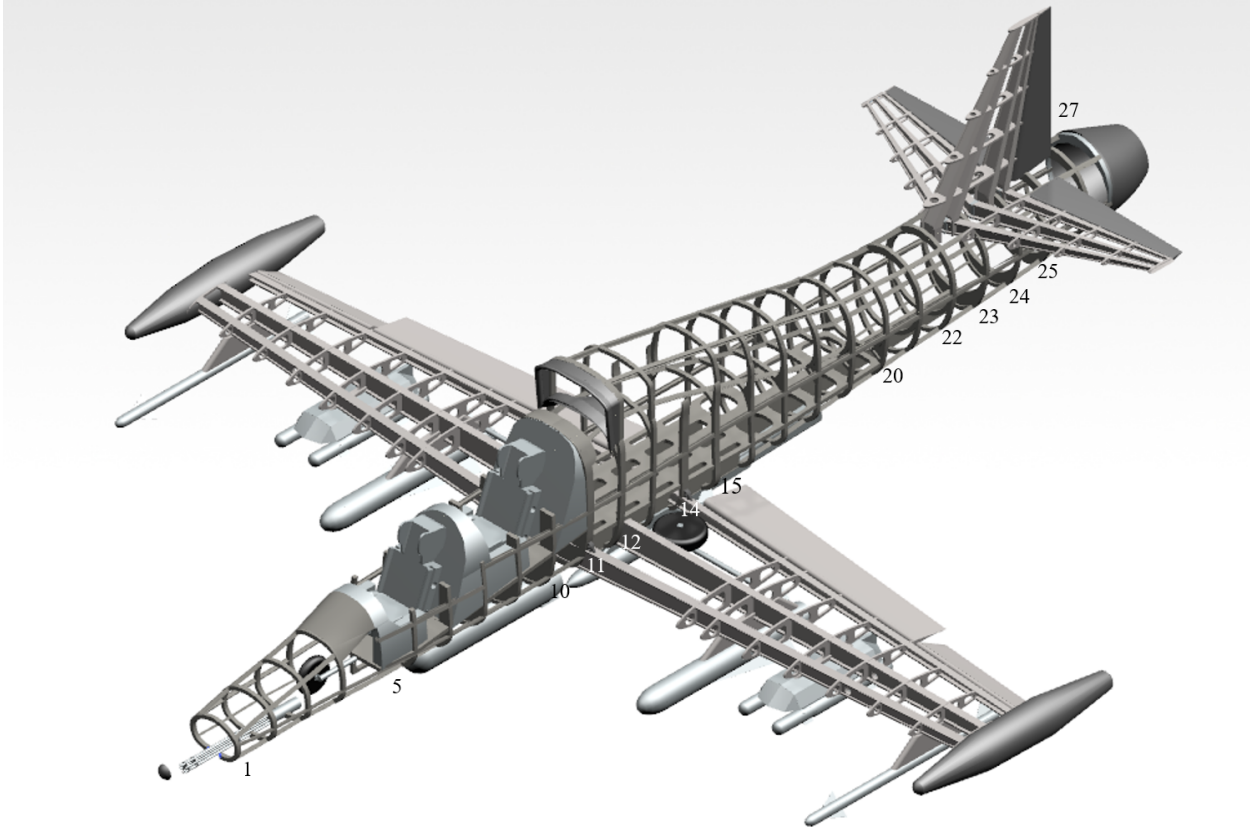


Fig. 44 Structural Arrangement of The Aircraft

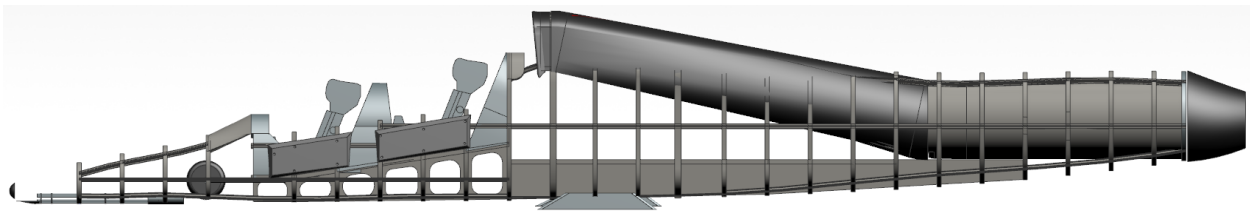


Fig. 45 Fuselage Side View

As shown in Fig. 45, a T-shape keel beam is installed across the entire fuselage with multiple I-shape longerons at the outer frame and between the inlet to distribute heavy loads. A maximum of eight longerons is implemented along the fuselage with a spacing of 12- 15 inches and 2-inch height.

In Fig. 46(a), the keel beam's top spar cap divides the fuselage into three compartments, two at the bottom and one at the top. The top compartment stores the cabin, engine, and internal fuel tank. The bottom compartments hold the main wings, armaments, system pipes and equipment. The keel beam's spar web is 1-inch, and the spar cap is 0.5-inch

thick. The top spar cap has a full width along the fuselage to divide the space. The nose landing gear is attached at the front of the keel beam for more manageable load carry during landing and at the ground. The tail wings and engine are mounted at the end of the keel beam with the same reason.

The wing carry-through structure for the main wing is a wing box structure integrated with the keel beam, and two wing attachment fittings between frames (11 and 14) and spars (front and rear) to account for shear, as shown in Fig. 46(b). The tail wings are a wing box structure connected at the top of the frame sections 22, 23, and 24. The hardpoints for fuselage are attached to the main wing's wing box structure.

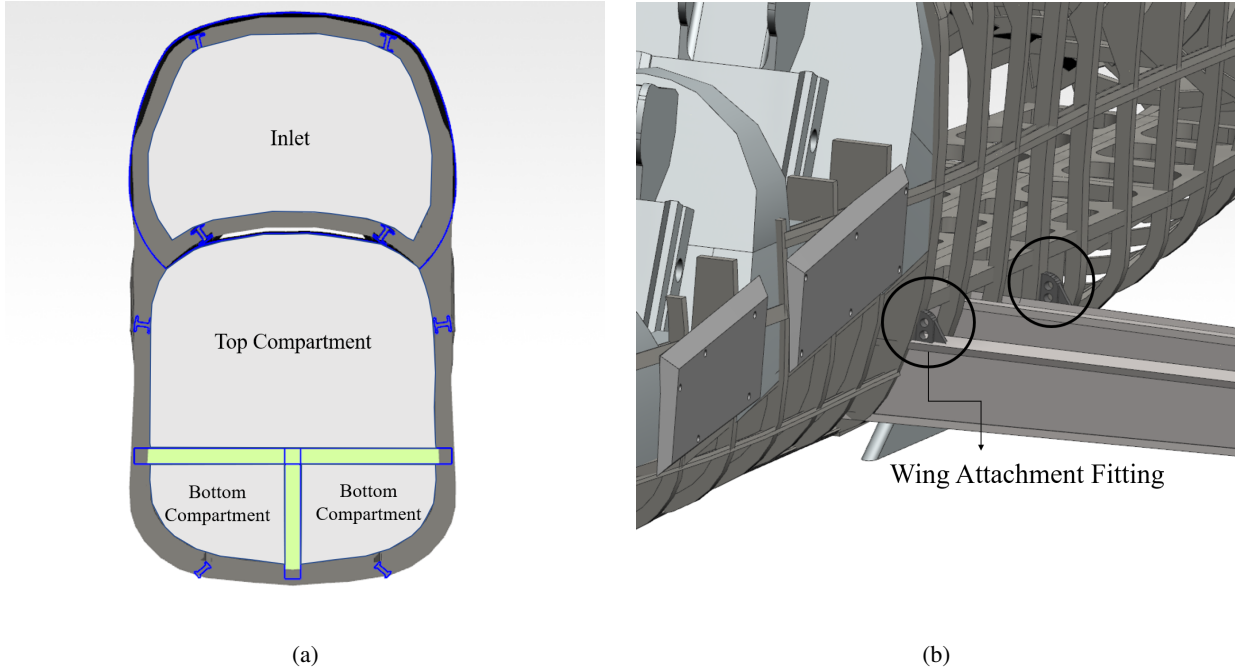


Fig. 46 (a) Compartment Division at Frame Section 12 (b) Wing Attachment Fittings

F. Pressurization & Skin Thickness

A pressurization system is required for the Orca, because it plays vital roles more than providing Oxygen to pilots. In addition to the oxygen masks, the entire cabin is pressurized using Environmental Control System (ECS), which is also used for other aircraft systems.

Using the ECS for cabin conditioning gives multiple benefits to pilots' performances. First, it prevents pilots from high skin temperatures and the effects of solar radiation through the canopy. The pilots' body temperature is efficiently controlled so that they can tolerate high-stress conditions. Second, high-pressure air is blown into the canopy and windscreens to avoid misting and icing, which will increase the pilot's visibility.

The cabin pressurization and conditioning system through the ECS follow MIL-E-19827E [31]. Using Moir[32], the automatic pressurization schedule for this aircraft is determined as shown in Fig. 47. The pressurization system starts when the altitude is above 5,000ft , and it restricts the cabin pressure from exceeding the cabin altitude of 20,000

ft in any situation.

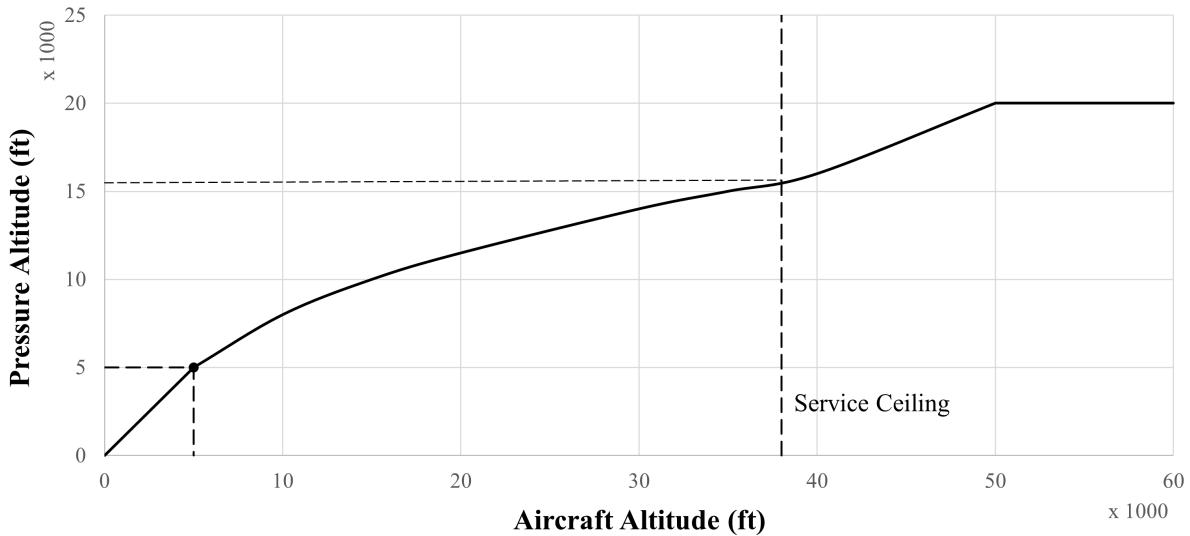


Fig. 47 Automatic Pressurization Schedule

Based on the difference between the cabin pressure and flying altitude at the service ceiling, a thin-walled cylindrical vessel analysis is done to find an optimal skin thickness, and an additional safety factor 1.2 are multiplied [33]. As a result, the skin thickness is set to be 0.1 inches for the entire aircraft. A fuselage stress in the cabin due to the pressurization is considered for the structural arrangement; the structure around the cabin is reinforced by implementing additional longerons, firewall, and a 0.5-inch thick metal plate at the bottom (part of the keel beam).

G. Landing Gear

The design of the landing gear components were driven by the need to effectively dissipate loads from an austere field and provide sufficient clearance from FOD.

The first parameter that was evaluated for the landing gear was the height and specific placement on the wing to provide clearance while taxiing as well as avoiding tail strike. With the current CG location it is seen from Raymer that the main landing gear should be positioned such that the tipback angle and tail strike angle are as close as possible [4]. From this it is calculated that the main landing gear should be 57 inches tall and positioned 21 inches aft of the CG. This positioning will prevent the aircraft from tipping over during maintenance but wont prevent the aircraft from rolling during takeoff because the angles are less than 25°[4]. Further, it is noted that with the landing gear 77 inches from the center line of the aircraft the wing is able to roll 5°during takeoff with sufficient wing clearance. All of these values can be seen below in table 40.

The nose gear of the aircraft will be positioned along the center line of the aircraft and was positioned to provide sufficient room for stowing and ensuring the overturn angle less than 63°[4]. The resulting distance from the nose of the aircraft and height can be seen below in table 40.

Table 40 Landing Gear Specifications

Parameters	Value
Main gear distance from nose	275.5 in
Nose gear distance from nose	106.75 in
Main gear height	57 in
Nose gear height	51 in
Tail strike angle	14°
Overturn angle	50.1°

With the heights determined the tire sizes and pressures can be determined. It is assumed that the main gear takes approximately 90 percent of the load of the aircraft. Additionally it is noted that the nose gear is typically about 75 percent the size of the main gear [4]. Utilizing table 11.1 in Raymer which covers statistical tire sizing, the tires were sized resulting in the main gear tire diameter and width being 24 inches and 6.5 inches respectively. This also results in the nose gear tire diameter and width being 17.75 inches and 4.75 inches respectively. Although these specific size of tires are not standard, specific tires were chosen from Michelin to be implemented on the aircraft [34]. The resulting main gear tires will be the Type VII 24 x 5.5 tires and the nose gear tires will be the Type VII 18 x 4.4 tires [34]. All of the tire pressures were determined using table 11.3 in Raymer and as a result the pressure of each tire should not exceed 50 psi to ensure safe operation of the aircraft while operating on Easter fields with a CBR rating of 5 [4] [1]. These values can be seen below in table 41.

The next major factor in the landing gear design is the shock absorbing system. It was determined that an in line oleo shock absorbing system will be utilized to dampen loads from the field due to the simplicity and compactness of the device along with the effectiveness of transferring loads into the structure of the aircraft [4]. The final oleo shock specs can be seen below in table 41 and were sized using the methods outlined in Raymer [4].

Table 41 Tire and Shock Specifications

Parameters	Value
Main tire size	Type VII 24 x 5.5 [34]
Nose tire size	Type VII 18 x 4.4 tires [34]
Tire pressure	50 psi
Shock diameter	6.25 in
Shock stroke length	13.5 in

1. Trade Study: Landing Gear Stowing

Due to the length requirement of the landing gear to satisfy the tip back angle, a trade study was performed on different stowing methods to ensure the choice was optimal for the situation. It had previously been determined that the landing gear should be stowed to minimize drag during cruise and as a result the three stowing options that were analyzed were retraction toward the fuselage into the wing, retraction forward into a pod, and a folding landing gear. The parameters used to evaluate the analysis are: structural impact, system integration, and aerodynamic impact.

The first method analyzed was for the main gear being stowed into the wing toward the fuselage. This is a design that is seen among many similar aircraft such as the L-39 and L-159 [6] [7]. The structural impact of this design is not a negligible one as there will need to be some adjustment in the overall layout of the ribs and spars to accommodate this design. This method also has a minimal aerodynamic impact during cruise because the landing gear has no external housing structure resulting in only a slight increase in drag due to protuberance of the seam. With regards to systems integration, this method is extremely simple because there will only be one axis of actuation necessary.

The next method that was analyzed was the wing podded landing gear location. This method was assumed to be a forward retracting system to allow for gravity assisted deployment in the event of a failure [4]. It is seen through the similarity analysis that was performed earlier that this style is rarely utilized with the exception of the A-10 [24]. With regards to the structural impact on the aircraft, it is nearly negligible because the main gear will be folding into its own structure. The aerodynamic impact of podded landing gear will be large due to the external architecture. This impact can be minimized by placing them at the trailing edge of the wing but is still not negligible [4]. Similar to the wing stowed landing gear, the systems impact is negligible with there only being one axis of actuation.

The last method to be analyzed was a folding style retraction of landing gear. This method also has a minimal impact on the structure of the aircraft because it will be able to fold into a specific position in between the ribs and spars that provide the most optimal structure. Similar to the standard folding gear, this design also has a negligible aerodynamic impact because the structure will be completely contained within the wing body. On the systems side the impact is very large. The added complexity of a multi axis retraction landing gear system will add additional weight to the design and also add additional points of maintenance and potential failure.

Due to the reasons outlined above, the main landing gear will be retracted into the body of the wing toward the fuselage. Although there will be a slight structural impact on the wing, this is able to be worked through and did not outweigh the aerodynamic and systems integration impact that the other two options had on the system. It is also noted that the nose landing gear will be retracted forward into the nose of the aircraft which will allow for a gravity assisted deployment in the event of a failure. The wing design of ribs was altered slightly to ensure the structure is sound and can fit the gear. The final landing gear configuration can be seen in its retracted state below in Fig. 48. Further, a drawing outlining the overall dimensions of the landing gear extended can be seen in section IV.C above.

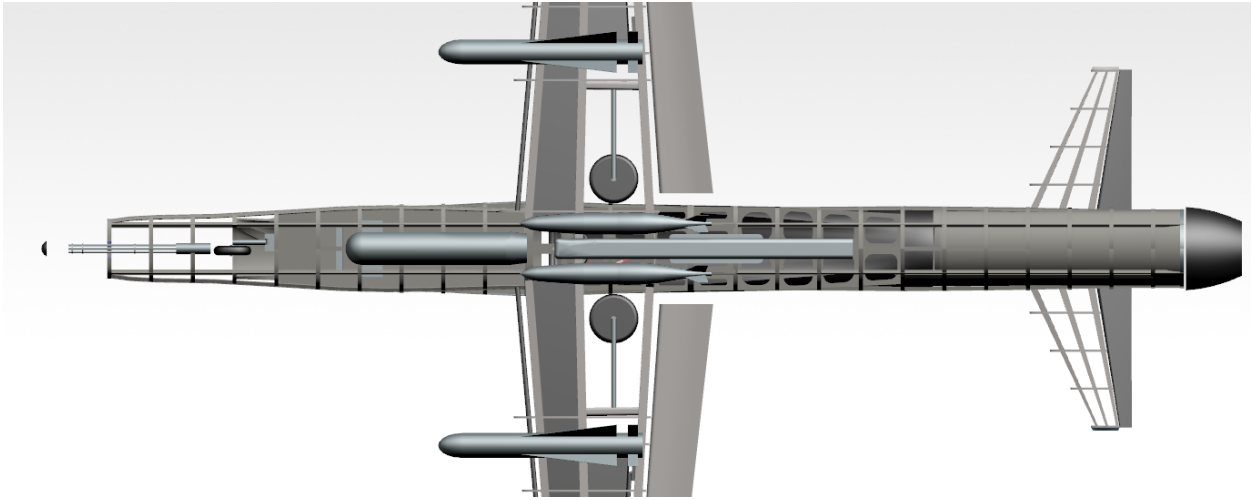


Fig. 48 Landing Gear Stowed

X. Mass Properties

A. Weight Estimations

To estimate the weight of the aircraft, the masses of the components were calculated first. In Part V of *Airplane Design* by Roskam [18], several methods are presented to calculate a component of an aircraft. Multiple combinations of the equations were tested using the parameters of actual aircraft, and the equations that best reflects the actual weight were selected for each components. GD method was mainly used, and few components were calculated using Torenbeek method. For the products with the defined manufacturers, the weight provided by the manufacturer was used. The detailed breakdown of the weights are found in Table 42.

To validate the estimation, the structural weight of Orca was compared with the weight obtained from Siemens NX 12.0, which the percent difference came out to be within 5%. The fuel weight is obtained from the calculation in performance section, Section VII.C, and the payload weight is set by the RFP. The total weight of the crews is set to be 462 lb as the weight requirement for the pilots in Air Force is between 160 lb to 231 lb.[36]

B. Longitudinal Center of Gravity

For the certification process, the center of gravity (CG) has to be defined thoroughly to handle the CG changes resulting from fuel usage, fuel loading, fuel migration due to pitch and roll, and payload drop. In order to find the center of gravity (CG) of the aircraft, the center of gravity was estimated for each component, using the method presented by Roskam Part V [18]. Then, the weights of each components were multiplied by their locations and divided by the total weight to find the CG location of the entire aircraft. The locations of the components were measured from the nose of the aircraft for length and from the ground for height. Detailed CG locations can be found in Table 42.

During the mission, the CG changes as fuel burns and armaments are deployed. As shown in Fig. 49, the CG stays

Table 42 Weights and CG Locations

Component	Weight [lb]	Methodology	CG Location [x,y,z] [in]
Wing	2015	GD	(236.4, 0, 7.896)
Empennage	187.0	Torenbeek	(474.5, 0, 69.58)
Fuselage	1608.2	Torenbeek	(139.2, 0, 25.16)
Landing Gear	685.5	GD	(244.1, 0, 6.241)
Structure Total	4434	-	(212.7, 0, 16.38)
Engine	1050	[11]	(458.3, 0, 34.69)
Air Induction	428.1	GD	(325.8, 0, 54.66)
Fuel System	280.7	GD	(252.0, 0, 27.12)
Propulsion System	116	Torenbeek	(454.8, 0, 34.69)
Powerplant Total	1875	-	(395.0, 0, 38.12)
Flight Control System	464.5	GD	(135.0, 0, 26.92)
Hydraulic/Pneumatic System	261.1	-	(398.8, 0, 15.70)
Electrical System	307.7	GD	(198.6, 0, 11.02)
Instrumentation, Avionics, and Electronics	247.7	GD	(76.27, 0, 14.85)
Air-Conditioning, Pressurization, Anti-/De-icing Systems	146.8	GD	(176.5, 0, 36.76)
Oxygen System	47.60	GD	(177.3, 0, 35.01)
Ejection Seat	350	[8]	(161.7, 0, 25.95)
Auxiliary Gear	85.62	-	(168.0, 0, 29.47)
Paint	69.62	-	(228.0, 0, 46.44)
Integrated gun	250	-	(32.40, 0, 5.000)
Chaff	9.9	[35]	(288, -9.304, 8.815)
Flare	12.9	[35]	(288, 9.304, 8.815)
Fixed Equipment Total	2253	-	(169.6, 0.001604, 20.31)
Empty Weight	8562	-	(242.8, 0, 18.67)
Payload	3000	-	(238.2, 0, -8.26)
Fuel	5380	-	(274.8, 0, 30.52)
Crew	462	-	(181.0, 0, 16.27)
Max Takeoff Weight	17404	-	(243.2, 0, 16.27)

in between the fore and aft CG limit of 19.5% MAC and 44.5% MAC during the flight. The component that affects longitudinal CG is fuel, so the CG limits are calculated by considering the CG at minimum and maximum angle of attack with different load of fuel. As the fuel is consumed from the fuel tank located in the wing to the tank in the fuselage, the CG of the aircraft moves toward aft for the first half of the consumption, then it moves forward as the fuel in the fuselage is fully consumed.

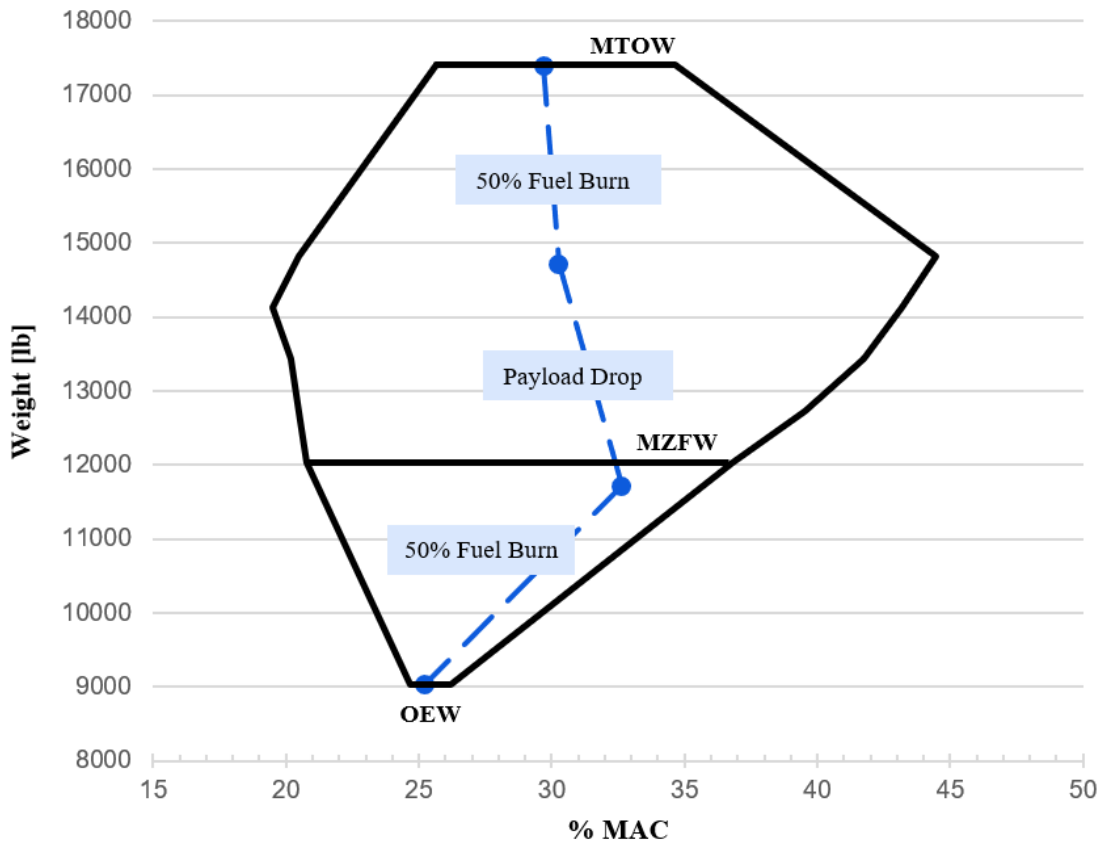


Fig. 49 Longitudinal CG envelope

C. Lateral Center of Gravity

According to AIAA RFP[1], the designed aircraft should be able to carry 3,000 pounds of armaments, which are consisted of rail-launched missiles, rockets, and bombs. The armaments change the lateral CG of Orca when they are deployed. The armament location of Orca is shown in Table 43. Also, as mentioned in previous section, fuel movement is a significant factor to the CG movement. In addition to the ordnance, fuel movement at loading and in flight was considered to find the lateral CG envelope of Orca. The lateral CG envelope is drawn in Fig. 50. To find the maximum CG imbalance, the CG change due to ordnance deployment was calculated after 50% of the fuel burn, and to calculate the in flight fuel movement, 15, 30, and 40 degrees of rolling were considered without payload weight.

Table 43 Armament Locations

Location in y-axis [in]	Weight [lb]
-201	190
-134	310
-89	500
-30	500
30	500
89	500
134	310
201	190

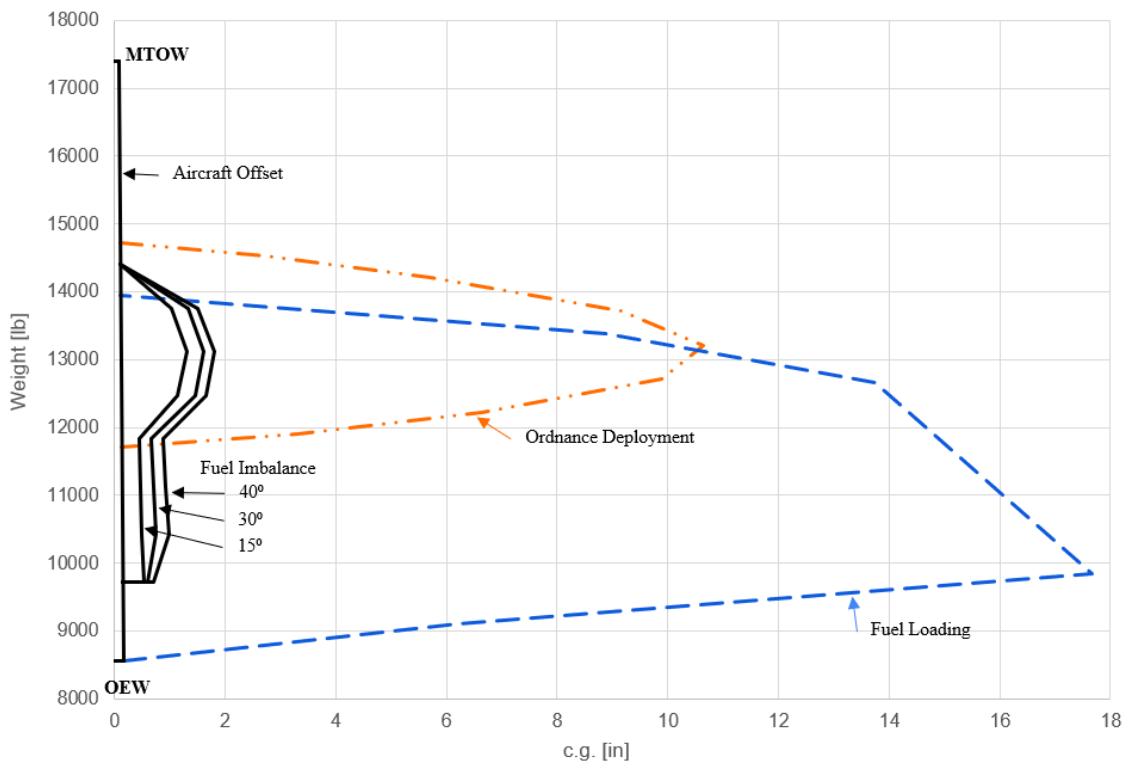


Fig. 50 Lateral CG envelope

The maximum CG change occurs during the fuel loading. When the fuel is loaded starting from the tank in the wing to the tank in the fuselage, the maximum CG change of 17.66 inches is recorded. Considering the location of the landing gear, this CG location can be supported sufficiently. Another factor that causes big lateral CG imbalance is

armament deployment. When all armaments under a wing are deployed at once, a maximum CG change of 10.64 inches occurs. This imbalance may be a problem when the armaments are deployed at a low speed and altitude, for example, during the loitering. Lastly, the fuel imbalance during the flight was calculated at different rolling angles. Comparing to the other factors, the change due to rolling is small. At 40 degrees of rolling, the maximum CG imbalance is 1.8 inches from the center of the fuselage.

D. Trade Study: Ordnance Location

In addition to the analysis that was done for lateral CG envelope, the CG imbalance due to ordnance location was tested. To find the relationship between ordnance CG location and the CG change of the entire aircraft, Figure 51 was drawn. The maximum CG change increases linearly as the armament CG moves away from the fuselage. As discussed in previous section, the ordnance configuration of Orca, Table 43, has the CG location of 92.82 inches from the center of the fuselage, having 10.64 inches of imbalance when all payload are deployed. To minimize the CG change, the location of the ordnance was chosen to make the ordnance CG close to the fuselage while distributing the load across the wing.

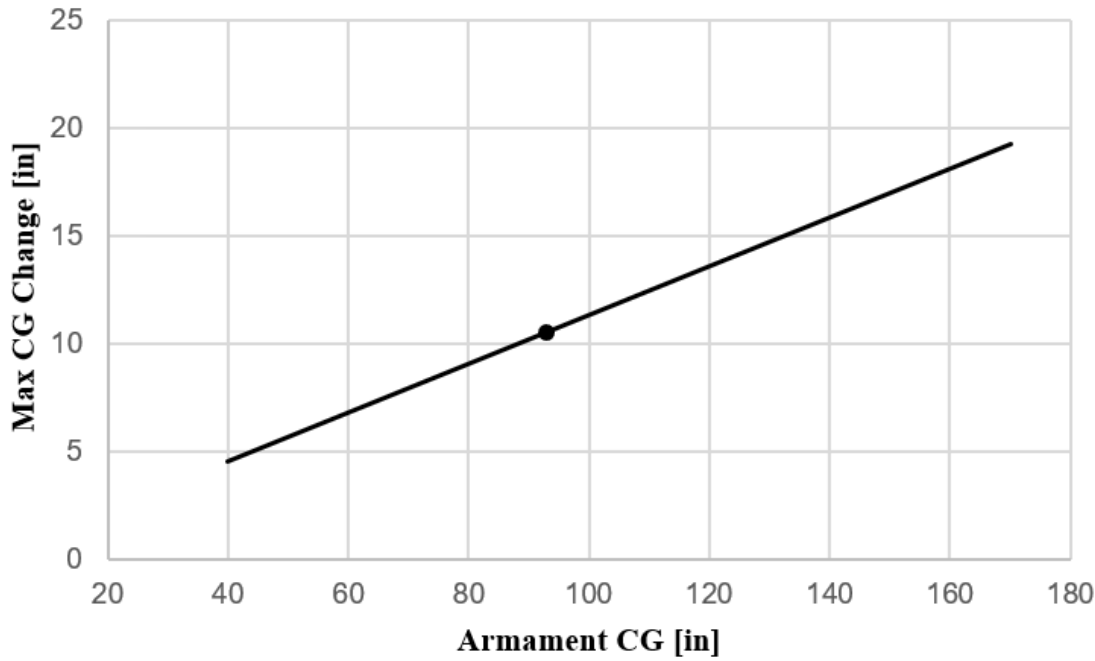


Fig. 51 CG Imbalance Due to Ordnance

XI. Auxiliary Systems

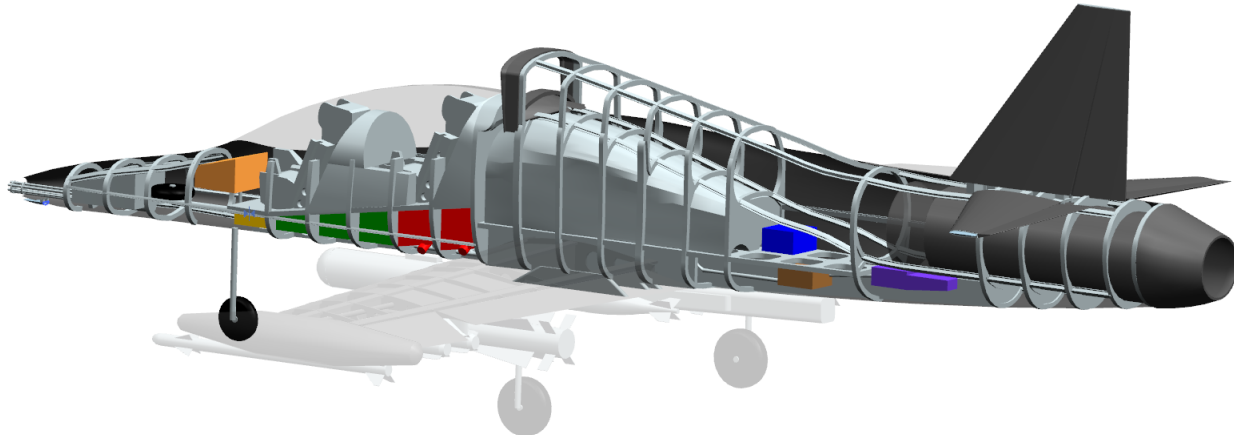


Fig. 52 Isometric view of all major auxiliary systems components

Within the Orca design, there are multiple auxiliary systems that help supplement functions necessary for maintaining the integrity of the aircraft. Above, in Fig 52, the major component locations of the auxiliary systems are highlighted. The colors correspond to components according to the table below.

Color	Component
Orange	Radar, Sensors
Yellow	Batteries
Green	ECS and Hydraulic Reservoir
Red	Chaff/Flare storage/deployment
Blue	APU
Brown	ECU
Purple	FCU

Table 44 Color Legend for Fig. 52

A. Fuel System

The fuel system consists of one main tank in the fuselage, one tank in each main wing, and two external tanks on the ends of the main wings. Performance calculated that the fuel weight required for the design mission is 5,380 lb. Using a fuel density of $50.8 \text{ lb}/\text{ft}^3$ and a margin for unusable fuel of 8% (estimated using Raymer [4]), the fuel volume required can be calculated using the below formula.

$$\text{Fuel Volume Required} = \frac{\text{Fuel Weight Required}}{\text{Fuel Density}} * 1.08 = 114.5 \text{ ft}^3 \quad (1)$$

As there was not enough empty room would in the wings and fuselage to carry that much fuel, the external tanks were added to compensate. These external tanks are drop tanks and as such are detachable. This allows for them to be taken off and stored during ferry missions where the extra fuel is not needed. This provides a fuel savings of 330 lb of fuel every time this is done. The layout of the fuel tanks is detailed below in Fig. 53.

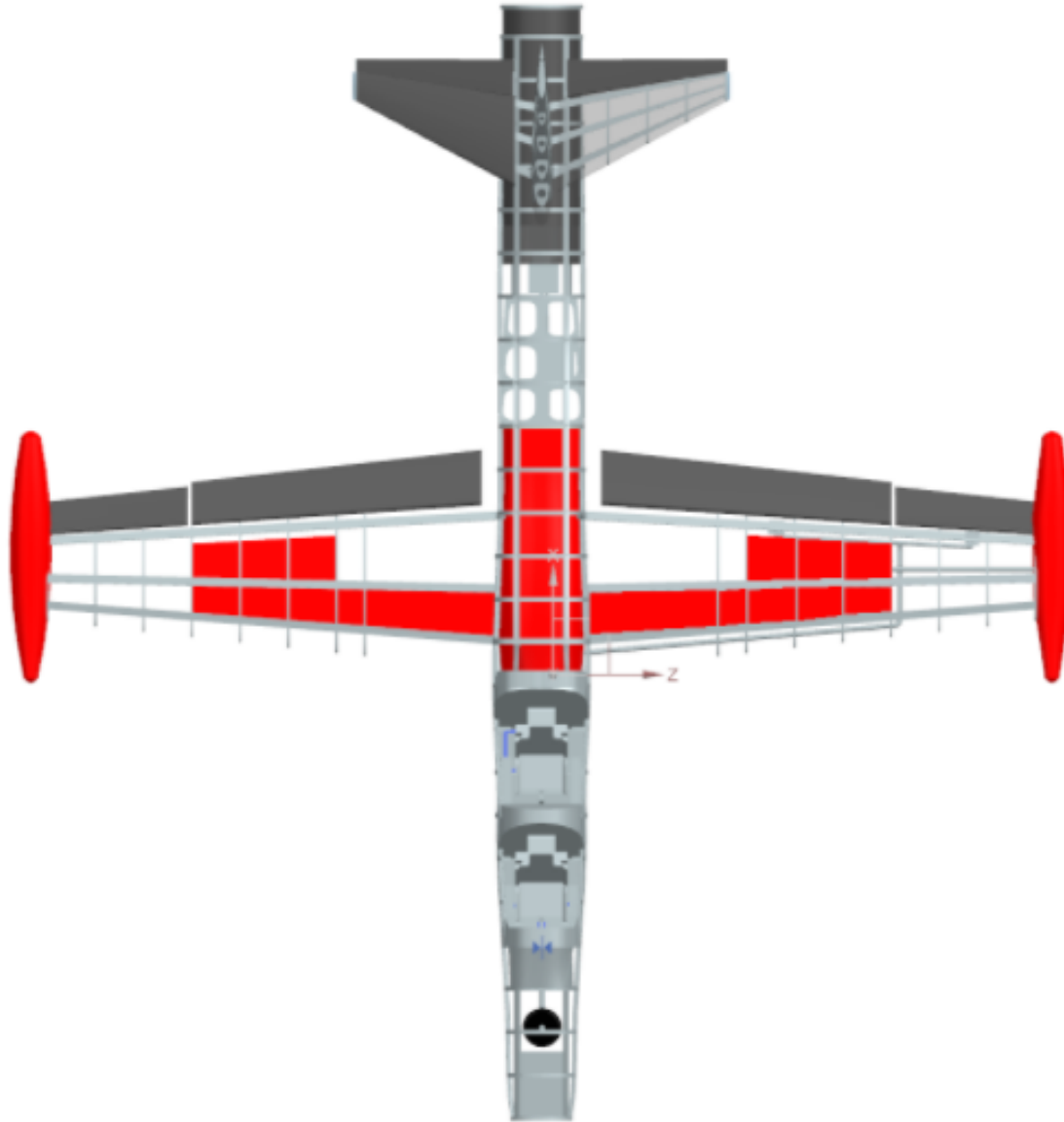


Fig. 53 Fuel Tank Layout

The fuselage tank is aluminum while the wing fuel tanks are rubber tanks. Using rubber tanks in the wings gives the tanks a resealing factor if damage is taken and minor punctures occur during flight. This helps prevent fuel loss as well

as reducing the risk of fires. The downside to this is that additional fuel is unusable due to the fuel being unable to be pumped out. This fuel loss is considered in the fuel volume calculation as a correction factor of 1.08 [4] where the 8% is the estimation for unusable fuel given above. The fuselage tank is solid because the added durability benefit of being rubber is considered unnecessary due to the more protected placement of the tank. The total fuel volume from the system shown above is detailed below in Table 45.

Type	Fuel Volume
Fuselage	65.82 ft ³
Wings (x2)	17.29 ft ³
External (x2)	12.93 ft ³
Total	126.24 ft ³

Table 45 Fuel Tank Volumes

The calculated fuel volume allows for a 9% margin. This is allowed as adverse weather conditions, pilot inefficiencies, and extra maneuvers need to be accounted for, especially due to the nature of performing close air support missions in contested areas.

The fuel is controlled using a system of multiple fuel pumps and check valves between each tank. The refuel point is on the starboard side of the aircraft on the main fuel line from the main fuel tank to the main engine. Fuel is dumped in emergency situations or when it is deemed necessary to lower the weight during flight or for landing. The complete system of check valves and pumps is shown below.

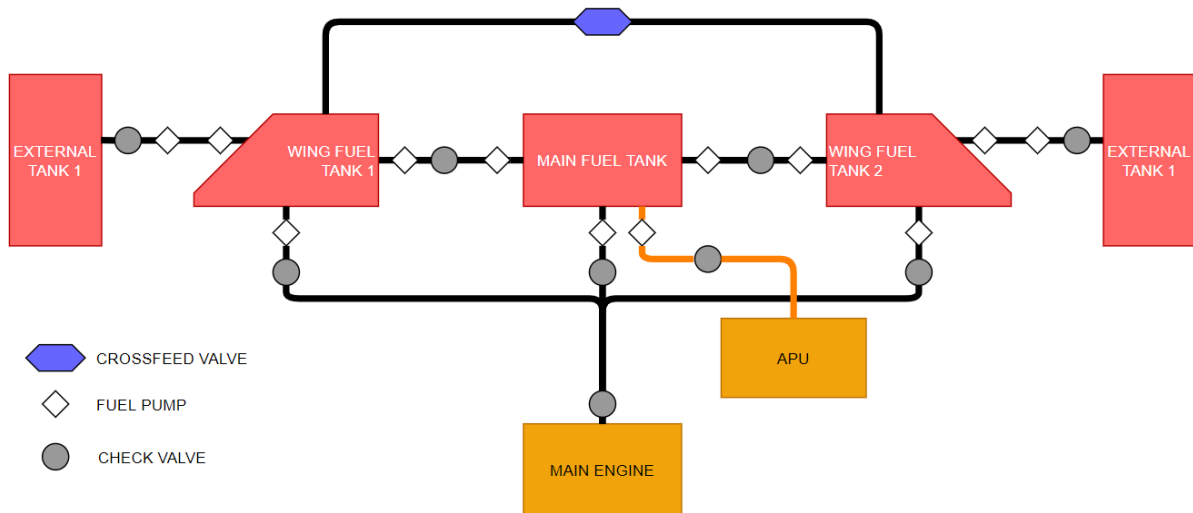


Fig. 54 Diagram of Fuel System

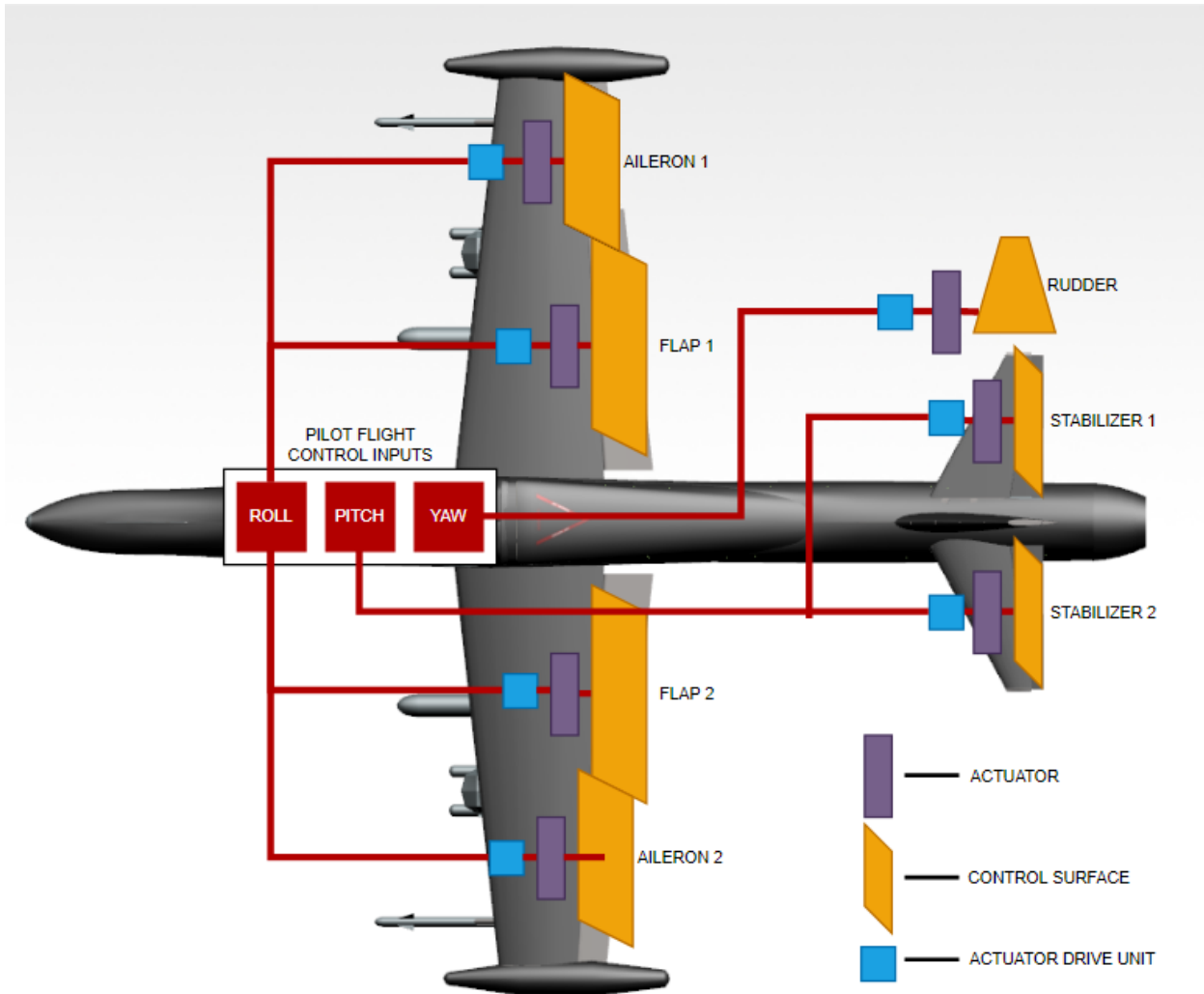


Fig. 55 Flight Control Diagram

B. Flight Controls

This aircraft will utilize a fly-by-wire system of flight controls. A fly-by-wire system uses a primary flight computer that sends electronic signals from the pilot controls to the control surfaces. There are a few reasons why the fly-by-wire system is a better choice than the conventional flight control systems for our design. Boeing gives six reasons to prefer this type of system: overall weight reduction, integration of several systems into one, better handling of the aircraft, ease of maintenance, ease of manufacturing, and greater flexibility with changes and integration of new systems into the aircraft. While the 777 is a commercial aircraft, the qualitative benefits outlined by Boeing are desirable for achieving a 'best value' design. While the manufacturing cost of the system is increased over a push-pull rod system, savings from reduced weight and maintenance ease are gained when the aircraft is in service. Cost will therefore be reduced over time during the proposed aircraft's service life.

Fly-by-wire also has some added safety benefits that come along with it. Because the system is running all of the

controls through the primary flight computer, it is easy to enact safety protocols that aid the pilot in emergency situations as well as keeping the aircraft out of emergency situations. The fly-by-wire system will be a 4-channel system that will run four times to each actuator in order to provide redundancy in the design and increase the overall safety. Fig. 55 shows a basic diagram of how the fly-by-wire system works and interacts with the rest of the design and Fig. ?? shows this system implemented in the model made for the Orca. This electronic system communicates the inputs to the actuators in order to obtain correct control output at the specified time. In the system, the flaps (one per wing), ailerons, rudder, and each side of the elevator will each have one actuator.

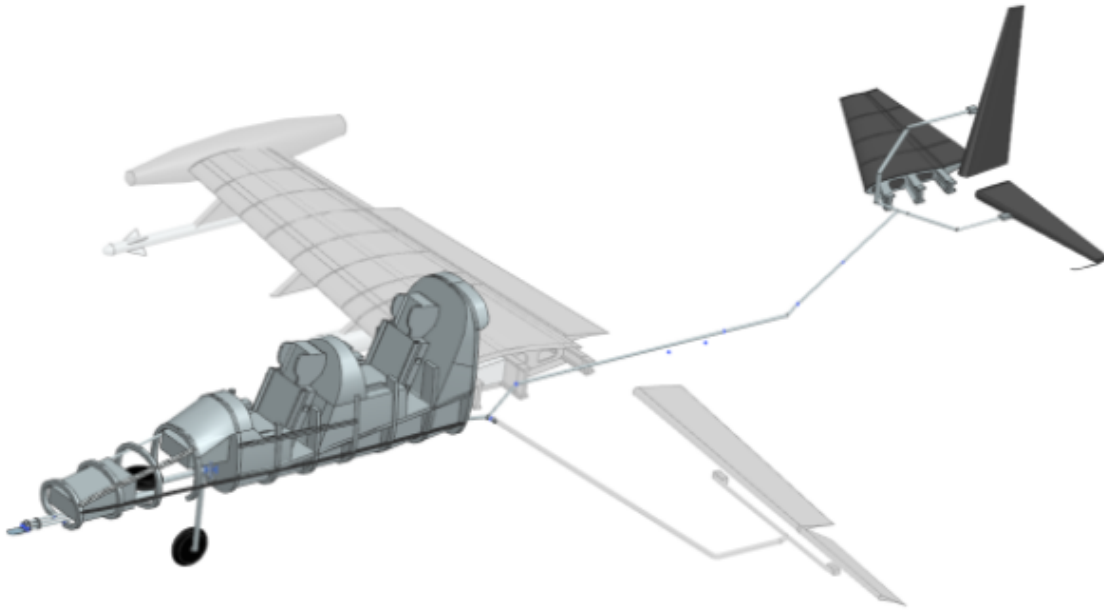


Fig. 56 Flight Control Model

Alongside the fly-by-wire system will be a power-by-wire system. This system is a redundant channel that runs to separate, electric actuators that are placed alongside the fly-by-wire electrohydraulic actuators. The benefits of a power-by-wire redundant system is additional redundancy in the case of hydraulic failure. The power-by-wire system is also comparatively light to the hydraulic system, so it is a good compliment. The power-by-wire system is also more responsive, than the fly-by-wire system, which is important in emergency situations where the fly-by-wire system fails.

C. Engine Controls

The engine control system on the proposed aircraft utilizes FADEC. The ECU is able to optimize fuel consumption, engine wear, and thrust output and calculate the adjustments to engine operating parameters. There are 2 ECU's in the aircraft for redundancy and they are located on the engine. However, the ECU's are meant to be used at all times due to the benefits of optimization described previously. The ECU system is shown in Fig. 57.

The ECU receives inputs from the air data collected by probes by the inlet and throttle. The fire switch opens the fuel valve and the fuel system lets fuel flow and publishes information on the fuel flow to the ECU. The FCU (Fuel Control

Unit) receives information from the ECU and fuel system to determine how much fuel the fuel pump should inject into the engine and how much air should be used as bleed air. There are also probes inside the engine that communicate air data and engine performance data inside the engine to the ECU.

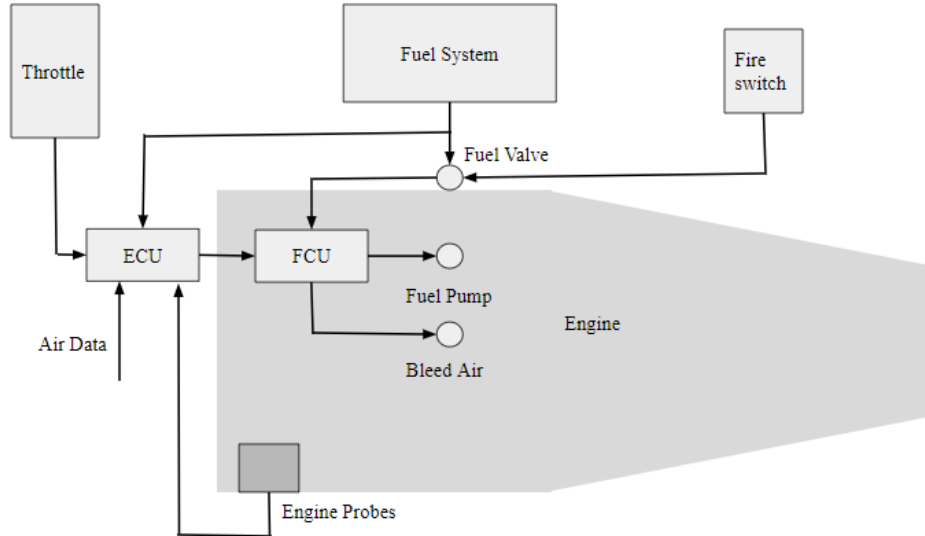


Fig. 57 ECU Diagram

Incorporating this system into the Orca, the locations of each system component is shown below in Fig. 58.

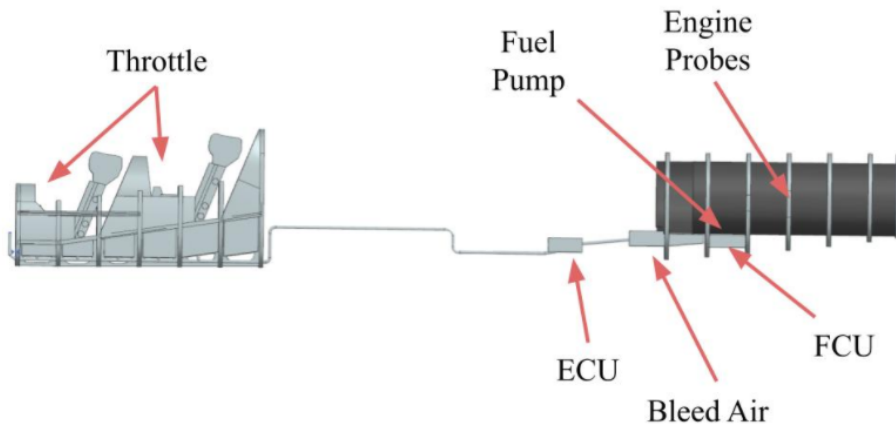


Fig. 58 ECU component locations

D. Hydraulics

The hydraulic system of this aircraft will be used for wheel braking, nose wheel steering, flight control actuation, and high lift device actuation. Figure 59 shows a basic layout of the hydraulic system layout of the Orca. This system offers redundancy in the case of single failures and leaks with two independent channel failures possible without complete loss of system control. To verify the location of the actuators, Actuator Drive Units (ADUs) are used on each channel of

the fly-by-wire system. An additional redundancy is given to this system in the form of the electric actuators for the power-by-wire system outline previously.

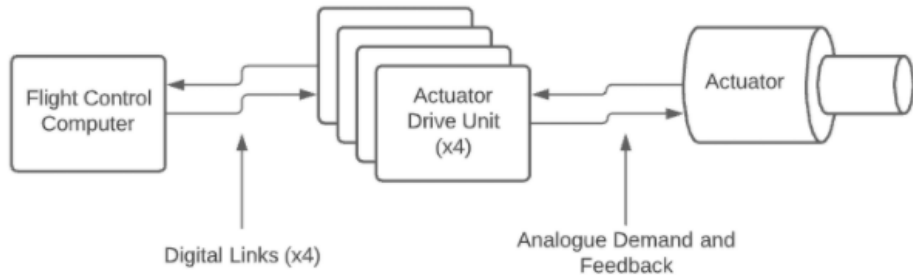


Fig. 59 Hydraulic System Diagram

E. Pneumatics

The pneumatic system provides air pressure to various parts of the aircraft. It does this by bleeding air out of the engine and supplying it to the necessary systems. Those systems include the environmental control system, pressurization, and engine starting. Figure 60 shows a simple diagram of the general layout of the pneumatic system.

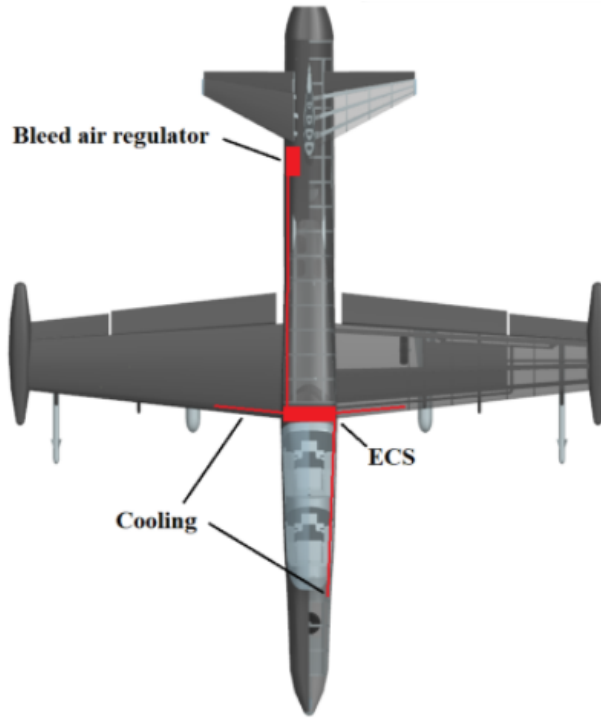


Fig. 60 Pneumatic System Diagram

F. Electric System

The electrical system consists of a generator driven by a drive shaft connected to the main engine and a battery for ignition and emergency situations. The efficiency loss from the Engine due to the power draw of other systems is on an

order of magnitude lower than the power required to produce the thrust necessary to meet performance expectations. An auxiliary power unit (APU) was installed alongside the main engine in order to power a separate generator. This allows for a 2 bus system, allowing for one system failure while still maintaining system integrity. In the case of both main and APU generator failure, there are two batteries installed underneath the cockpit which aid in both these emergency situations as well as ignition of the engines. A layout of the electrical system structure is shown below.

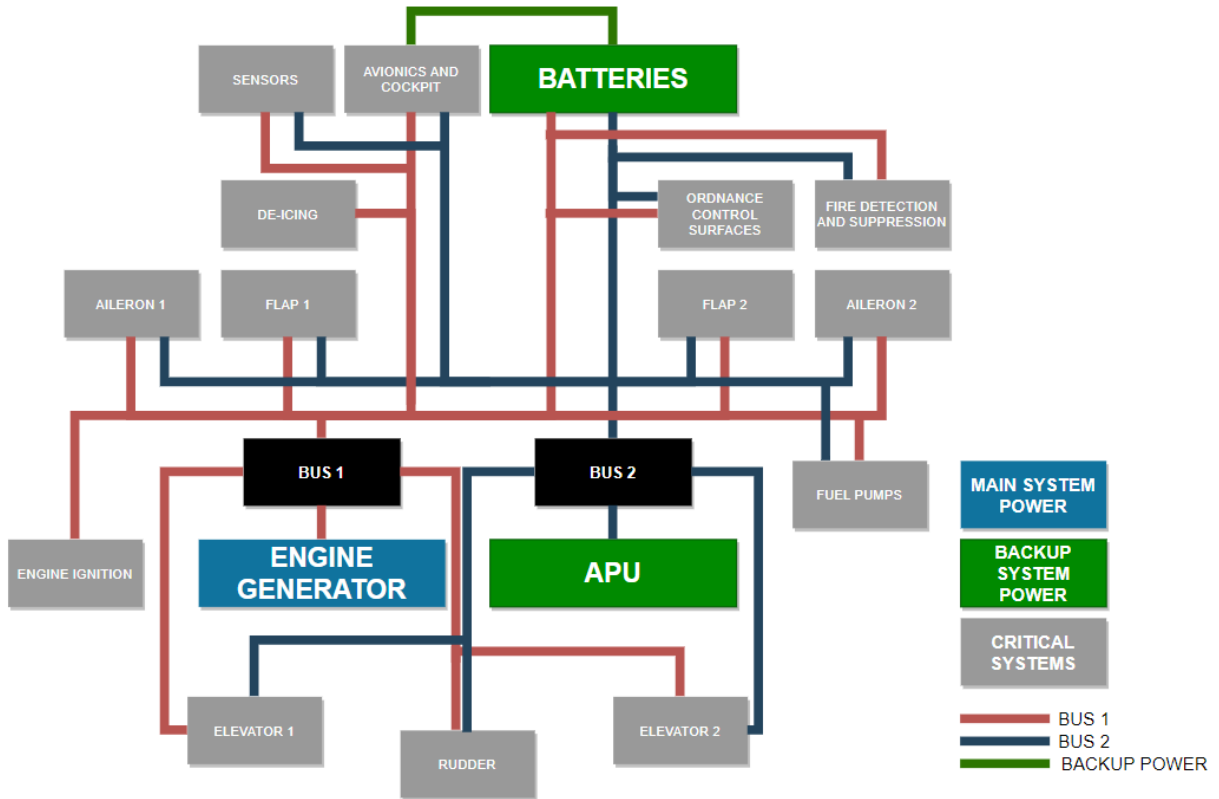


Fig. 61 Electrical System Diagram

G. Avionics

The avionics suite chosen for the proposed aircraft is the CMC Cockpit 4000 [37]. A suite was chosen over individual parts since a suite is guaranteed to be compatible with its parts while a part by part avionics approach does not have that same guarantee. Some advantages of this avionics suite is that it has a centralized cockpit management and 3 master modes for the pilot to chose as they are performing tasks: Navigation, Air-to-Air, and Air-to-Ground. The CMC Cockpit 4000 uses HOTAS and is made to use many standard interfaces like MIL-STD-1553B, Ethernet, Discrete signals, and others. There will be two integrated avionics computers for redundancy. This avionics suite has a modular design meaning the parts desired can be chosen while the parts that are not needed can be left out. Table 46 shows the parts and software programs that were selected for the Orca. In addition to the CMC Cockpit 4000, the Litening Targeting Pod was used for ordnance targeting [38]. The Litening Pod is located just behind the nose landing gear.

Table 46 Avionics

Name	Name
Continuously Computed Impact Point (CCIP)	Continuously Computed Impact Line (CCIL)
HUD Repeater	Primary Flight Display (PFD)
Navigation Display (NAV)	Tactical Situation Display (TSD)
Stores Management System (SMS)	Communication Navigation Management (CNM)
Engine Instruments Caution Advisory System (EICAS)	Data Transfer System
HUD Display	HUD Camera
Multi-Function Display (MFD)	Litening Advance Targeting Pod

The trade study shown in Table 47 was conducted to identify which targeting pod would be the best for the Orca. The considerations for this trade study are relevance of purpose to the Orca's design mission, weight, length and width. Most of the pods' purpose matched very well with one being over capable. The lowest weight possible was desired so a minimal amount of thrust would be spent to carry the pod. The lowest possible length and width were also desired to reduce drag.

Table 47 Targeting Pod Trade Study

	Purpose	Weight	Length	Diameter	Score
Weight Coefficient	2	3	1	2	
Litening	3	3	3	1	20
Sniper Pods	2	2	2	3	18
TIALD	3	1	1	3	16

Fig. 62 shows the avionics lay out for the Orca. The Litening Pod is not included in this layout since it is outside the cockpit.

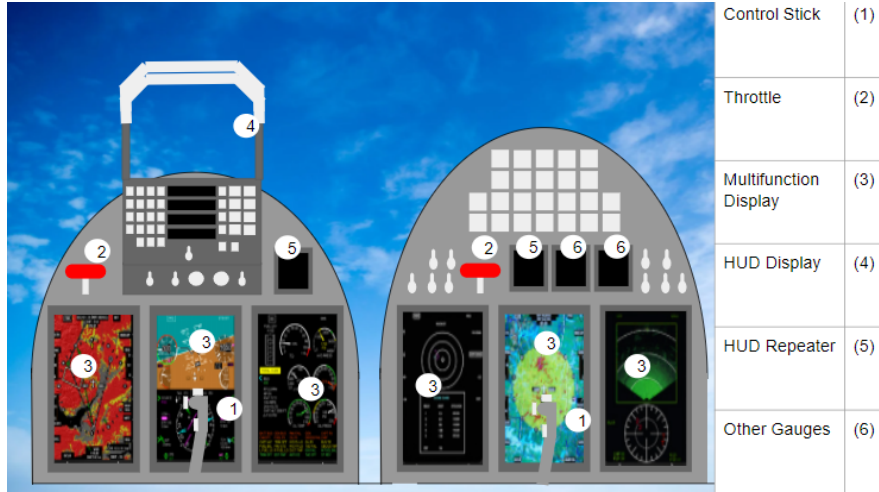


Fig. 62 Avionics Layout

H. Emergency Systems

A zero/zero ejection seat system will be included on this proposed design. The seats are angled at 20 degrees for pilot g-force tolerance. Angling the seats more would increase the g-force tolerance further but it has been shown in designs like the F-16 that this may induce neck pain from incorrect posture while sitting. The process of pilot ejection is covered in Section IV.B.

I. Environmental Control System

The environmental control system (ECS) is responsible for a variety of functions. First and foremost, the ECS provides an environment within the cockpit where the pilots can operate the proposed aircraft in a comfortable cabin. ECS utilizes pneumatic air in order to cool both the cabin and other specific systems. These systems that are given cooling include: avionics, the M61A2 integrated gun, the engine, and the ECS itself.

XII. Cost Analysis

A. Inaccuracies

Cost estimation for the aircraft was conducted using Roskam [18] based around the requirements listed in the RFP from AIAA [1]. This model is based mostly around the aircraft maximum takeoff weight, maximum velocity, and number of aircraft being produced, these categories are weighted toward cost with considerations to aircraft development, production, and operational costs from 1989. The method requires a clear idea of the price of avionics development and pricing beforehand which is difficult to have at this point in the design process. These things lead to a certain degree of inaccuracy but will produce a reasonable approximation of the price of an aircraft in 2021 dollars.

B. Major Costs

The roskam[18] method provides estimation of the cost of research and development for an aircraft with the same parameters that have been discussed in the report. The estimation is summed using calculations of the cost of airframe engineering and design, development support, flight test airplanes, flight test operations, and financing.

The total operations cost of the aircraft is made up of the price of all materials used in the upkeep of the aircraft including manhours of aircrews and maintenance, this total is about 2.1B USD over nearly 650,000 total flight hours for the program. This results in a cost of approximately 3,276 dollars per flight hour.

The production cost is a measure of the costs of a production run of aircraft over the length of the program. For this analysis 25 years was chosen as the length for the given 50 aircraft production run based on the approximate program lengths given in the appendix of Roskam II [18]. The major considerations of production are the cost of producing aircraft through engineering, tooling, manufacturing and cost of personnel. This includes the cost of oil, loss rate of aircraft and spares. For this aircraft based on its parameters the major costs are listed in table 49.

Table 48 Major Costs For a 25 Year Program (Millions of Dollars)

Category	Cost
RDTE	\$408.2
Operations	\$2,123.4
Acquisition	\$917.22
Unit Price per Aircraft	\$26.51

C. Cost Reduction Methods

To market this aircraft program to a wide range of countries, designing for value and is a major priority. Orca incorporates multiple cost reducing design methodologies but further methods are worth considering before any actual production occurs and are listed in Nicolai and Carichner [16]. One such method is to reduce the total development cost by combining the engineering and quality testing into one process rather than two; the cost of quality testing is over \$140M which is a small percentage of the RDTE but if reduced would result in a lower unit cost. Another method is to make the aircraft tooling multipurpose, many aircraft have complex maintenance requirements and have high cost per flight hour and require more man hours to keep running as well. To reduce this, the parts on the aircraft can be both symmetrical and use many common parts therefore reducing the amount of tooling to purchase and resulting a sharp decrease to program cost.

D. Unit Cost

Unit cost was estimated using the total cost of RDTE, Acquisition, and Operations for the total number of production aircraft. Multiple production quantities were considered for Orca, decreasing the unit cost as total production increased making the price more competitive to other aircraft in this class. 200 aircraft was decided to be a reasonable goal as the Super Tucano has around that number in production right now. At this production point the Orca is much cheaper in 2021 dollars.

Table 49 Unit Cost of Aircraft Based on Production

Production Aircraft	Cost
50 A/C	\$ 26.51
100 A/C	\$ 19.71
150 A/C	\$ 17.02
200 A/C	\$ 15.52
250 A/C	\$ 14.56
300 A/C	\$ 13.88

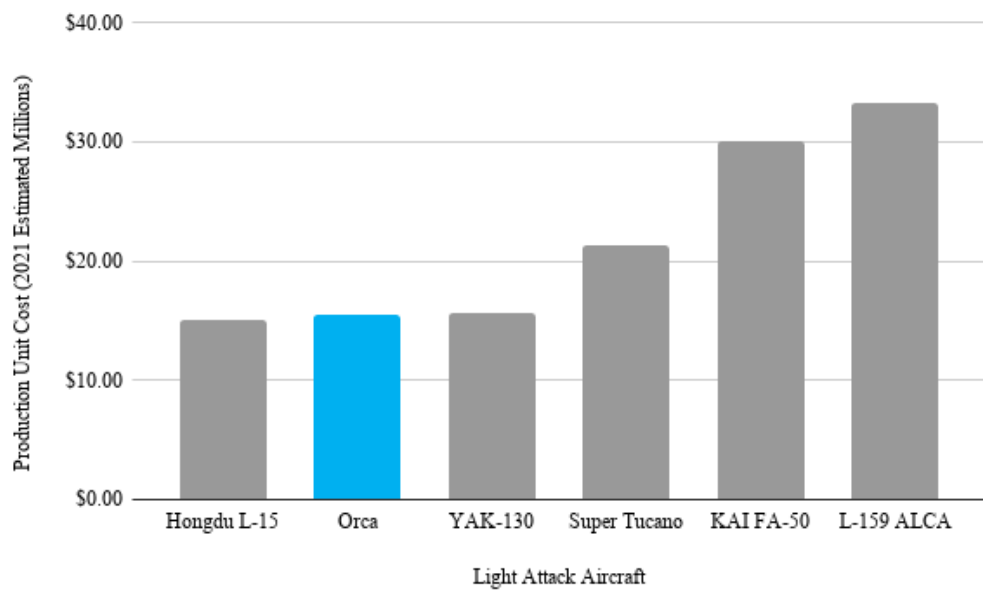


Fig. 63 Comparison of Unit Cost to Similar Aircraft

XIII. Ordnance

A. Requirements and Design

The requirements for ordnance listed in the RFP from AIAA are to have an integrated gun, a maximum of 3000 pounds of ordnance and a maximum bomb weight of 500 pounds per bomb [1]. The weight of the gun was not part of the 3000 pounds, but the ammunition is included since the ammunition is expended during a mission. These requirements drove design by making the bombs and missiles sought after be relatively small. The decision was made to not use rockets due to their high drag on the aircraft. As the Orca is not a fighter, there are not many air-to-air weapons and is quite weak to enemy fighters. The proper situations to use the Orca are missions into uncontested space or contested space with a small escort or other assistance. The only air-to-air offensive capability the Orca has is a sidewinder missile on the farthest pylon on each wing [38]. The lack of air-to-air offensive capabilities is due to the weight limit for ordnance. The more weight given to air-to-air weapons reduces the amount of weight for air-to-surface weapons, which is what the Orca is designed for. The two air-to-surface missiles chosen for the Orca are the AGM-65 Maverick and the Brimstone missile. The Maverick is a close air support weapon that has a wide range of targets including bunkers, tanks, radar sites, and more [38]. The Brimstone is much smaller and is specialized for tanks [39]. The Brimstone is launched from the AGML III launching rack that can hold 3 missiles and the launching rack is mounted in place of the pylon. The weight of the AGML III rack is 76 pounds. The two bombs used for the proposed aircraft are the GBU-39B Small Diameter Bomb (SDB) and the BLU-111/B [40], [41]. Both of these bombs are guided since guided bombs hit their targets at much higher rates than unguided bombs [42]. The SDB is much smaller than the BLU-111/B, which is a modified Mk 82 bomb, but comes in sets of 4 on the BRU-61/A bomb carriage. The integrated gun requirement will be satisfied by having one M61A2 integrated in the nose, along the bottom of the fuselage, and in front of the landing gear shown in Fig. 64 [43]. The gun can be used to deter enemy fighters, however its real purpose is to destroy lighter enemy vehicles with its 20mm ammunition. The gun specifications are shown in Table 51. In order to avoid protruding outside the fuselage and causing aerodynamic concerns, the gun is stowed inside the nose and has a slot cutout in front of it for firing out the front. Table 50 shows the specifications of the ordnance used on the proposed aircraft.

Table 50 Ordnance Specifications

Name	Weight [lb]	Length [in]	Diameter [in]
Aim-9 Sidewinder	190	113	5
AGM-65 Maverick	485	98	12
Brimstone	108	71	7
GBU-39B	285	71	7.5
BLU-111/B	500	92	11

Table 51 Gun Specifications

Name	M61A2
Gun Weight [lb]	202
Length [in]	71.9
Barrel Diameter [mm]	20
RPM	4000/6000
Bullet Count	250
Ammunition Weight [lb]	141

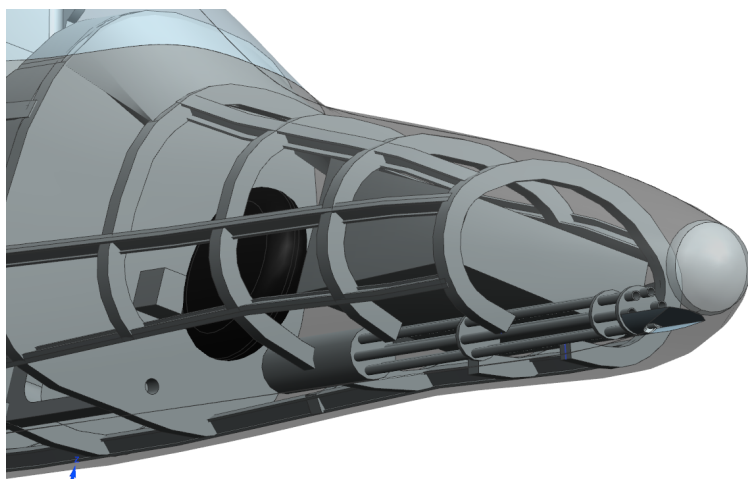


Fig. 64 Gun Location

B. Ordnance Configurations

Figure 65 shows the different pylons or launching platforms to launch ordnance from. Table 52 shows the different ordnance configurations that all satisfy the requirements set in the RFP. The configuration naming system uses a C for contested air space and U for uncontested airspace. Configurations C1 and U1 are designed for missions targeting structures, C2 is designed for anti armor missions, while U2 and U3 are designed to be more flexible and balanced in terms of targets. The difference between U2 and U3 is that U2 uses more bombs that are smaller, so U2 is better for hitting multiple smaller targets than U3.

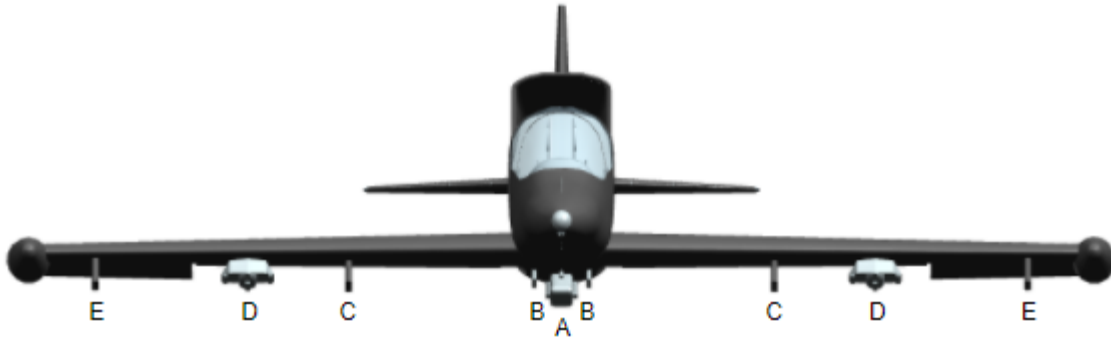


Fig. 65 Pylon Locations

Table 52 Ordnance Configurations

Name	A	B	C	D	E	Total Weight [lb]
C1	GBU-39B (4x)	none	BLU-111/B	Brimstone (1x)	Aim-9	2877
C2	none	BLU-111/B	AGM-65	Brimstone (2x)	Aim-9	2923
U1	GBU-39B (4x)	none	BLU-111/B	Brimstone (3x)	none	2929
U2	GBU-39B (4x)	none	AGM-65	Brimstone (3x)	none	2899
U3	none	BLU-111/B	AGM-65	Brimstone (3x)	none	2759

C. Inaccuracies

The first notable inaccuracy is the weight of the Brimstone launching rack. This was calculated by using the weight ratio of the SDB to its launching rack and comparing that to the weight of three Brimstone missiles. Most of the specifications given for the different ordnances are older since the USAF and Royal Airforce are not willing to publish their up to date data. This means they could be lighter if technological advancements were made to make things smaller or they could be heavier if the new devices are added that did not exist when the data was published.

XIV. Survivability

The design philosophy for survivability considerations is centered around the discussions found in Roskam Part IV Chapter 13 [18]. In general, survivability considerations are heavily influenced by the airworthiness of the design and whether it is able to meet all requirements set out. In this way, we are then limited by how safe we can make the design. As it is with the AIAA RFP [1], we have conflicting interests in both making the design "best value" by lowering the cost and by having "considerations" for survivability, which would increase the cost. Therefore, we will begin by employing the standard design considerations for survivability in military aircraft and add more as seen necessary. This will keep our cost as low as possible while meeting the standards for survivability concerns seen in modern aircraft.

We then must consider what sources do we need to protect the pilots and the plane from? The answer is that there are two sources: crashes and enemy ordnance. The first source can be accounted for using ejection methods which are accounted for in the design. The Orca is also built in such a way as to ensure pilot safety during these emergency situations. This has been discussed previously in section IV.B (Interior Design).

For the second source of enemy ordnance, the Orca must consider radar detection, radar-guided weaponry, infared detection, infared-guided weaponry, acoustic detection, and other non-guided weaponry. We will split these sections into the survivability considerations taken by the Orca: radar, infared, and other.

A. Radar

In order to prevent detection from radar, a few considerations are employed in the Orca design. The most prominent of these features is the unique placement of the Orca's inlet. Inlets are considered to be one of the worst aspects to the acoustic profile of a plane, both for audible and inaudible waves [4]. Radar waves bounce around the inlet and scatter in all directions in front of itself, making the plane much more detectable if radar manages to make it inside the inlet. However, by placing the inlet on top of the airplane, the chances of radar reaching inside the inlet from a ground source is drastically reduced. This placement reduces the need for additional radar wave emission reduction methods such as RAM paint or inlet coverings. Both of which would increase the cost and in the case of inlet covers, would decrease the performance of the design. The final design consideration that aids in the radar detectability of this design is the shape of the inlet. The inlet shape was made to be flush with the fuselage at its sides as shown in Fig. 12. Radar waves are more easily detectable when design features of aircraft make concave corners or cups (this is why inlets are considered the worst aspect to aircraft radar detectability). Previous iterations of the inlet were a simple circle design which created a cusp with the fuselage. This feature was eliminated so as to limit the number of design features on the fuselage that would propagate radar waves to hostile forces.

Chaff is the chief countermeasure employed in order to protect the Orca against radar-guided weaponry. Radar-guided missiles may be employed against this aircraft and in that case the only way to prevent detection altogether is by jamming or by deploying chaff. Since jamming is more costly both in equipment needed as well as power draw required (on the order of kW), chaff will be employed instead. This option is much cheaper overall and has a low space cost inside the fuselage. The pilot will control when to deploy this if it is detected by the instrumentation if a radar-guided missile is approaching.

B. Infared

The heat signature of the aircraft is another concern. In order to prevent infared detection two considerations are taken into account. First, the use of pneumatic air will be used to cool the engine. This cool air will also be mixed in with the exhaust air, which will act as a form of optical blocking of the exhaust. This is a cost-effective method for reducing the radar signature as it does not require paneling to cover the engine that would require maintenance. Instead,

the existing pneumatic system will be employed to act as an ECS for the engine.

Flares will also be at the pilot's disposal if an infrared missile is detected. This is a common countermeasure along with chaff that allows for some amount of protection in the event that ordnance has been deployed against the aircraft. The locations for chaff and flare deployment are shown above in Fig. 52. These countermeasures are deployed in such a way as to avoid both structures and ordnance behind the deploy points. To do this, the flares and chaff are deployed on both sides at a 45 degree decline to the horizontal of the aircraft.

C. Acoustic

The audible sound profile of the aircraft is another concern. Because of the nature of the turbofan engine, some amount of control is granted as to where the sound is directed. Because the inlet is placed on top of the fuselage, the sound will be directed to the front and back of the aircraft. Because there is only one inlet, this also means that all sound from the engine will be mainly out the front and back of the aircraft. An additional benefit to the inlet placement is that because the inlet is on the top of the fuselage, direct noise waves will not reach ground targets and instead will be bounced off the top of the fuselage. Propagated waves will still reach ground targets, but these waves are reduced in noise level compared to direct noise.

D. Other

Included in the cockpit for each pilot's headgear include the capability for night vision goggles. These will allow for better visibility at night so that the Orca is not limited to daytime missions only. Utilizing the cover of night also helps increase the survivability of the design as it is visually harder to detect aircraft during these times.

The armor employed on this aircraft includes both integrated and exterior armor. The integrated armor will be placed in key locations on the aircraft to minimize the chances of a complete loss of control due to heavy damage sustained. These locations include: the bases of the main wings, the nose of the plane, and around the engine. This is shown in Fig. 66.

The exterior armor is bolted on to the side of the aircraft next to the fuselage fuel tank. The exact location is shown below in Figure 67. This armor is included in this location in order to protect the fuel tank inside the fuselage (shown Section XI.A). Using exterior armor decreases manufacturing costs and also allows for a different configuration depending on the mission. For instance, it may be determined that during the ferry mission (outlined by the AIAA RFP), armor is deemed unnecessary as this mission is a low-risk flight. This reduces the weight and therefore decreases the fuel consumption of the design during this mission. The downside to this design is that the aerodynamic profile is negatively impacted when the armor is attached. However, the aerodynamic effect was deemed minimal enough that the overall fuel consumption increase caused by this would be negligible enough that the cost savings during the ferry mission would more than make up for the cost of using armor during the design mission. The choice to add external armor also aids in the maintenance ease and manufacturing costs associated with this design. As the goal of this project is to provide a

"best value" design (as per the AIAA RFP [1]), the benefits of this design therefore aid in accomplishing this goal.

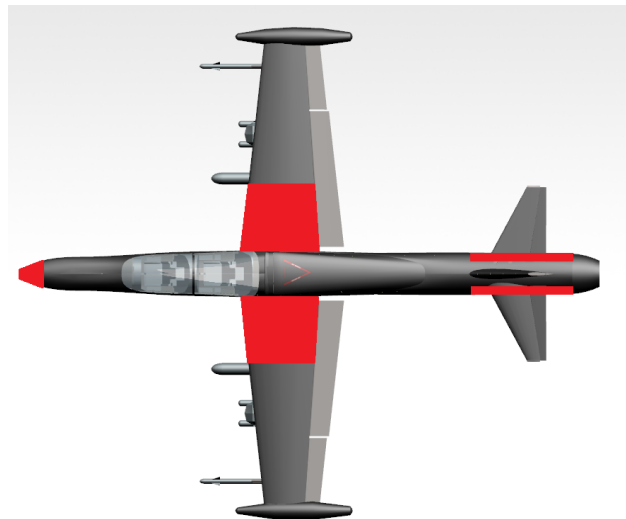


Fig. 66 Internal Armor Placement

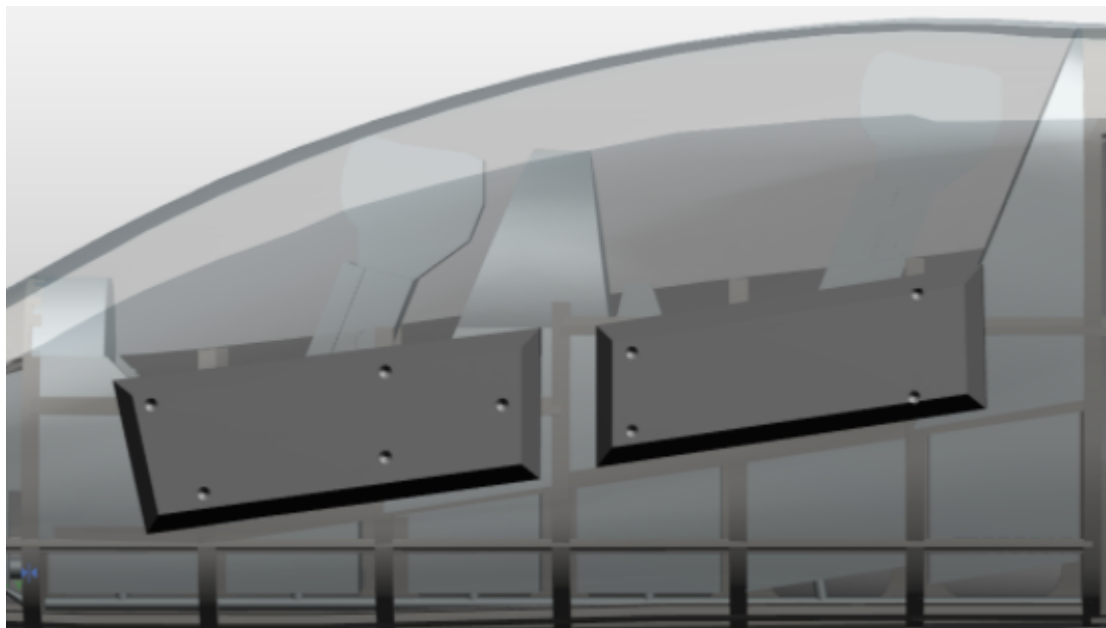


Fig. 67 External Armor Placement

It should be noted that while this armor may be transported by the Orca itself, it is not necessary. The external armor may be shipped in as needed by cargo vehicles at any time. This also aides in maintenance ease as multiple sets of external armor plates may be stored in bases for quick and easy replacement as needed. This is key due to the need for fast response times in close air support missions.

XV. Conclusion

For the missions of close air support in austere fields, there are currently very few airplane options available. The default has been mostly helicopters in the modern era. This presents an opportunity to fill a gap in the market and provide a new design to fill this role. In order to do this, a light attack aircraft was proposed in this paper. This possible aircraft design, the Orca, adheres to the AIAA RFP [1] and proves to meet or exceed all of the requirements laid out. This is outlined by Table 1.

The Orca aims to fulfill the RFP's desire for a 'best value' design. To achieve this, preference was given to cost reduction measures that allowed the aircraft to approach a unit cost of \$15.52 million for a fleet size of 200. This makes the Orca very competitive in the market of light attack aircraft while still achieving all requirements laid out by the RFP. The Orca also has the distinguishing design feature of a top inlet which is a rarity across all aircraft. This design choice was verified to still meet the performance requirements and justified by the survivability benefits it provides.

It was also desired to provide a design that is unique and distinct from the competition in this field. In order to do this, a top inlet design was chosen. This provided many benefits that are unique to our design, including: ground radar signature reduction, better certification for austere field performance, and better horizontal visual range for pilots. These traits are important for the role of close air support as this role mainly focuses on providing support for ground troops and as such benefits greatly from these traits. There are some concerns associated with the top inlet design. There are valid reasons for avoiding this due to boundary layer separation during maneuvers. In order to alleviate this concern, an aerodynamic performance analysis of the top inlet was performed in order to validate our design. It was found that the inlet was still able to provide enough air to the engine during the maneuvers required by our concept of operations, thus validating the design.

Future study should be done on the top inlet design. While our performance analysis of the inlet (done in Section V.F) showed that the inlet was sufficient in providing air to the engine during rise and descent, the analysis done did not consider advanced maneuvers that could be done during evasive action or emergency situations. These extreme actions should be taken into account in order to ensure the design does not fail under these conditions as air flow is harder to model under these conditions and may reveal areas where the inlet design may be improved.

References

- [1] AIAA, “Request for Proposal,” , 2021.
- [2] “Global Light Attack & Reconnaissance Aircraft Market Research Report,” , 2021. URL <https://www.marketresearchfuture.com/reports/light-attack-reconnaissance-aircraft-market-5925>.
- [3] “Global military expenditure sees largest annual increase in a decade—says SIPRI—reaching 1917 billion in 2019,” , 2020. URL <https://www.sipri.org/media/press-release/2020/global-military-expenditure-sees-largest-annual-increase-decade-says-sipri-reaching-1917-billion>.
- [4] Raymer, D. P., *Aircraft Design: A Conceptual Approach*, 6th ed., AIAA, California, 2018.
- [5] Jackson, P., *Jane's All the World's Aircraft 2010 - 2011*, Janes Information Group, London, England, 2010.
- [6] Taylor, J. W. R., *Jane's All the World's Aircraft 1988 - 89*, Jane's Publishing Company, London, England, 1988.
- [7] Jackson, P., *Jane's All the World's Aircraft 2003 - 2004*, Janes Information Group, London, England, 2003.
- [8] “ACES 5® ADVANCED CONCEPT EJECTION SEATS,” , Feb 2021. URL <https://www.collinsaerospace.com/-/media/project/collinsaerospace/collinsaerospace-website/product-assets/marketing/a/aces-5/aces-5-united-states-air-force-next-generation-ejection-seat.pdf?rev=dcf164f5028445879a80e86eb5d3a07a>.
- [9] Currey, N. S., *Aircraft Landing Gear Design: Principles and Practices*, American Institute of Aeronautics and Astronautics, Washington DC, 1988.
- [10] “Type-Certificate Data Sheet for PW305 PW306 Engines,” , Nov 2015. URL https://www.easa.europa.eu/sites/default/files/dfu/TCDS%20IM.E.051%20_issue04_200151711_1.0.pdf.
- [11] “F124 Turbofan Engine,” , May 2017. URL <https://aerospace.honeywell.com/content/dam/aero/en-us/documents/learn/products/engines/brochures/N61-1646-000-000-F124TurbofanEngine-bro.pdf>.
- [12] “A light attack aircraft fleet: Could it change the fight or put lives at risk?” , Feb 2018. URL <https://www.airforcetimes.com/news/your-air-force/2018/02/20/a-light-attack-aircraft-fleet-could-it-change-the-fight-or-put-lives-at-risk/>.
- [13] “EJ200 turbofan engine,” , Feb 2021. URL https://www.mtu.de/fileadmin/EN/7_News_Media/2_Media/Brochures/Engines/EJ200.pdf.
- [14] “M88: Proven performance and reliability,” , Feb 2021. URL <https://www.safran-aircraft-engines.com/military-engines/training-and-combat-aircraft/m88>.
- [15] “AI-222-25F/AI-322F,” , Feb 2021. URL <http://www.motorsich.com/eng/products/aircraft/tde/ai-222-25f>.
- [16] Leland M. Nicolai, G. E. C., *Fundamentals of Aircraft and Airship Design*, AIAA, Virginia, 2010.

- [17] Abbott, I., and Doenhoff, A. V., *Theory of Wing Sections*, dover ed., Dover Publications, New York, 1958.
- [18] Roskam, J., *Airplane Design*, 6th ed., DARcorporation, Kansas, 2019.
- [19] McCormick, B. W., *Aerodynamics, Aeronautics and Flight Mechanics*, Wiley, New York, 1995.
- [20] Sadraey, M. H., *Aircraft Design: A system engineering approach*, Wiley, Chichester, 2013.
- [21] J.R. Davis, D. . A., *ASM Specialty Handbook - Carbon and Alloy Steels*, ASM International, Metals Park, OH, 1996.
- [22] *Metals Handbook, Vol.2 - Properties and Selection: Nonferrous Alloys and Special-Purpose Materials*, ASM International, 1990.
- [23] Bolthouse, J., “Republic P-47 Thunderbolt,” , July 2003. URL <https://www.asminternational.org/documents/10192/1881847/amp16107p041.pdf>
- [24] Matthew G. Richards, A. M. R., “Two Empirical Tests of Design Principles for Survivable System Architecture,” , 2008. URL http://seari.mit.edu/documents/preprints/RICHARDS_INCOSE08.pdf.
- [25] “TenCate selected by Embraer for supplying ballistic protection for Embraer A-29 Super Tucano military aircraft,” , ????
- [26] Bauccio, M., *ASM Engineered Materials Reference Book, Second Edition*, ASM International, Materials Park, OH, 1996.
- [27] “MIL-A-8861: Military Specification, airplane Strength and Rigidity Flight Load.” , Feb 1986.
- [28] “MIL-A-8860: Military Specification, airplane Strength and Rigidity General Specification For,” , May 1987.
- [29] “aeroMETAL™ Honeycomb Panels,” , 2021. URL <https://www.collinsaerospace.com/what-we-do/Business-Aviation/Cabin/Structures/Honeycomb-Panels/Aerometal>.
- [30] FEDERAL AVIATION ADMINISTRATION, D. O. T., “14 CFR 25.1191 - Firewalls.” , 2001. URL <https://www.govinfo.gov/app/details/CFR-2001-title14-vol1/CFR-2001-title14-vol1-sec25-1191>.
- [31] “MIL-E-18927E: Military Specification, Environmental Control Systems, Aircraft, General Requirement For,” , Aug 1983.
- [32] Ian Moir, A. S., *Aircraft Systems: Mechanical, Electrical, and Avionics Subsystems Integration*, 3rd ed., AIAA, California, 2008.
- [33] Pierre, F., *Mechanics of Materials*, 3rd ed., McGraw-Hill, 2001.
- [34] “Michelin Military Aircraft Tires.” , March 2021. URL <https://aircraft.michelin.com/wp-content/uploads/sites/15/2020/05/DataSheets-MILITARY-segment%20%93-April-update.pdf>.
- [35] “M-130 General Purpose Dispenser.” , Feb 2000. URL <https://fas.org/man/dod-101/sys/ac/equip/m-130.htm>.
- [36] “Air Force Fighter Pilot Qualifications.” , Jan 2020. URL <https://work.chron.com/air-force-fighter-pilot-qualifications-8456.html>.
- [37] “Cockpit 4000 Avionics Suite.” , 2020. URL <https://cmcelectronics.ca/Portals/17/Documents/en-us/CMC-COCKPIT4000-19-003.pdf>.

- [38] “Air Force Fact Sheets,” , 2014. URL <https://www.af.mil/About-Us/Fact-Sheets/Category/728/>.
- [39] Thomas, P., *Royal Air Force Aircraft and Weapons*, 2003.
- [40] “Boeing / Lockheed Martin SDB (Small Diameter Bomb),” , 2008. URL <http://www.designation-systems.net/dusrm/app5/sdb.html>.
- [41] “Gallery of USAF Weapons,” , 2016. URL <https://www.airforcemag.com/PDF/MagazineArchive/Magazine%20Documents/2016/May%202016/0516weapons.pdf>.
- [42] “Precision Guided Munitions and the New Era of Warfare,” , 1995. URL <https://fas.org/man/dod-101/sys/smарт/docs/paper53.htm>.
- [43] “F/A-18 E/F 20mm Gatling Gun System,” , July 2002. URL <https://www.gd-ots.com/wp-content/uploads/2017/11/F-A-18-E-F.pdf>.